REPUBLIQUE ALGERIENNE DEMOCRATIQUE ET POPULAIRE

MINISTÈRE DE L'ENSEIGNEMENT SUPERIEUR
ET DE LA RECHERCHE SCIENTIFIQUE

UNIVERSITE DJILLALI LIABES DE SIDI BEL ABBES

FACULTE DE TECHNOLOGIE

DÉPARTEMENT DE GENIE MECANIQUE

Thèse en Vue de l'Obtention du Diplôme de Doctorat LMD en Génie Mécanique

Option : Energétique et environnement

Présentée par Monsieur

HADDOUCHE Mohammed Réda

Intitulé de la thèse

Investigation numérique des capteurs solaires cylindro-parabolique sous conditions climatiques Algérienne

---

Devant le jury composé de :

Mr MAKHLOUF MOHAMED	Pr	Président	Université de Sidi Bel Abbes
Mr RETIEL NOURREDINE	Pr	Examinateur	Université de Mostaganem
Mr BOUCHAM BELHADJ	Pr	Examinateur	Université de Sidi Bel Abbes
Mr BENAZZA ABDELYLAH	Pr	Encadreur	Université de Sidi Bel Abbes

Année Universitaire : 2021-2022

Thanks

I would like to address my sincere thanks to my family, my father, my mother and my brothers Zakaria and Abdelhadi for their support all the time

Also, to all the professors of the MECHANICAL ENGINEERING department of the Djillali Liabes University of Sidi Bel-Abbes, in particular Mr. Benazza Abdelylah who was of precious help and unfailing assistance to me and also the members of the jury for agreeing to evaluate my work

Abstract

Solar energy is one of the renewable, free, clean and available energies in the whole globe. In order to be useful, this energy must be concentrated and collected. The Parabolic Trough Collector is the most mature and developed technology on this field. The aim of this thesis is to evaluate the thermo-hydraulic performance and the increase of the heat transfer inside an enhanced tube of parabolic trough solar collector.

Passive and active methods are used by introducing different type of inserts inside the absorber tube and a secondary reflector is used to homogenise the circumferential temperature of the receiver tube. In the other hand, the Algerian climatic condition and geographical parameters of different region are analysed to calculate the direct normal irradiance. The simulation's results indicate that the inserts enhance the heat transfer inside the absorber tube. The use of the Secondary Reflector decreases the circumferential temperature gradient of the absorber tube and the geographical analysis shows that the direct normal irradiance is higher in the Saharan regions.

Resumé

L'énergie solaire est l'une des énergies renouvelables, gratuites, propres et disponibles dans le monde entier. Pour être utile, cette énergie doit être convertie et collectée. Le collecteur à cylindro-parabolique est la technologie la plus mature et la plus développée dans ce domaine. Le but de cette thèse est d'évaluer les performances thermo-hydrauliques et l'amélioration du transfert de chaleur à l'intérieur du tube récepteur du capteur solaire cylindro-parabolique.

Des méthodes passives et actives sont utilisées en introduisant différents types d'inserts à l'intérieur du tube absorbeur, un réflecteur secondaire est utilisé pour homogénéiser la température circonférentielle du tube récepteur. D'ailleurs, les conditions climatiques algériennes et les paramètres géographiques des différentes régions sont analysés pour calculer l'irradiance normale directe. Les résultats de la simulation indiquent que les inserts améliorent le transfert de chaleur à l'intérieur du tube absorbeur. L'utilisation du réflecteur secondaire diminue le gradient de température circonférentiel du tube absorbeur et l'analyse géographique montre que l'irradiance normale directe est plus élevée dans les régions sahariennes.

ملخص

الطاقة الشمسية هي واحدة من الطاقات المتجددة والنظيفة والمتجددة في العالم بأسره. لكي تكون هذه الطاقة مفيدة، يجب تركيزها وجمعها. يعتبر مجمع Parabolic Trough Collector من أكثر التقنيات تطوراً وتطوراً في هذا المجال. الهدف من هذه الأطروحة هو تقييم الأداء الحراري الهيدروليكي وزيادة نقل الحرارة داخل أنبوب محسّن لمجمع الطاقة الشمسية المكافئ.

يتم استخدام الطرق السلبية والفعالة عن طريق إدخال أنواع مختلفة من المدخلات داخل أنبوب الامتصاص ويتم استخدام عاكس ثانوي لمجانسة درجة الحرارة المحيطية لأنبوب المستقبل. من ناحية أخرى ، يتم تحليل الحالة المناخية الجزائرية والمعايير الجغرافية للمنطقة المختلفة لحساب الإشعاع الطبيعي المباشر. تشير نتائج المحاكاة إلى أن الإضافات تعزز انتقال الحرارة داخل أنبوب الامتصاص.

شير نتائج المحاكاة إلى أن الإضافات تعزز انتقال الحرارة داخل أنبوب الامتصاص. يقلل استخدام العاكس الثانوي من التدرج الحراري المحيطي لأنبوب الامتصاص ويظهر التحليل الجغرافي أن الإشعاع الطبيعي المباشر أعلى في المناطق الصحراوية.

Content

Chapter I: Solar Radiation

Chapter II: Solar thermal collectors

Chapter III: Mathematical model and numerical approach

Chapter IV: results and discussion

Chapter V: Solar irradiation Estimation

Figures list

Nomenclature

Nomenclature

A	Surface	(m^2)
Cp	Heat capacity	(J/kgK)
D	Diameter	(m)
E	Power	(W)
e	Eccentricity	(m)
f	Friction factor	(-)
G	Irradiance	(W/m^2)
g	Gravity	(m/s^2)
H	Height	(m)
h	Convective Heat transfer coefficient	(W/m^2k)
Hs	Solar height	(Degree)
L	Longitude	(m)
N	Day number	(-)
Nu	Nusselt number	(-)
Pr	Prandt number	(-)
Q	Heat flux	(w/m^2)
R	Radius	(m)
Re	Reynolds number	(-)
T	Temperature	(K)
u,v,w	Velocity	(m/s)

Greek letters

δ	Declination	(Degree)
ε	Turbulence dissipation	(-)
θz	Zenith angle	(Degree)
λ	Conductive heat transfer coefficient	(W/mk)
μ	Viscosity	(m^2/s)
π	Number Pi	(3.14)
ρ	Density	(Kg/m^3)
σ	Stephan Boltzmann constant	(5.6697x10-8 $W/m^2.K4$)
τ	transmittance	(-)

Subscripts

a	Absorber tube
amb	Ambient
g	Glass cover
i	Inner
o	Outer
sky	Sky
sol	Solar
w	wind

Abbreviation

DNI	Direct normal irradiance
HTF	Heat transfer fluid
LCR	Local concentration ratio
MCRT	Monte Carlo ray tracing
NREL	National renewable energy laboratory

PEC	Performance coefficient
PTC	Parabolic trough collector
SR	Secondary reflector
TST	True solar time

Introduction

Securing a reliable, economic and sustainable energy supply as well as environmental and climate protection are important global challenges of the 21Stcentury. Renewable energy and improving energy efficiency are the most important steps to achieve these goals of energy policy. While impressive efficiency gains have already been achieved in the past two decades, energy use and CO2 emissions in manufacturing industries could be reduced further, if best available technologies were to be applied worldwide.

Solar energy has become increasingly important in the world as a technology to improve energy efficiency and reduce CO2 emissions. In particular solar concentrators offer various opportunities to all types of manufacturing processes and operations. These concentrators are using solar radiation as the heat source, deliver heat at higher temperature for use in industrial processes, heating or preheating, or for space heating and cooling in industry. Also it can significantly reduce fossil fuel consumption and green-house gas emissions.

Algeria with an area of 2.381.741 km² and an irradiance of 2650kWh/m² per year has a potential solar energetic.

The thesis consists of five chapters. In the first chapter the solar radiation and the earth-sun relationship is discussed and the mathematical equations to calculate the different parameters are presented.

In the second one, the solar thermal collector technologies are presented and illustrated. Also the different elements of the Parabolic Through collector are shown in details.

In the third chapter the mathematical modelling and the different equations used to calculate the thermo-hydraulic parameters of the fluid flow and the heat transfer mechanism are presented. The chapter four the numerical results of the simulation are presented and

discussed and the different parameters that identify the fluid flow and the thermo-hydraulic performance of the receiver tube.

In the fifth and final chapter, the Algerian climatic conditions are introduced in order to calculate the direct normal irradiance using the Hottel's method and using an Excel program for different region of Algeria.

Chapter I

I.1. Introduction

The operation of solar thermal collectors is related to the earth-Sun relationship since it is essential to know the radiation and the energy produced by the sun and reaches the earth's surface. For this, it is necessary to study the factors that characterize the solar radiation that reaches the Earth's surface and can be summarized in two categories: geometric factors and climatic factors. In this chapter we will explain all the phenomena and equations of the solar radiation required for the solar thermal calculations.

I.2. Energy of the sun:

The Sun is a star within the category of yellow dwarf stars with a spherical shape with a diameter of 1,392x10^6 km. In its interior complex and continuous fusion reactions making it the most advanced and powerful of the nuclear reactors, being its power of about 3,844 10^{23} kW. Its composition, mainly hydrogen and helium, are in the gaseous and plasma state. The figure I.1 illustrates the reaction mechanism of the sun's particles [1].

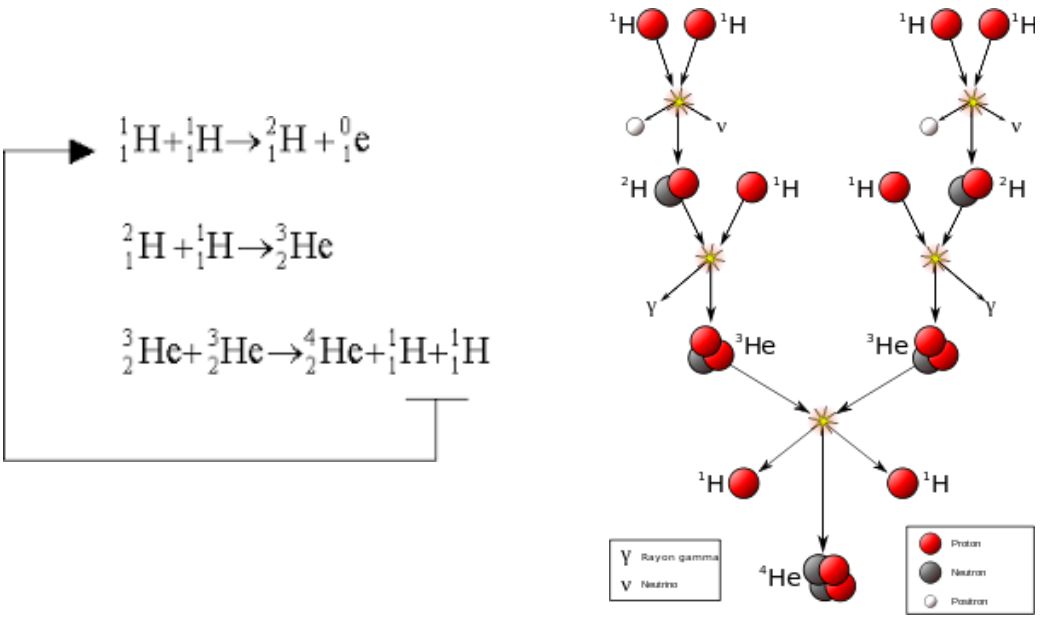

Figure I.1: *Reaction mechanism of the sun's particles*

The solar mass is estimated to be around $2 \cdot 10^{30}$ kg (332000 times bigger than that the Earth) with a conversion of mass into energy that supposes a loss of 4 million tons per second, but despite this impressive speed of mass loss, the life of the Sun in its current state is guaranteed for more than 6000 million years. The Sun disperses the energy produced in all directions, reaching the earth's surface of the order of $1{,}743 \cdot 10^{14}$ kW. For the purposes of solar energy received on earth, the Sun behaves as a black body at 5777 K, with 96% of the energy being distributed between wavelengths λ, from 0.2 to 2.4 µm. Figure I.2 shows the spectrum of actual radiation received from the Sun and is compared with the theoretical radiation spectrum produced by a black body at 5777 K [2].

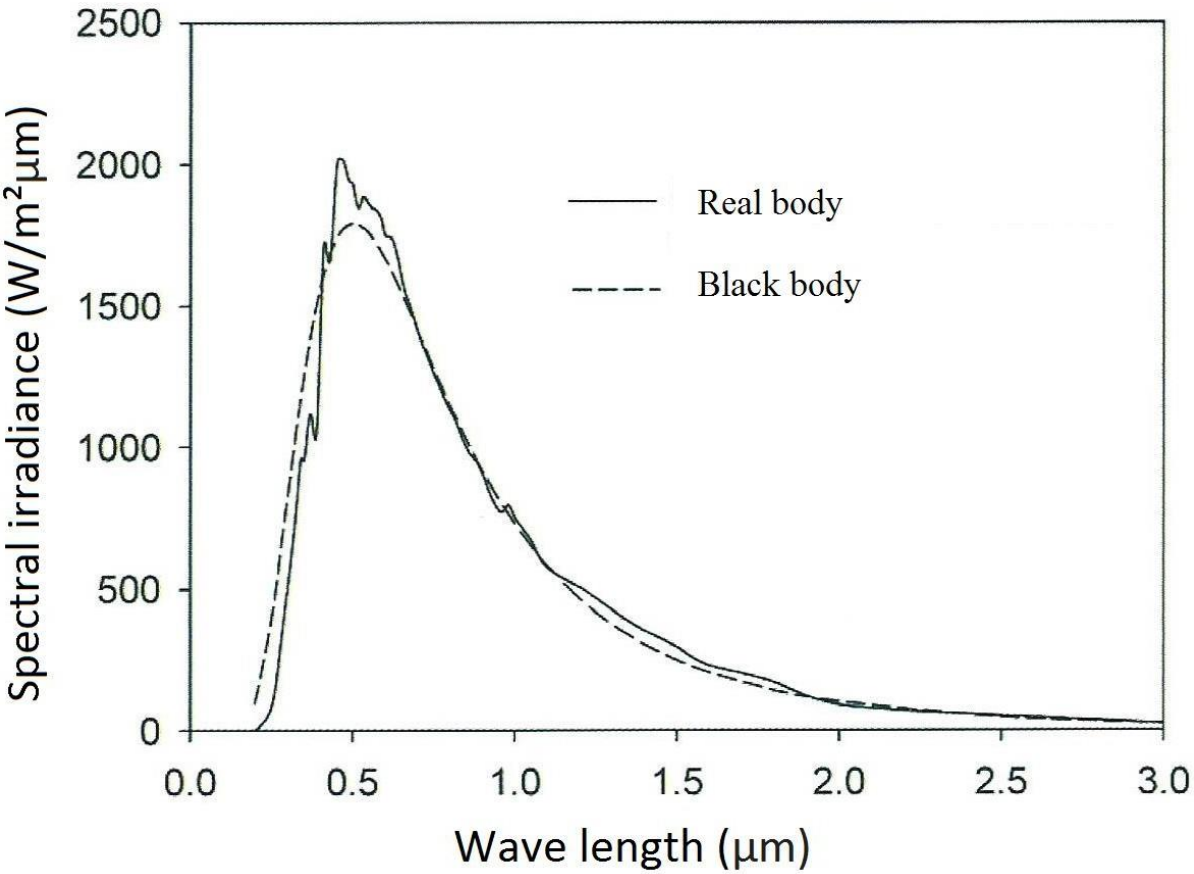

Figure I.2: *Spectrum of actual radiation received from the Sun*

I.3. Earth-Sun motion

I.3.1 Solar constant

The total energy per unit time emitted by the sun (Considered as a black body) is [2]:

$$E_{sun} = A_{sun} \cdot \sigma \cdot T_{sun}^4$$

I.1

Where A_{sol} is the external area of the sun and it is defined as $A_{sol} = 4 \cdot \pi \cdot R_0^2$, σ is the Stephan Boltzmann constant ($5.6697 \cdot 10^{-8}$ W/m²·K^4) and T_{sol} is the effective temperature defined as a black body temperature and its value is 5774 K [2].

At the end the Total energy is estimated as:

$$E_{sun} = 3.884 \cdot 10^{26} \qquad \text{I.2}$$

It is considered that the energy produced by the sun is distributed uniformly in all directions

And per square meter perpendicular to the radiation reached the external surface of the atmosphere of the earth when we considered the average distance earth-sun d_{e-s} (149.598×10^6km)

$$G_{sc} = \frac{A_{sun} \sigma \, T_{sun}^4}{4 \, \pi r_{e-s}^{\,2}} \qquad \text{I.3}$$

And the solar constant is:

$$G_{sc} = 1367 \ (\text{W} \cdot \text{m}^{-2}) \qquad \text{I.4}$$

The incidence solar radiation (G_s) changes every day because of the change of the earth-sun distance, and it is estimated ±1.7% and it can be calculated by the following expression

$$G_s = G_{sc} \ [1 + 0.034 \cos (\frac{360(N-3)}{365.25})] \qquad \text{I.5}$$

Where, N is the day number calculated from the first of January. Figure I.3 shows the graphical representation of the equation.

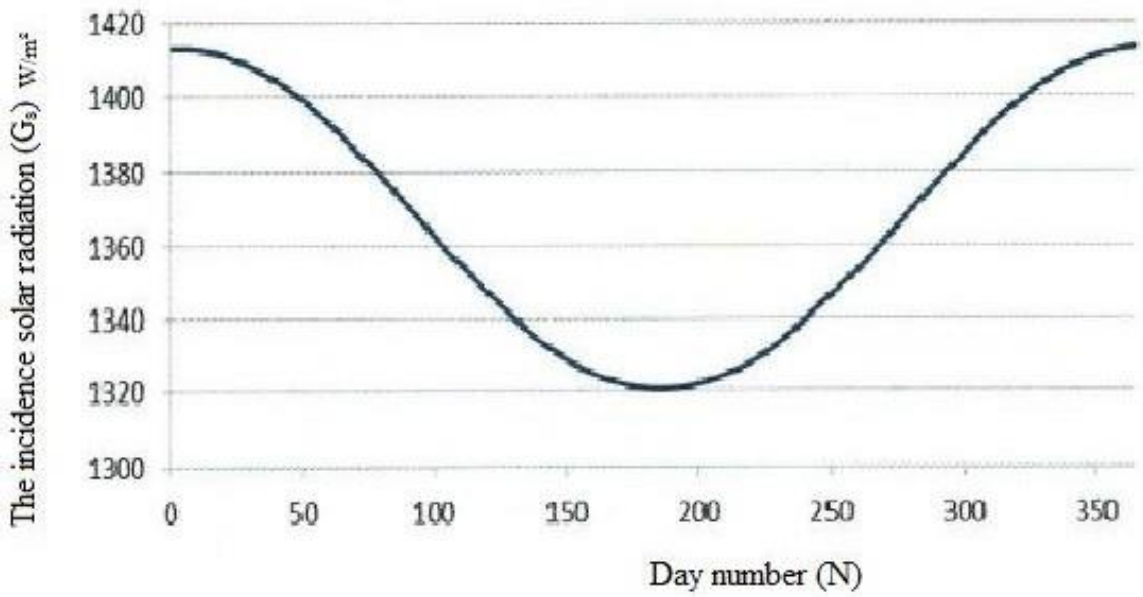

Figure I.3: *Incidence solar radiation in function of day number*

I.3.2. Geographical coordinates of the earth

In order to situate any location on earth is established a reference system that consists of determine two angles: the latitude (φ) and the longitude (λ) as it's shown in figure I.4.

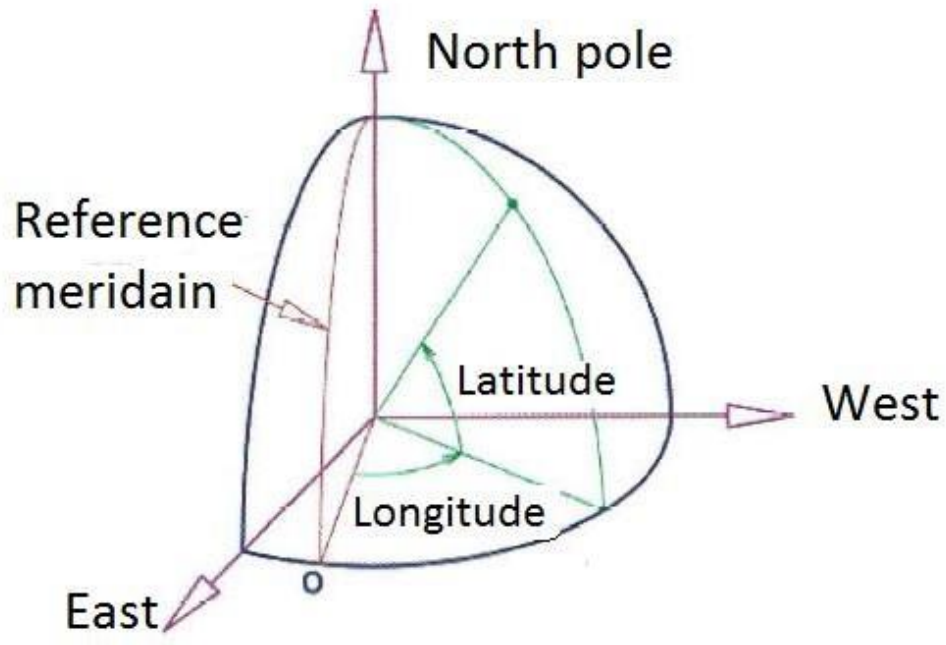

Figure I.4: *Reference system*

The latitude (φ) of a place is the angle formed by the terrestrial radius that passes through that point and the plane that forms the equator. All points of equal latitude are located in the same plane, called the terrestrial parallel.

The longitude (λ) of a place is the angle formed by the radial plane that contains the earth's axis and that passes through that point with a plane that contains the earth's axis are taken as a reference. The radial planes that contain the earth's axis are called meridians, the meridian plane that is taken as a reference is the one that passes through Greenwich [3].

I.3.3. Celestial and equinox

The daily rotational movement of the earth around its own axis causes the differences between day and night. The earth axis is the union of the earth poles, has an inclination of 23.25° with respect to the perpendicular to the plane of the ecliptic. The tilt of the earth axis is responsible of the seasons that are produced by the translational movement of earth around

the sun. The tilt of the earth axis leads to the definition of Cancer and Capricorn and of the Arctic and Antarctic polar circles as shown in the figure I.5.

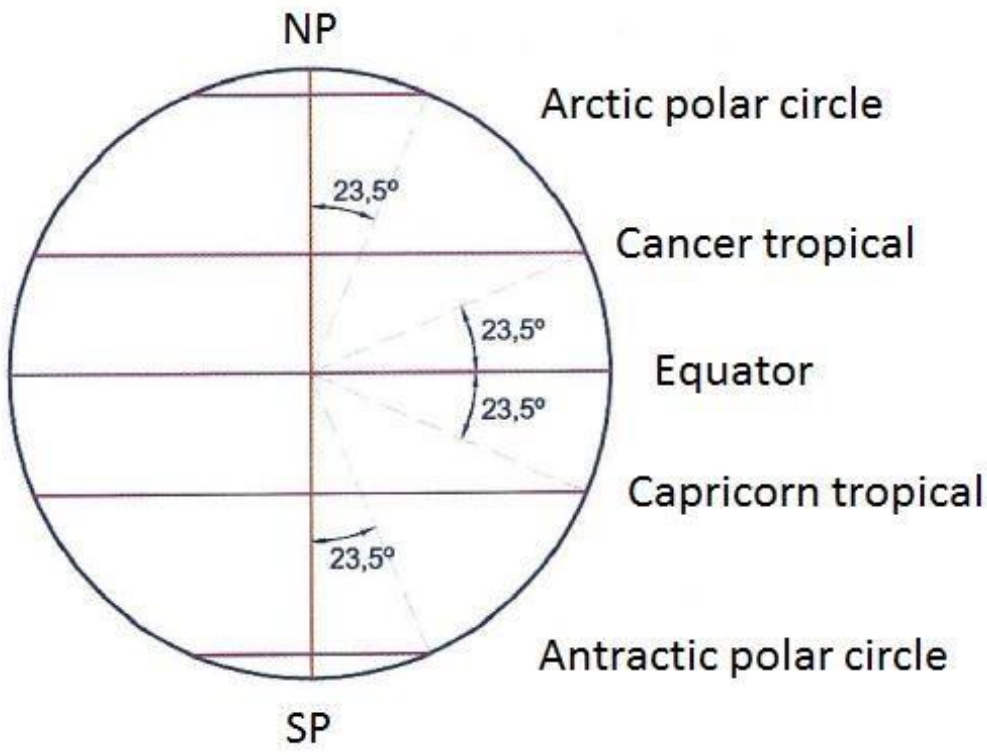

Figure I.5: *Earth's polar circles*

I.3.4. Declination

The declination δ is a variable magnitude that is defined as the angle formed by the line that joins the centres of the earth and the Sun with the circle that contains the earth's equator. The declination has a daily variation of less than 0.5°, and the average daily declination can be calculated using the following equation [3]:

$$\delta = 23.45 \sin\left[\frac{360}{365.25}(N + 284)\right] \qquad \text{I.6}$$

Where, N is the day number calculated from the first of January.

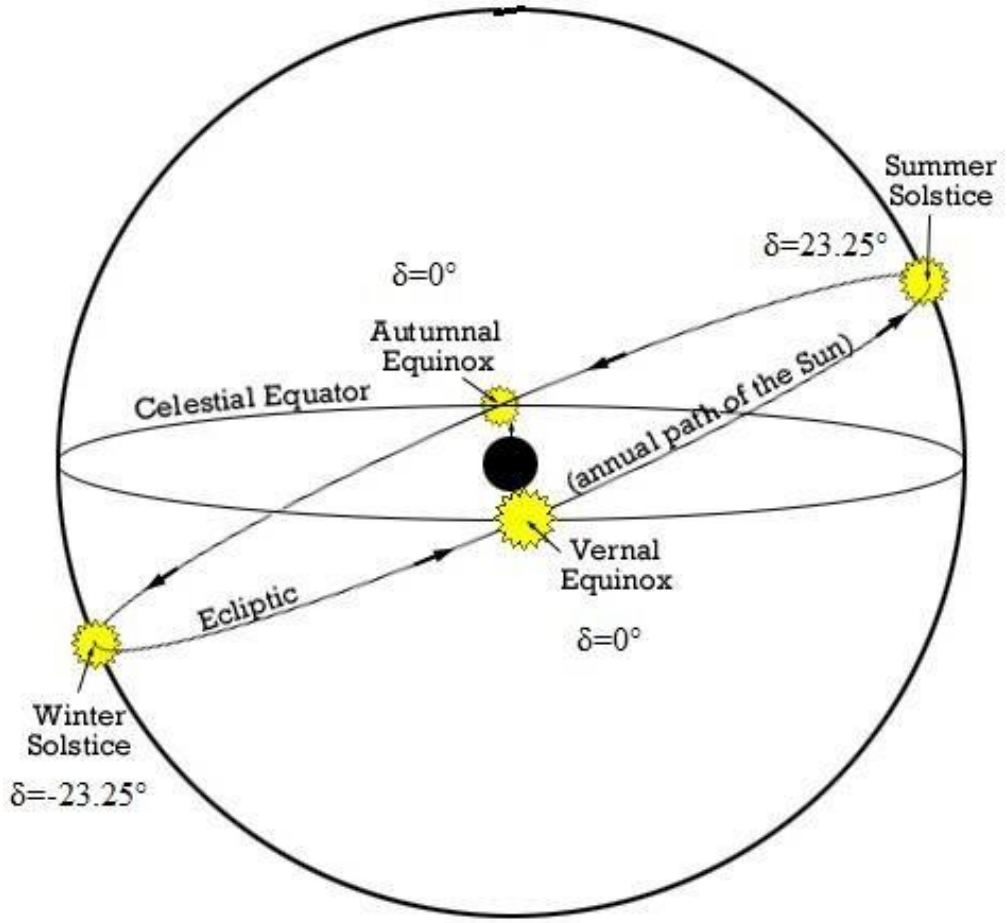

Figure I.6: *Earth's* declination

- The summer solstice: June 21-22 (N=172-173). It corresponds to the day for which the diurnal part of the northern hemisphere is maximum and the declination at this time is maximum with a value of δ=23.25°. The sun rays are perpendicular to the surface of the earth in the tropic of Cancer.
- The winter solstice: December 21-22 (N=355-356). Corresponds to the day for which the diurnal part in the northern hemisphere is minimum (maximum in the southern hemisphere). The declination at this time is minimal (δ=-23.25°). The sun's rays are perpendicular to the surface of the earth in the tropic of Capricorn.
- The vernal equinox: March 20-21 (N=79-80). Day and night last 12h (δ=0°). The sun's rays are perpendicular to the earth's surface at the equator.

- The autumnal equinox: September 22-23 (N=256-266). The sun's rays are perpendicular to the earth surface of the equator.

I.3.5. Sun geometry

It is necessary to create a reference system to fix the position of a star in the celestial sphere. The most useful and appropriate for the study of solar radiation are the horizontal reference system and the equatorial reference system.

I.3.5.1. Horizontal reference system

To fix the position of the sun, it is necessary to use only two angular coordinates (The azimuth and the sun height) since the distance of the sun is not an interesting concept as it shown in the figure I.7.

I.3.5.1.1. Azimuth

The azimuth (A_z) is the angle formed by the vertical plane or that contains the sun with the vertical plane that passes but the south. The angle is measured in the celestial astronomical horizon starting from the south to the vertical plane that contains the sun. It is usually measured from 0 to 180° if we start from the South point to the West and from 0 to -180° if we start from the South point to the East.

At a practical level, we call the solar azimuth the angle formed by our south with the projection of the solar rays on the horizon plane [3].

I.3.5.1.2. Solar height

The Solar height (H_s) is the angle measured in the vertical plane of the sun, between the celestial astronomic horizon and the sun. It is measured from 0 to 90° if we move toward the

zenith or from 0 to -90°. In a practical purpose we call the solar height is the angle that the horizon plane formed with the direction in which we observe the sun.

I.3.5.1.3. Zenith angle

The Zenith angle (θ) is defined as the compliment of the solar height

$$\theta = 90 - H_s \qquad \text{I.7}$$

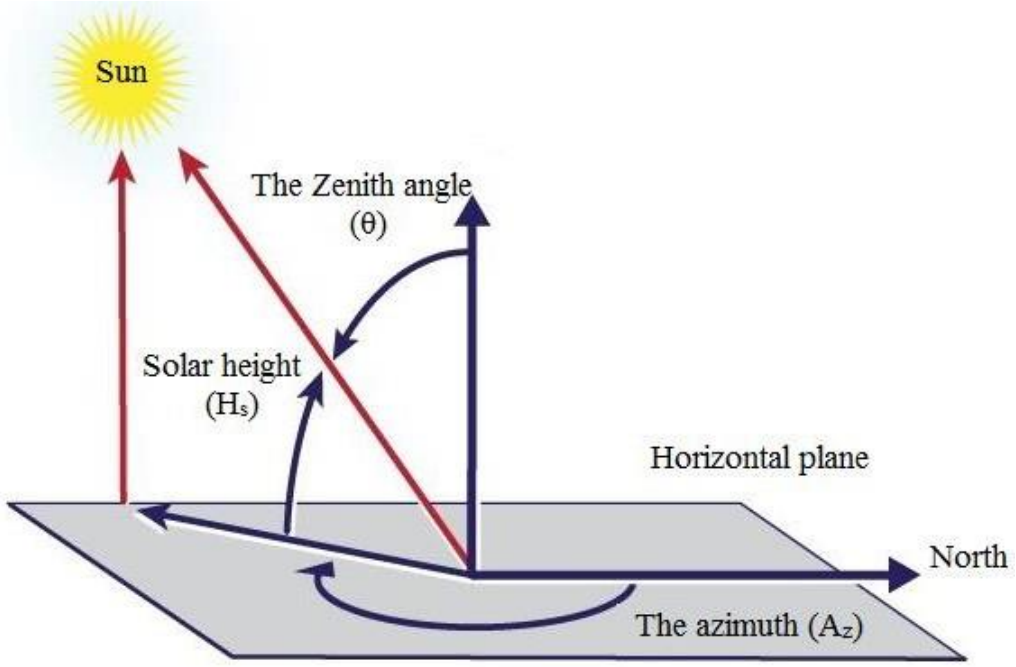

Figure I.7: Zenith angle

I.3.5.2. Equatorial reference system

I.3.5.2.1. Hour angle

The hour angle (ω) is the angle measured on the celestial equator starting from the point belonging the meridian of the place to the meridian of the sun. It is usually measured from 0 to 360° in the clockwise direction or 0 to 24h. Since the principle, each hour corresponds to

15°. Knowing the solar time, the hour angle can be calculated in degrees from the True Solar Time (TST) such as:

$$\omega = 15\ (TST - 12) \qquad \text{I.8}$$

I.3.5.2.2. Declination of the sun

This angle is considered a universal angle, since at a given instant the declination of star is the same for all points on earth, because they are so far from earth and maintain a constant decline through the year. However, for the sun the declination varies as the same equation of the earth's declination. (This variable is usually doesn't considered in calculations). The daily variation of the declination makes the sun moves through different celestial parallels day after day; in fact, the movement of the sun follows the path of a spiral [2].

I.3.5.3. Relationship between both reference systems

To obtain the relationship between both reference systems, spherical geometry is used.it should be taken in consideration that the height and the Azimuth of the sun are easily measurable angles from any point on earth [4].

$$\sin H_s = \sin\varphi \sin\delta + \cos\varphi \cos\delta \cos\omega \qquad \text{I.9}$$

And

$$\cos A_z = \frac{-sin\delta + \sin\varphi \sin H_z}{\cos\varphi \cos H_z} \qquad \text{I.10}$$

Therefore, with these two equations it is possible to calculate in a simple way the azimuth and the height of the sun, knowing the latitude (φ), the declination (δ) and the hour angle (ω).

I.4 Solar radiation

In the beginning of this chapter, we analysed the sun activity which produces electromagnetic radiations, most of them are at wavelength between 0.2 and 2.4µm with a spectral distribution practically invariable over the time. These electromagnetic radiations cause of the warming of the earth, they provide the energy necessary for our lives. In this section we will analyse the part of the solar energy that is capable to reach the earth ‘s surface and therefore is potentially usable is solar thermal installations.

Before proceeding farther, it is convenient to introduce some basic concepts that will help to simplify and understand the nomenclature used and its physical meaning [5].

I.4.1. Irradiance

The irradiance (G) is the incident energy on the unit surface in unit time. In some way it called the surface power, and its unit is $W \cdot m^{-2}$.

I.4.2. Irradiation

The irradiation (I) is the energy received by the surface during a certain time period and it is obtained by the integration of the irradiance throughout time period and its unit is $J \cdot m^{-2}$.

I.4.3. Incidence angle of solar radiation on a horizontal plane

The incidence angle (θ_h) of solar rays on a surface outside the earth’s atmosphere is defined as the angle of the sun’s rays and the perpendicular to the surface. This definition is also applicable to solar radiation on the earth’s surface when speaking exclusively of direct solar radiation.

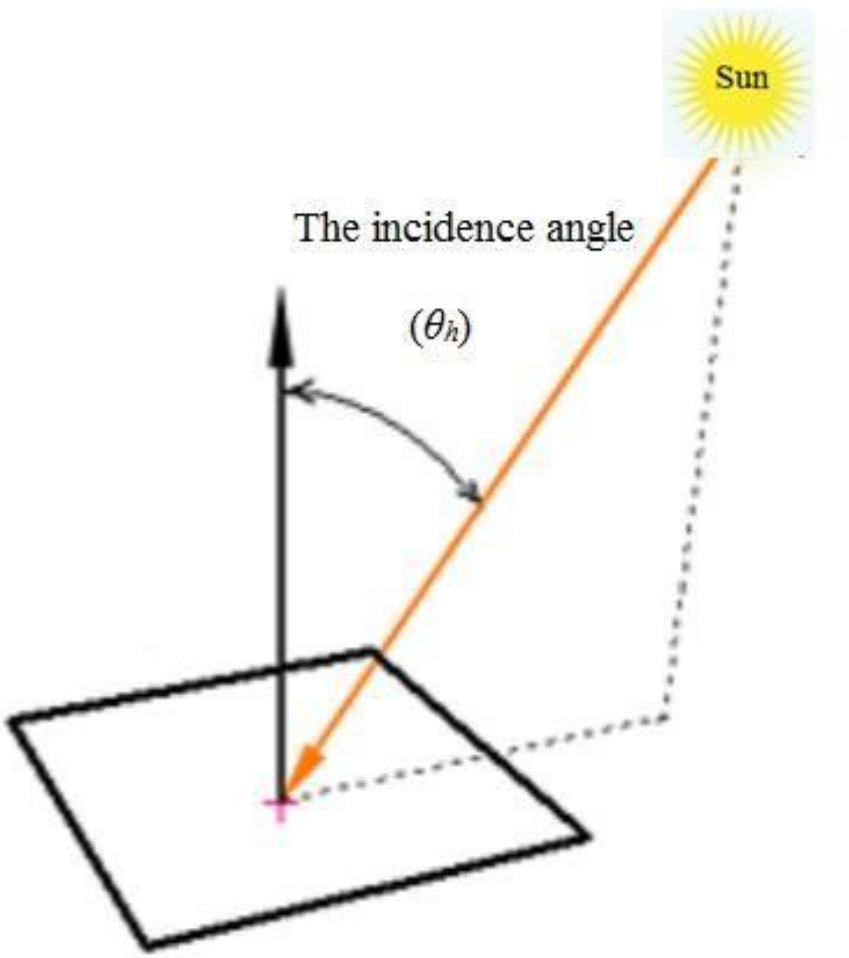

Figure I.8: *Incidence angle of solar radiation on a horizontal plane*

The incidence angle at each moment on earth is given by [6]:

$$\sin H_s = \cos\theta_h = \sin\varphi \sin\delta + \cos\varphi \cos\delta \cos\omega \qquad \text{I.11}$$

When θ_h is the incident angle, in the case of horizontal plane, is equal to the zenith angle (θ) or the compliment of the solar height (H_s).

I.5. Extra-terrestrial solar irradiance

The extra-terrestrial solar irradiance is on a surface perpendicular to the solar beam (G_{on}), is inversely proportional to the square of the distance between the earth and the sun. it is uniformly distributed in the celestial sphere.

$$\frac{G_{on}}{G_{sc}} = \left(\frac{R_0}{R}\right)^2 \qquad \text{I.12}$$

Where G_{sc} is the solar constant, R_0 is the mean earth-sun distance, R is the earth-sun distance on day N; N is the day number calculated from the first of January.

The expression $\left(\frac{R_0}{R}\right)$ is the correction factor of the earth eccentricity or the correction factor of earth-sun distance.

$$E_0 = \left(\frac{R_0}{R}\right) = 1 + 0.034\cos\left(\frac{360(N-3)}{365.25}\right) \qquad \text{I.13}$$

Thus, the solar irradiance on a surface perpendicular to the solar rays will be given by the following expression:

$$G_{on} = G_{sc}\left(\frac{R_0}{R}\right)^2 = G_{sc}\left[1 + 0.034\cos\left(\frac{360(N-3)}{365.25}\right)\right] \qquad \text{I.14}$$

I.6. Terrestrial solar irradiance

The main characteristics of the solar radiation that reaches the outside of the earth's atmosphere are already defined, however, the use of solar resources take place on the earth's surface and that is why the atmosphere becomes the main factor determining the characteristics of such radiation at the earth's level. It is in the first 80 km of the atmosphere where most of the activities that influence the earth's climate take place. In the same way, it is

in this layer where the main phenomena occur that make it an attenuating medium for solar radiation [5].

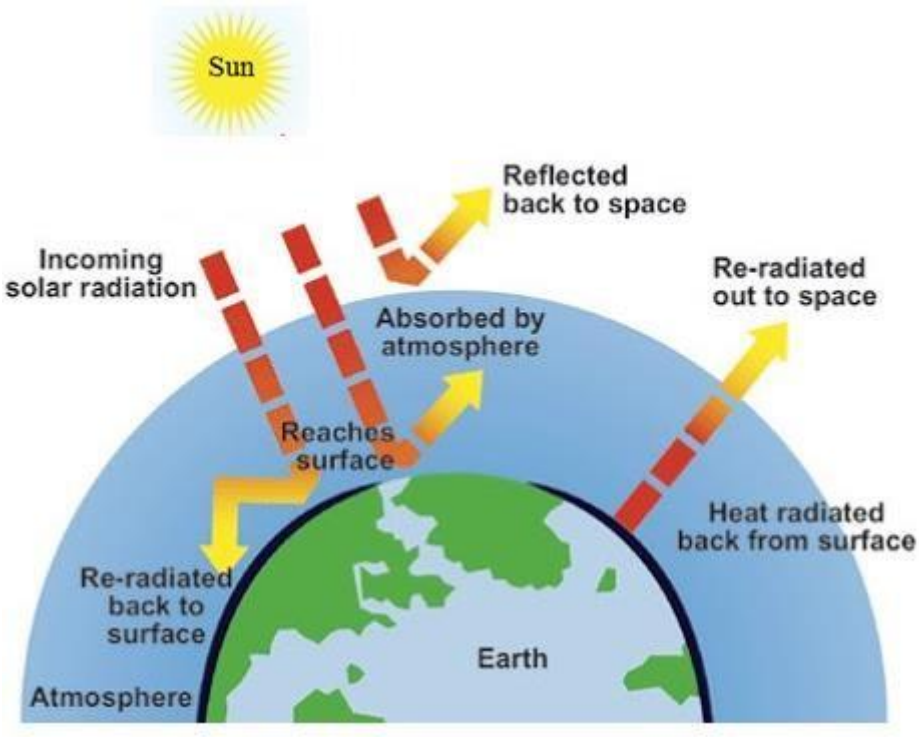

Figure I.9: *Terrestrial solar irradiance*

The main components of the atmosphere are in the gaseous state and are mainly oxygen (21% volume) and nitrogen (78% volume). There are another series of components of variable presence such as ozone, water both in liquid and vapour state, methane, carbon dioxide, aerosols, etc. The main phenomena on solar radiation due to the presence of these elements are the absorption and dispersion of solar radiation. The components of the atmosphere become new energy emitters when solar radiation falls on them, so that part of this captured energy is again radiated in all directions (dispersion phenomenon) and on the other hand they can become authentic energy sinks (absorption phenomenon) to originate different chemical reactions to maintain the atmospheric balance, for example the ozone cycle.

At the terrestrial level there are two components of solar radiation:

The direct component: radiation that has not been interfered with by the Earth's atmosphere and that has a perfectly defined direction by the hypothetical line that joins the Earth and the Sun. It is the one that produces the shadows.

The diffuse component: solar radiation that has undergone dispersion processes by the components of the atmosphere and comes from all points of the celestial vault. On a covered day, all radiation is diffuse [5].

I.7. Conclusion

The factors that characterize the solar radiation that reaches the Earth's surface can be summarized in two categories: geometrical factors and climatic factors. The geometric factors depend on the relative Earth-Sun position and the geometric coordinates of the site. The climatic factors: once the effects of geometric factors are "discounted", it continues to be observed that solar radiation has different characteristics from those expected. This is they diffused, absorbed, and reflected part of the solar radiation in a random way due to the presence of clouds, aerosols, ozone, etc…

Chapter II

II.1. Introduction

Enhancing heat transfer surface are used in many engineering applications, such as parabolic trough absorber hence many techniques have been investigated on enhancement of heat transfer rate and decrease the size and cost of the involving equipment one of the most important techniques used are passive heat transfer technique. These techniques when adopted in Heat exchanger proved that the overall thermal performance improved significantly. This chapter reviews experimental and numerical works taken by researchers on these techniques such as twisted tape, wire-coil, etc.

II.2. Solar thermal collector

A solar thermal collector is a heat exchanger that converts solar radiation into a usable thermal energy for different applications [7, 8 and 9]. Solar collectors can basically be classified between those that are stationary and those that have the ability to follow the movement of the sun.

The main objective of a solar thermal collector is to convert the electromagnetic radiations that come from the Sun to useful energy by increasing the temperature of the heat transfer fluid [10, 11]. Its behaviour depends on the geometrical and optical properties of its elements. The absorption, reflection and transmittance are the key parameters in the design of the different part of the installation [10].

II.3. Solar concentrating technologies

Currently, there are four main commercially available technologies to concentrate the direct solar radiation, where this radiation will be transformed in thermal energy. Two of these solar

concentrating technologies are linear-focusing technologies and the other two are point-focusing technologies [11].

II.3.1. Line focusses solar concentrators

Line focusses solar concentrators have reflectors that concentrate solar radiation onto a linear receiver. The two dominant concentrator technologies are parabolic troughs and linear Fresnel. A linear Fresnel concentrator approximates a parabolic trough by having independent reflectors rather than a more continuous reflector surface. While there may be some loss of optical efficiency from having independent reflectors, there may be other advantages that contribute to the overall collector efficiency or cost effectiveness.

II.3.1.1. Parabolic trough

A conventional parabolic trough solar concentrator comprises a parabolic reflector and a receiver tube see figure. The troughs collectors are laid out in parallel rows as a solar field with spacing between the rows to minimize shading of the reflectors, while allowing sufficient access for maintenance and minimizing the pipework and parasitic pumping energy for the heat transfer fluid. The heat transfer fluid normally enters at one end of the trough and leaves at the other one.

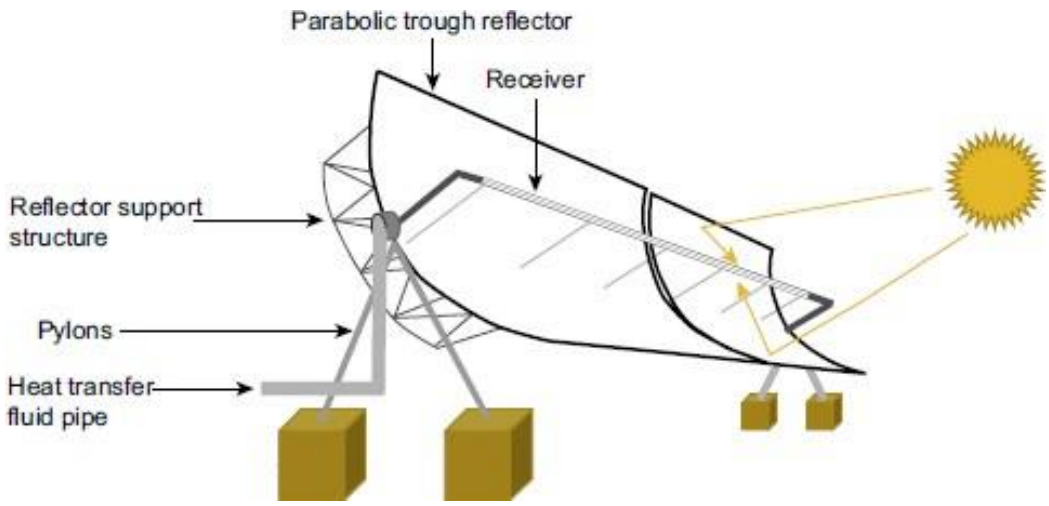

Figure II.1: *parabolic trough collector*

II.3.1.2. Linear Fresnel

A conventional linear Fresnel solar concentrator comprises reflectors that may be flat or slightly parabolic. The individual reflectors are laid out parallel to the ground such that each reflector has a different focal length to its receiver. The spacing of the reflectors is close to minimize the discontinuity in the reflective area or aperture. The width of the reflectors is optimized to allow access to the reflectors for maintenance, while not being too large to complicate the support structure or tracking.

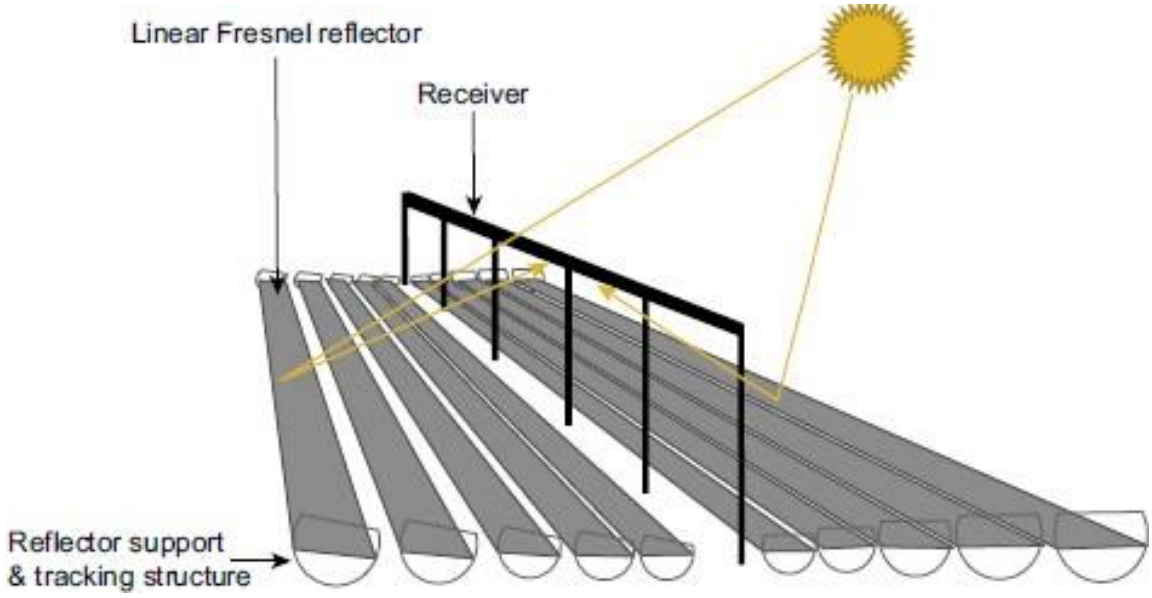

Figure II.2: *Linear Fresnel collectors*

II.3.2. Point-focus solar concentrators

Point-focus systems have reflectors that concentrate solar radiation onto a central receiver that is effectively a point compared to the reflector. The two dominant technologies are parabolic dishes and central receiver systems, known as solar towers. The solar tower has independent reflector facets, known as heliostats, rather than a more continuous reflector surface. While there may be some loss of optical efficiency from having heliostats, there may be other advantages that contribute to the overall collector efficiency or cost effectiveness.

II.3.2.1. Parabolic dish

A conventional parabolic dish collector comprises a dish parabolic reflector. The parabolic reflectors may be continuous or comprise of discrete elements conforming to a parabolic shape. The receiver is fixed to the reflector support structure so that both the dish and receiver track the sun. The size of the receiver needs to be optimized to minimize the shadow it, and its support structure, might create on the reflector. The mass of the receiver needs to be

optimized to minimize the mass that needs to track the sun. The most common consideration is for a parabolic dish to have a Stirling engine placed at the receiver. Alternatively, the receiver might have a heat transfer fluid to drive an independent process or heat engine.

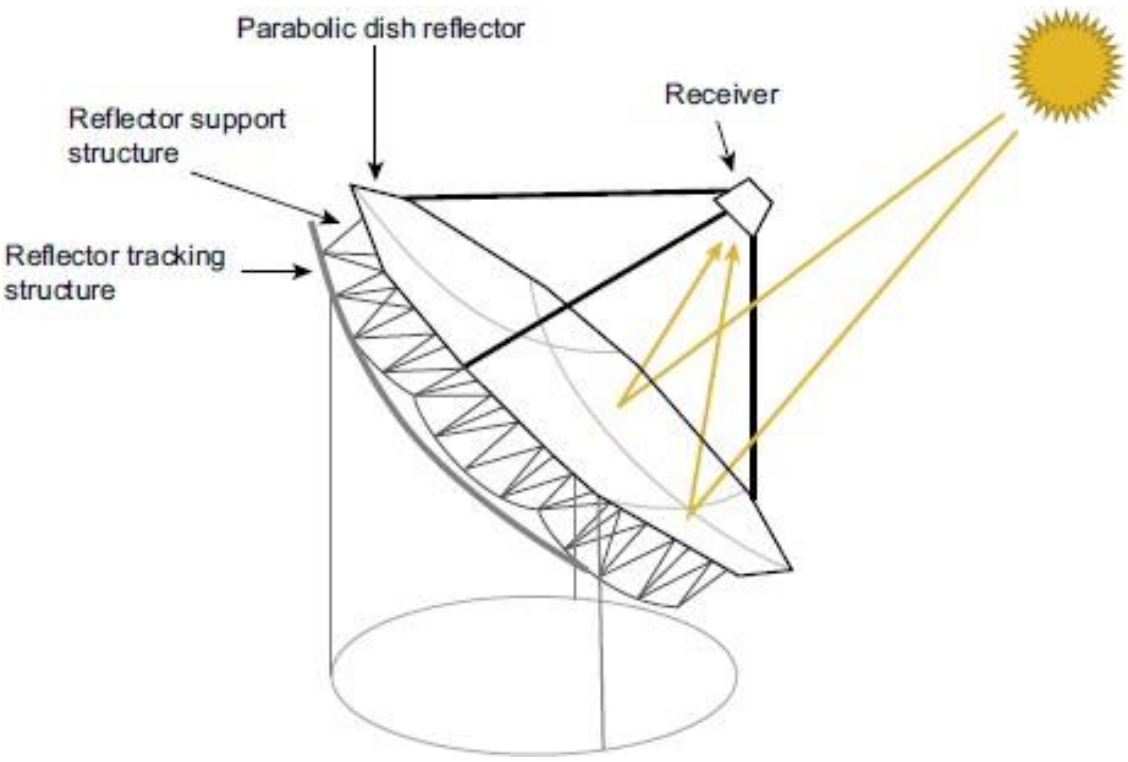

Figure II.3: *Parabolic dish collector*

II.3.2.2. Heliostat field-central receiver

A conventional heliostat field-central receiver solar concentrator comprises heliostat reflectors, which may be flat or slightly parabolic. The heliostat reflectors are placed in a solar field surrounding the tower. The receiver and tower need to be optimized to minimize the shadow they might create on the solar field. The solar field needs to be optimized in terms of the heliostat size, closeness to minimize the discontinuity in the reflective area, or aperture, spacing to minimize collisions, while also allowing sufficient access for maintenance. The

system layout needs to be optimized to minimize the pipework and parasitic pumping energy for the heat transfer fluid.

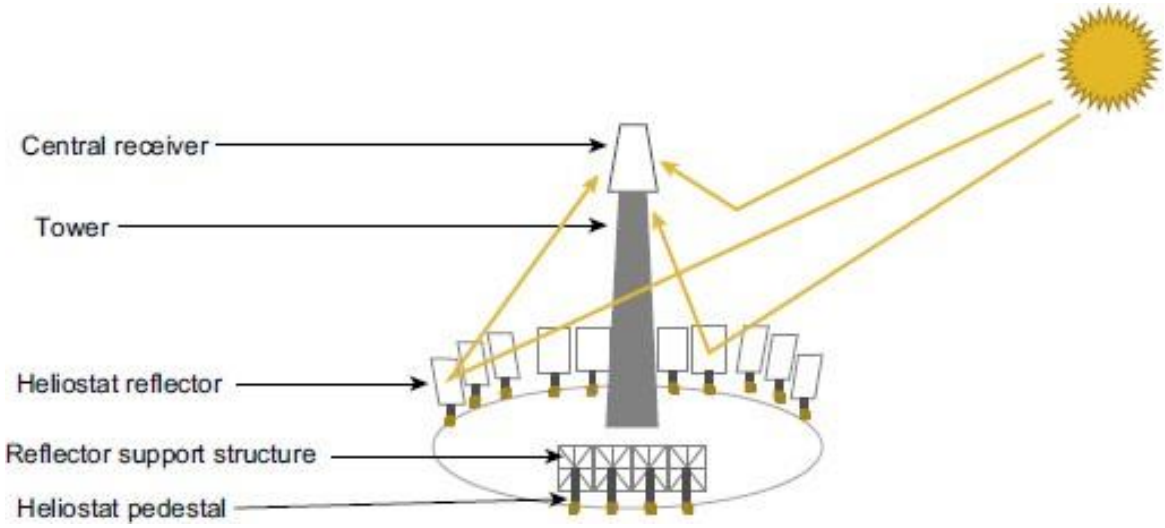

Figure II.4: *Tower solar concentrating*

II.4. Parabolic Trough Solar Collector

Among all the concentrating solar collectors mentioned above, the most common technology is that of the parabolic trough collector [8]. The Parabolic Trough Solar collectors are the type of concentrating solar collector that can track the sun's motion around its own axis. The need to move the collector and follow the position of the sun is taking the advantage of solar radiation in wide range of incidence angle. The orientation of a Parabolic Trough Solar collector may be aligned with the North-South or East-West direction [12]. It consists of two major components, the concentrator and the receiver tube as shown in the figure II.5.

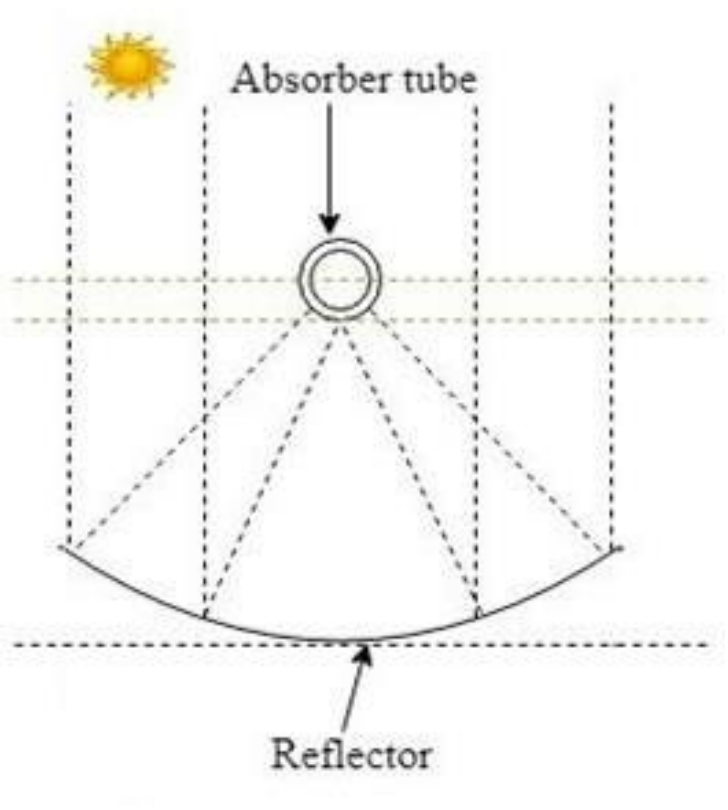

Figure II.5: *PTC technology*

II.4.1. Concentrator

The main role of the concentrator or (the reflector) is to reflect the maximum amount of solar radiation to the receiver. In PTCs, concentrators have the shape of a cylindrical parabola, a structure which has the property to reflect each normal incident solar ray to a line belonging to the parabola itself and called focal line, where the receiver is located.

In order to correctly concentrate the solar radiation on the receiver, it is crucial to obtain a concentrator with good characteristics. This can be achieved by designing an accurate model and by choosing appropriate materials for both the concentrator structure itself and the reflective foil attached to it.

II.4.2. Receiver tube

The receiver tube or (the absorber tube) is the key element in the parabolic trough concentrators a (PTC) where the solar radiation is concentrated and collected. PTC receivers are tubes of various diameters located in the focal line of the concentrator and can be distinguished into two parts: the absorber, i.e., the metallic tube in which the heat transfer fluid (HTF) flows, and the glass cover, an external tube generally made of glass, adopted to reduce convective thermal losses. The absorber tube collects the solar radiation reflected and focused by the concentrator and transfers the absorbed heat to the HTF by conduction and then by convection. Due to their function, receivers should have high thermal conductivity. The latter condition is generally realized by painting the outer surface of the receiver with special black coatings [13].

There are several methods to enhance the heat transfer of a receiver tube; active method, this method involves some external power in put for the enhancement of heat transfer, passive method, this method generally uses surface or geometrical modifications to the flow channel by incorporating inserts or additional devices and compound method Combination of the above two methods [14]. Moreover, many researchers focus on the heat transfer enhancement between the HTF and the absorber tube by different technics [15]. Jie Deng et al. [16] investigated the heat transfer enhancement of a receiver tube by introducing concentric and eccentric rod inserts and using molten salt as HTF.

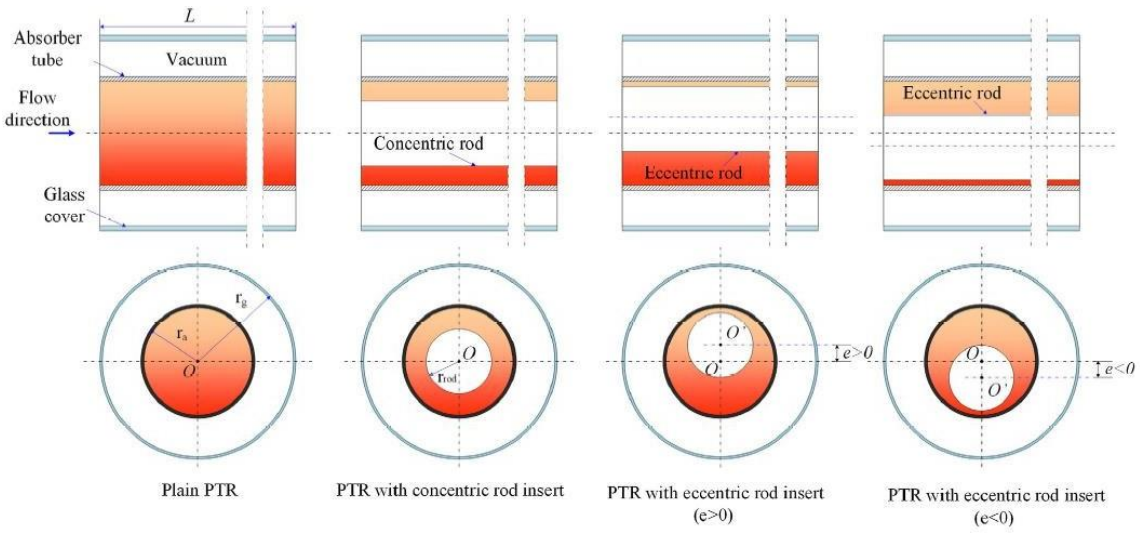

Figure II.6: *Concentric and eccentric rod*

Their results show that the usage of rod insert can enhance the heat transfer performance and reduces of the maximum tube wall temperature and by comparing the concentric and eccentric rod insert, an eccentric rod insert for parabolic trough receiver can further improve the heat transfer performance.

Evangelos Bellos et al. [17] investigated a flow insert with a star shape in parabolic trough collector.

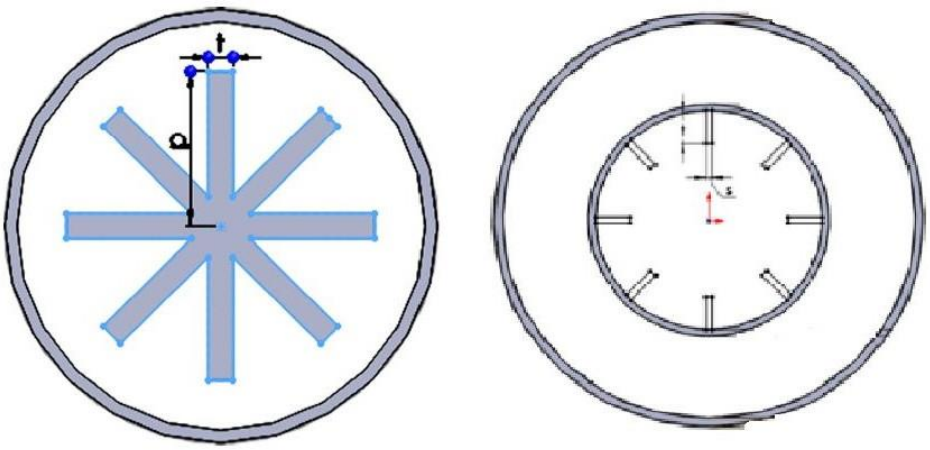

Figure II.7: *Star shape and inserts*

They concluded that the use of this type of inserts enhance the Nusselt number and decrease the thermal losses. In another work they investigated the usage of multiple cylindrical inserts for parabolic trough solar collector [18]. Their results show that the use of a higher number of internal cylindrical inserts leads to higher thermal efficiency enhancement.

Gong Xiangtao et al. [19] analysed the Heat transfer enhancement of a parabolic trough solar receiver with pin-fin arrays inserting.

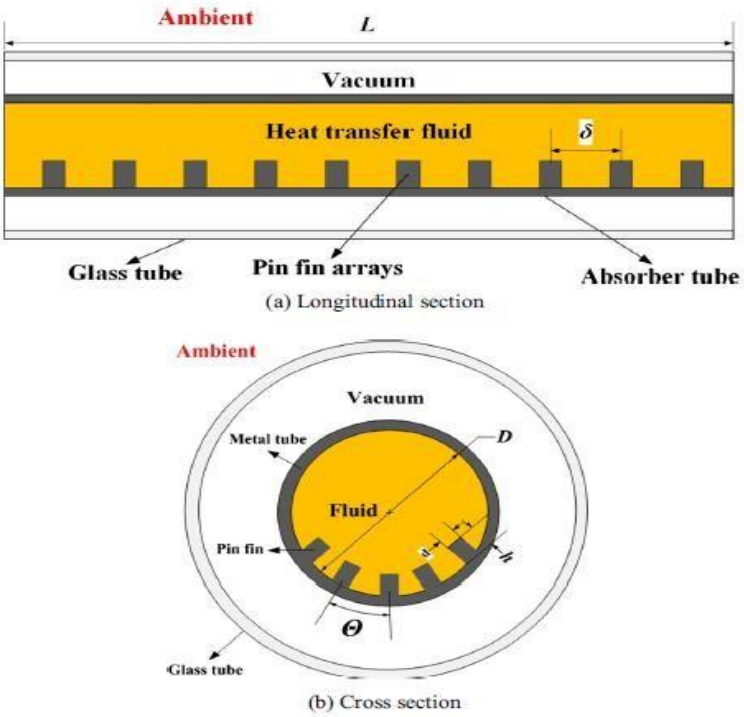

Figure II.8: *Pin Fin Array Inserting*

Their results show that by using of pin-fin arrays inserting the Nusselt number and pressure drop of PFAI-PTR increases with the decrease of d/L values and decrease with the increase of the pin fin array inserting in one section. And the overall heat transfer performance of PFAI-PTR with different d/L values and different number of pin fin arrays inserting in one section is always higher than that of conventional PTR.

Wei Wang et al. [20] studied numerically the heat transfer on fully developed turbulent flow in inward corrugated tubes.

Figure II.9: *Corrugated tube*

They found that the spiral flow exerts a low inhibiting effect on the heat transfer performance and causes a significant reduction in the pressure drop.

Aggrey Mwesigye et al. [21] evaluated the heat transfer and the thermodynamic performance of a parabolic trough receiver with centrally placed perforated plate inserts.

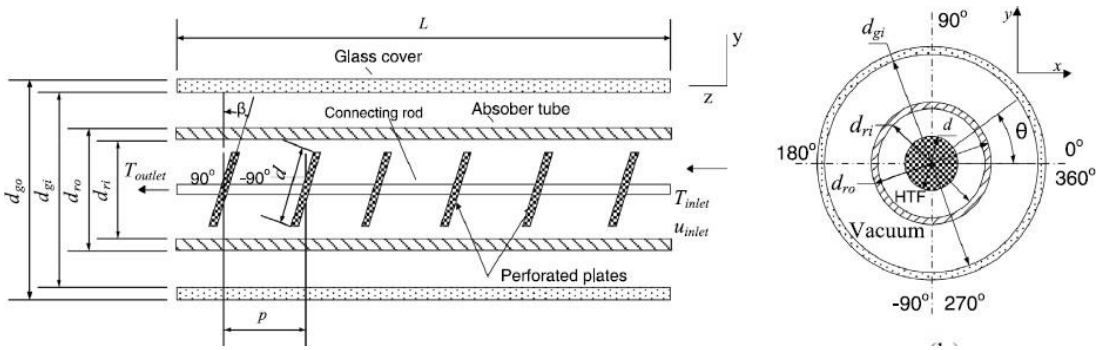

Figure II.10: *Perforated plate inserts*

They reported that the use of inserts improves the thermodynamic performance of the receiver by minimizing the entropy generation rates. They conclude also that the Nusselt number and

friction factor are dependent on the spacing and the size of the insert as well as flow Reynolds number and Significant reductions in absorber tube temperature gradients and peak temperatures were noticed.

Zhen Huang et al. [22] investigated numerically a dimpled parabolic trough receiver tubes under uniform and non-uniform heat flux.

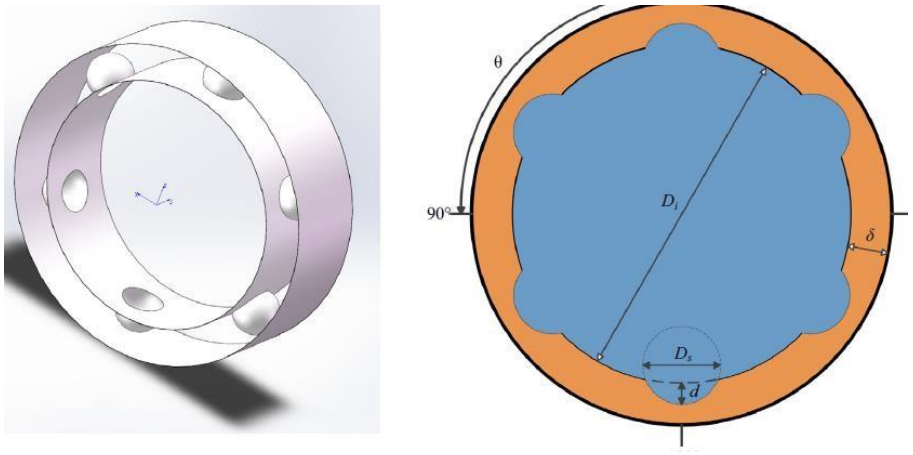

Figure II.11: *Dimpled parabolic trough receiver tubes*

They concluded that the deep dimples are far superior to the shallow dimples. But with the further increase of dimple depth, the comprehensive performance decreases.

Evangelos Bellos et al. [23] analysed the thermal enhancement of solar parabolic trough collectors by using nanofluids and converging-diverging absorber tube.

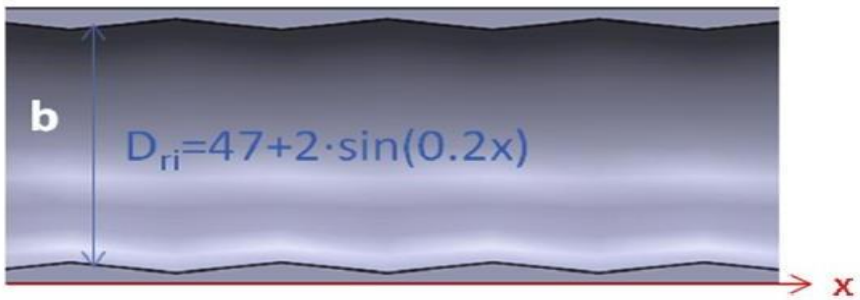

Figure II.12*: Converging-diverging absorber tube*

Their results showed that the use of nanoparticles improves the mean efficiency, and on the other hand, the converging-diverging absorber tube creates more turbulent conditions in the flow with a sacrifice of pressure inside the tube.

Zaid S.Kareem et al. [24] carried out an experimental and numerical study on heat transfer enhancement in three-start spirally corrugated tube.

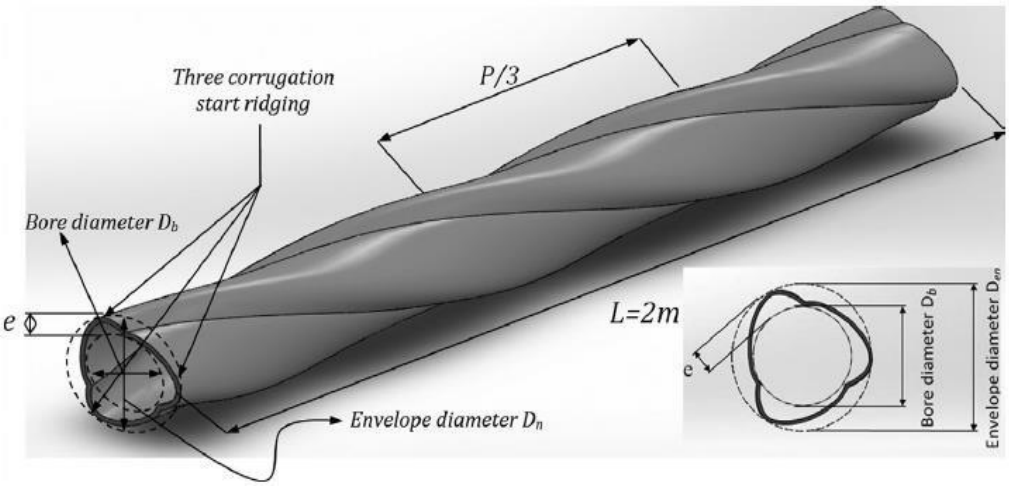

Figure II.13: *Three-start spirally corrugated tube*

They concluded that the tube with spiral corrugations can improve the heat transfer with an increase in the friction factor and the key to obtain a better heat transfer with the lowest pressure drop is the corrugation profile.

P. Wang et al. [25] analysed the heat transfer enhancement in the receiver tube of parabolic trough collector for direct steam generation by inserting metal foams.

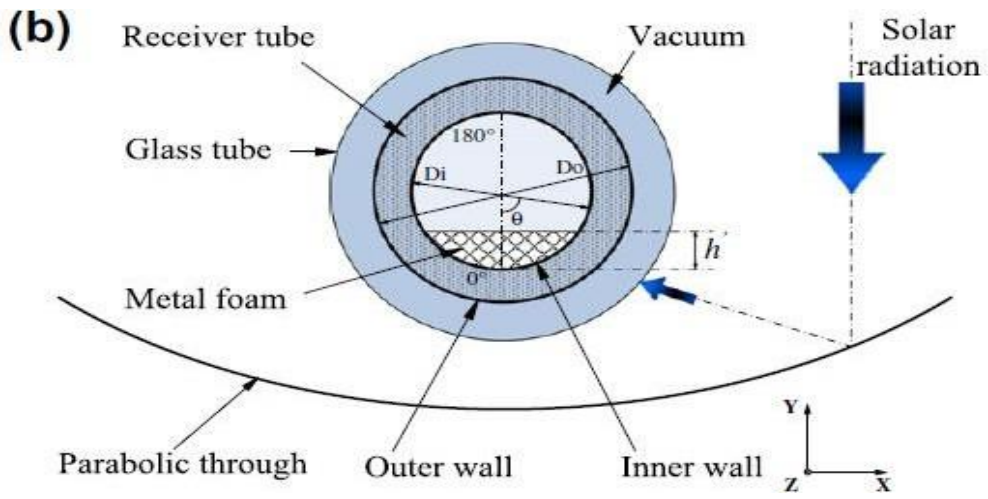

Figure II.14: *Metal foams inserts*

They concluded that the use of the metal foams improves the heat transfer efficiency and decreases the circumferential temperature difference which leads to extend the lifetime of the receiver tube.

Aggrey Mwesigye et al. [26, 27] studied the heat transfer and thermodynamic performance of a parabolic trough receiver with centrally placed perforated plate inserts and receiver with wall-detached twisted tape inserts.

They concluded that the Nusselt number and friction factor are dependent on the spacing and size of the insert and also a significant reduction in absorber tube temperature gradients. A considerable reduction in the entropy generation rates was obtained with the use of inserts at low Reynolds numbers.

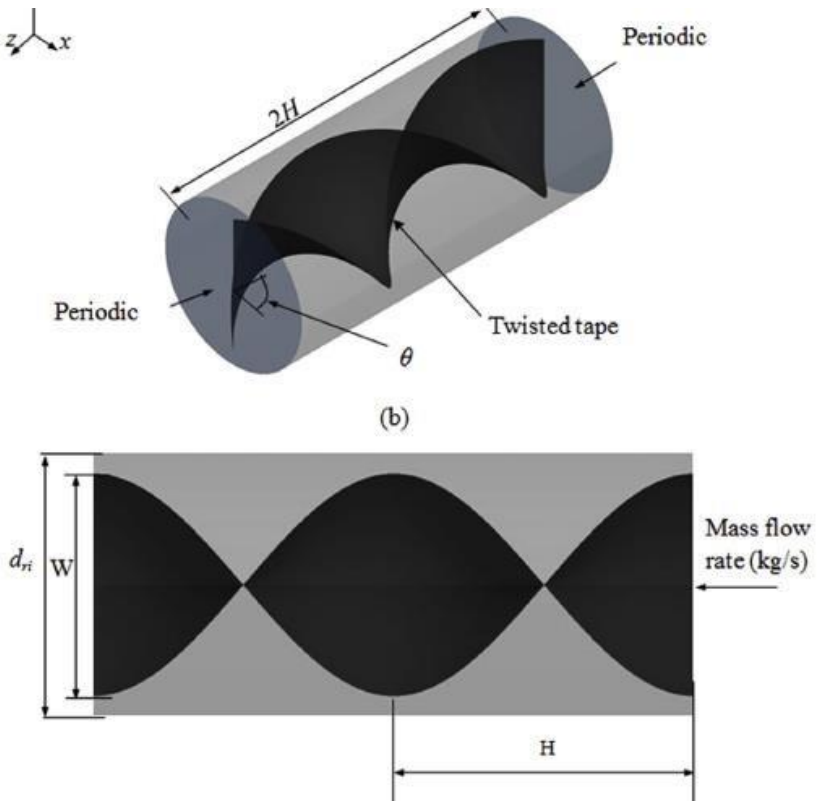

Figure II.15: *Wall-detached twisted tape inserts*

They concluded also that due to improved mixing and a longer helical path followed by the heat transfer fluid, high heat transfer enhancement was achieved with the use of wall detached twisted tape inserts and both the heat transfer performance and fluid friction performance increase as the twist ratio reduces and as the width ratio increases.

Xingwang Song et al. [28] carried out a numerical study of parabolic trough receiver with non-uniform heat flux and helical screw-tape inserts.

Figure II.16: *Helical screw-tape inserts*

They investigated the effect of solar incidence angle on heat flux distribution, the heat loss of a receiver, the maximum temperature on absorber tube outer surface and the maximum circumferential temperature difference. Their results show that within the range of Reynolds number studied, the helical screw-tape inserts of given geometrical parameters greatly reduce the maximum temperature and the temperature difference and as the flow rate increases to 0.6 kg s^{-1}, heat loss in SATPTR is as nearly 3 times as that in HST-PTR. Correspondingly, the pressure loss in SAT-PTR increases by 4 times as flow rate increase, and that increase 23 times in HST-PTR. Similar results are obtained when inlet temperature is 640 K.

Z. Huang et al. [29] studied numerically the heat transfer enhancement in a receiver tube of parabolic trough solar collector with dimples, protrusions, and helical fins.

Figure II.17: *Dimples, protrusions and helical fins*

The demonstrated that the dimples with deeper depth, narrower pitch and more numbers in the circumferential direction is benefit for improving the performance of heat transfer enhancement while the dimple arrangements have no obvious influence.

Z.D. Cheng et al. [30] They presented a numerical study of heat transfer enhancement by unilateral longitudinal vortex generators inside parabolic trough solar receivers.

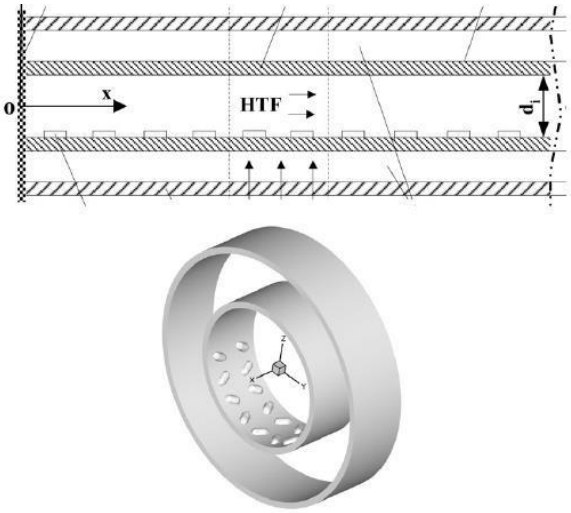

Figure II.18: *Unilateral longitudinal vortex generators insert*

They showed that the enhanced parabolic trough receiver has better comprehensive heat transfer performance than that of the smooth one at the equal given pumping power. With the increase of the Reynolds number, both the average wall temperature and the thermal loss decrease, and the average wall temperature and the thermal loss increase with the increasing HTF inlet temperature.

In the other hand the biggest problem that can be encountered in the Parabolic Trough Collector is the tube wear, and this is due to the non-uniformity of the temperature distribution over the circumferential angle of the tube. The non-uniformity of the solar flux distribution over the outer surface of the absorber tube leads to a large difference on the temperature distribution which can cause damages and failures. Nowadays the researchers and engineers in the field search to decrease the circumferential temperature gradient to avoid failures and increase the lifetime of the absorber tube. Moreover, many researchers try to modify the geometry of the receiver tube or by adding another reflector (cavity).

Yogender Pal Chandra et al. [31] Analysed numerically the optimization and convective thermal losses of improved solar parabolic trough collector receiver system. They noticed that a maximum of 20% reduction in overall heat transfer when reformed receiver was used under the defined experimental conditions and boundary conditions. A remarkable uniformity and homogeneous angular temperature distribution in the absorber tube are noticed.

Wang Fuqiang et al. [32] analysed numerically the effects of glass cover on heat flux distribution on the tube receiver of a parabolic trough collector. And a glass cover with elliptic–circular cross section was proposed.

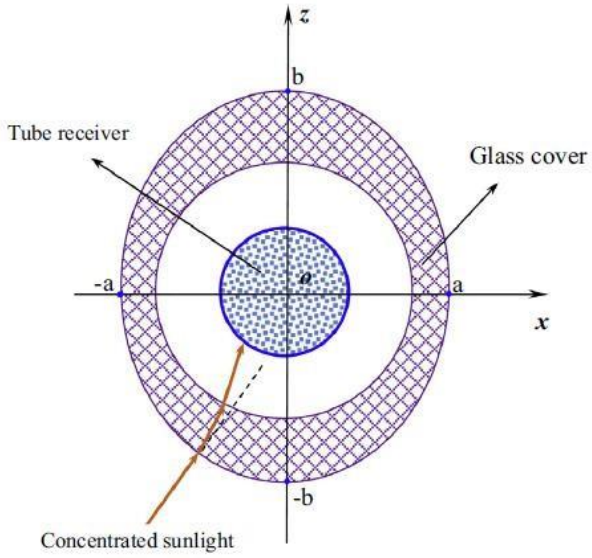

Figure II.18: *Glass cover with elliptic–circular cross section*

The conventional glass covers with different thickness have little impact on the heat flux distribution. In order to minimize heat flux distribution gradient on the tube receiver surface, which in turn it can reduce the thermal stress of the tube receiver. The glass cover with elliptic–circular cross section can effectively decrease the heat flux gradient and peak magnitude.

Fei Cao et al. [33] proposed a design of elliptical cavity tube receivers in the parabolic trough solar collector.

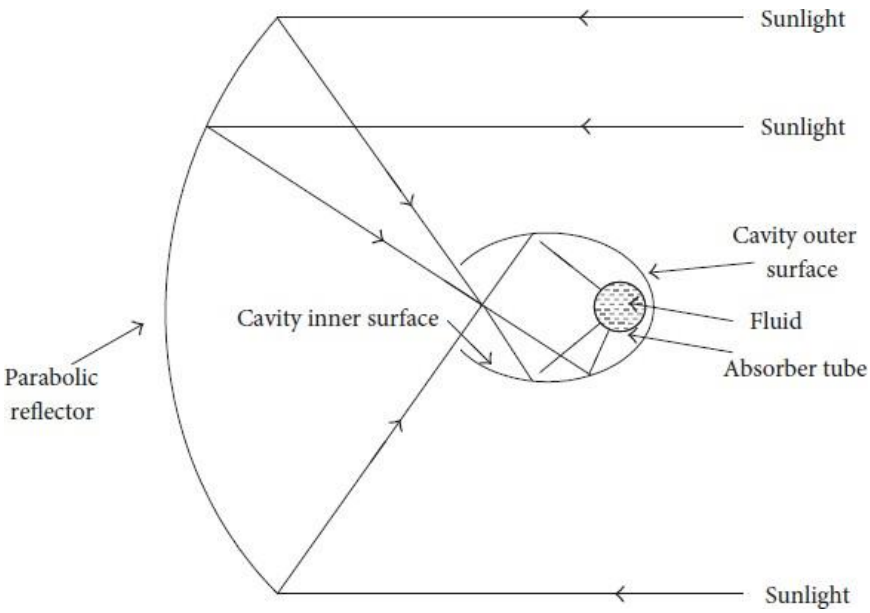

Figure II.19: *Elliptical cavity tube receivers*

They concluded that the light distribution on the tube receiver is asymmetrical. On increasing the tracking error angle, more lights are sheltered by the cavity outer surface and less lights reach the below section of the tube receivers.

Wang Kun et al. [34] proposed a design method and numerical study for a new type of parabolic trough solar collector with uniform solar flux distribution.

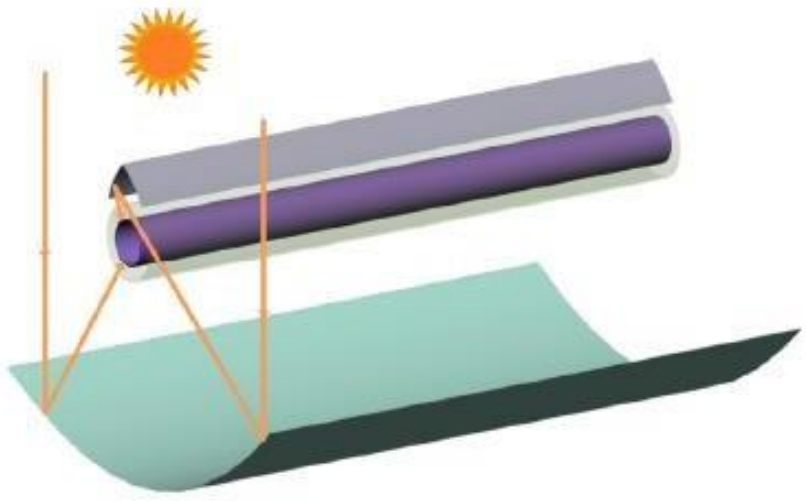

Figure II.20: *Homogenized reflector*

They found that the solar flux distribution can be homogenized by moving the absorber tube away from the focal line of the parabolic trough concentrator toward the concentrator and adding a homogenized reflector. However, the absorber tube is heated uniformly at the expense of slightly increased optical loss. Although the collector efficiency tends to decrease slightly, the maximum temperature and the circumferential temperature difference of the absorber tube wall can be reduced significantly and thus the reliability of the PTSC may be improved.

Yassine Demagh et al. [35] proposed a design method of an S-curved parabolic trough collector absorber with a three-dimensional heat flux density distribution.

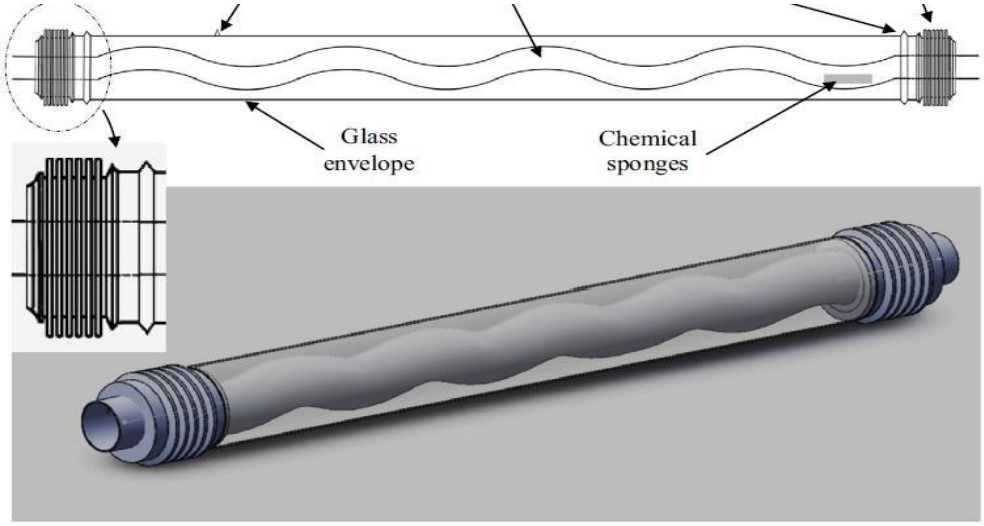

Figure II.21: *S-curved receiver tube*

They found that the highest values of the heat flux density decrease, what reduces the heat flux circumferential gradient and leads to a reduced temperature gradient on almost the entire absorber outer surface. The design should achieve other indirect benefits, as the reduction of the absorber pipe deflection in consequence of a better flux distribution around the pipe.

Hongbo Liang et al. [36] presented a Monte Carlo method and finite volume method coupled optical simulation method for cavity parabolic trough solar collector's receiver.

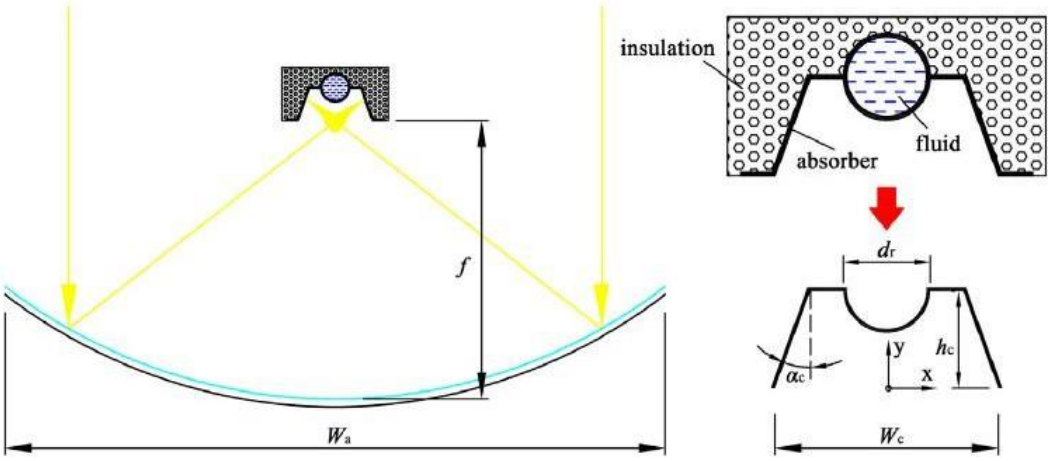

Figure II.22: *Cavity parabolic trough solar collector's receiver*

Roman Bader et al. [37] they examined a new design of an air-based receiver for solar trough concentrators that features a tubular absorber contained in an insulated cavity, with a rectangular aperture closed by a quartz window. They showed that the main heat losses were caused by incoming solar radiation being spilled and reflected at the receiver aperture. With decreasing mass flow rates and, consequently, increasing receiver temperatures, convection losses at the cavity outer surface and radiation losses became predominant. They conclude also that the higher receiver's absorption efficiency is achievable by optimizing the receiver geometry, improving the cavity insulation.

X. Xiao et al. [38] analysed experimentally and numerically the heat transfer of a V-cavity absorber for linear parabolic trough solar collector.

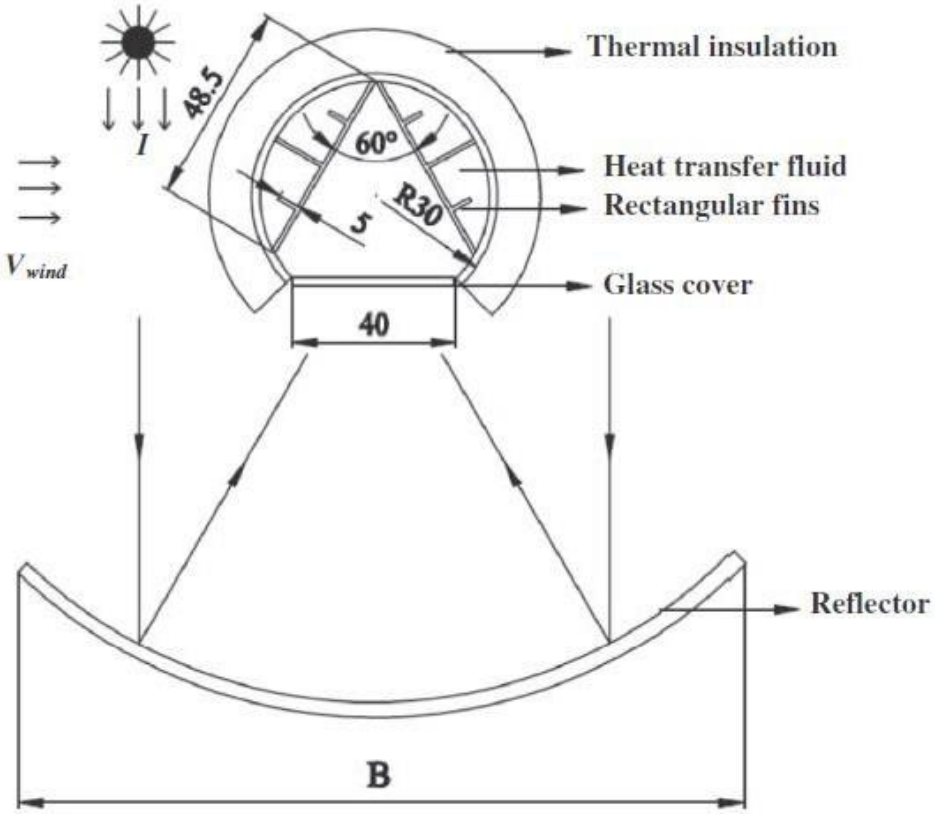

Figure II.23: *V-cavity absorber*

They found that the calculated results of MCRT method show that the sunlight can be reflected repeatedly by the triangle shape and nearly no sunlight escapes, so the V-cavity absorber has a high optical efficiency. The realistic heat flux distribution of the heating surface of the V-cavity absorber is heterogeneous. They found also that the absorber with the rectangular fins has a better heat transfer performance, which confirms that the rectangular fins in the absorber can enhance the heat transfer and decrease the heat loss.

II.5. Conclusion

It can be concluded that there are several technics to enhance the heat transfer between the receiver tube and the heat transfer fluid and increase the efficiency of the absorber tube with different manners. There are two manners to improve the heat transfer of the absorber tube, active and passive technics. In the chapter bellow we will present two passive technics and active technic.

Chapter III

III.1. Introduction

The biggest problem that can be encountered in the Parabolic Trough Collector is the tube wear, with the aim to enhance the heat transfer between the absorber tube and the heat transfer fluid and decrease the circumferential temperature gradient of the receiver, as it is explicated in the chapter before there are several technics to enhance and protect the receiver tube from failures. In this chapter we will explain the mechanism of the heat transfer inside and outside the receiver tube and the governing equation to analyse the heat transfer, and present three technics to enhance the heat transfer and increase the lifetime of the absorber tube.

III.2. Physical model

The parabolic trough collector is designed to capture the direct solar irradiance over a large parabolic shaped surface and concentrate it onto its focal line in which a black metal tube is located (fig III.1). It must accurately track the sun's motion to maintain the parabola axis parallel to the incident rays of the sun. The absorber tube is the key element of this device which contains a heat transfer fluid. It must have high radiation absorption and low thermal losses. To reach that performance, its absorption must be high in the visible light range and its emissivity must be low in the infrared range. In order to reach low convective heat losses, it is covered by another tube made from glass. The annular space between the two tubes is maintained evacuated, so that the convective and conductive heat losses are reduced further [39, 40]. The geometrical parameters of the tube studied are illustrated in table III.1.

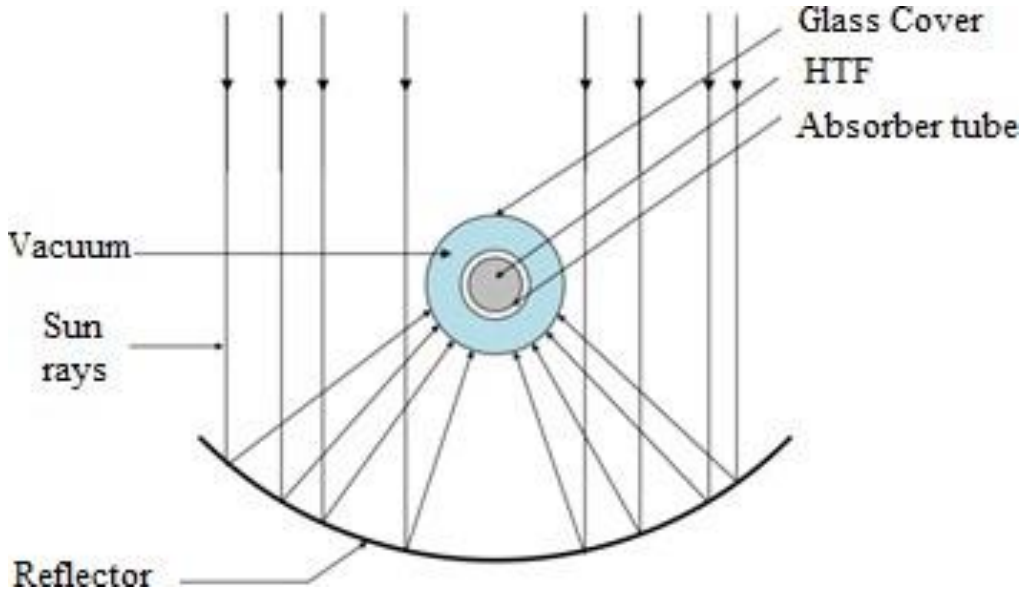

Figure III.1: *Schematic diagram of PTC*

Table III.1: The geometrical parameters of the receiver [40].

Focal length	1.71 m
Aperture width	5.77 m
Absorber inner radius	3.2 cm
Absorber outer radius	3.5 cm
Material of the glass cover	Borosilicate glass
Transmittance of the glass pipe	96%
Cover inner radius	5.95 cm
Cover outer radius	6.25 cm
Coating absorbance	95%

The heat transfer phenomena [41] inside and outside the absorber tube are shown in the figure III.2.

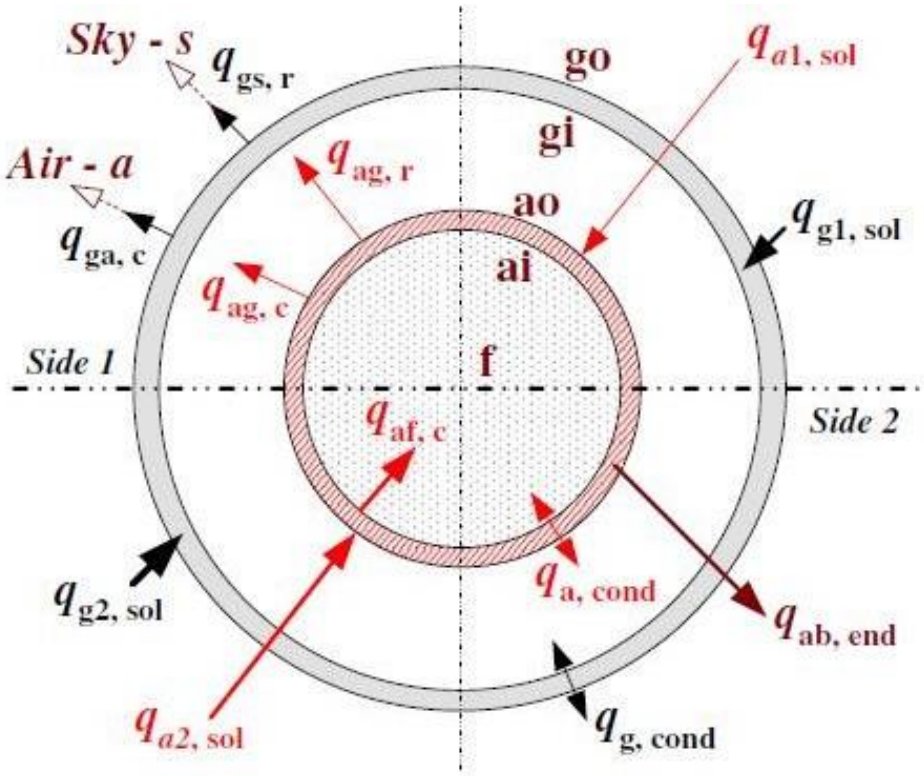

Figure III.2: *Heat transfer phenomena within the absorber tube*

The figure III.2 shows the receiver of a Parabolic Trough Collector. It can be seen that there are two concentric tubes. The absorber tube is a metallic tube covered by a selective coat generally black colour and has a high absorbance characteristic. The glass cover is a transparent tube to allow transmittance of the rays and maintain a greenhouse phenomenon. The space between the two concentric tubes is maintained under vacuum [42] to eliminate heat losses by convection.

III.3. Mathematical model and boundary conditions

A three-dimensional numerical simulation is employed to analyse the impact of the flow and heat transfer inside the receiver tube. The MCRT method was adopted to predict the heat flux distribution on the outer surface of the absorber tube [40]. The finite Volume Method is used to resolve the governing equations using fluent program and it is a useful tool to simulate the heat transfer and the thermo-hydraulic performance of the systems.

III.3.1. Governing equations

The equations which govern the physical phenomena inside the receiver tube are: continuity, momentum, energy and the standard *k-ε* equations [43] with the introduction of the following hypothesis:

- Steady state
- The fluid is incompressible and Newtonian.
- Developed Turbulent flow.
- The thermo-physical properties of the fluid are taken constant

The equations can be written as follow:

III.3.1.1. Continuity equation

$$\frac{\partial}{\partial x_j}(\rho u_i) = 0 \qquad \text{III.1}$$

III.3.1.2. Momentum equation

$$\frac{\partial}{\partial x_i}(\rho u_i u_j) = -\frac{\partial P}{\partial x_i} + \frac{\partial}{\partial x_j}\left[(\mu + \mu_t)\left(\frac{\partial u_i}{\partial x_j} + \frac{\partial u_j}{\partial x_i}\right) - \frac{2}{3}(\mu + \mu_t)\frac{\partial u_i}{\partial x_i}\delta_{ij}\right] + \rho g_i \qquad \text{III.2}$$

III.3.1.3. Energy equation

$$\frac{\partial}{\partial x_i}(\rho u_i T) = \frac{\partial}{\partial x_i}\left[\left(\frac{\mu}{Pr} + \frac{}{\sigma_t}\right)\frac{\partial T}{\partial x_i}\right] \qquad \text{III.3}$$

The standard k-ε model has two model equations, one for k and one for ε [44]:

III.3.1.4. k-equation

$$\frac{\partial}{\partial x_i}(\rho u_i k) = \frac{\partial}{\partial x_i}\left[\left(\mu + \frac{\mu_t}{\sigma_k}\right)\frac{\partial k}{\partial x_i}\right] + G_k - \rho\varepsilon \qquad \text{III.4}$$

III.3.1.5. ε- equation

$$\frac{\partial}{\partial x_i}(\rho u_i \varepsilon) = \frac{\partial}{\partial x_i}\left[\left(\mu + \frac{\mu_t}{\sigma_s}\right)\frac{\partial s}{\partial x_i}\right] + \frac{s}{k}(c_{1s} G_k - c_{2s}\rho\varepsilon) \qquad \text{III.5}$$

Where G_k represent the generation of turbulent kinetic energy

$$\frac{\partial}{\partial x_i}(\rho u_i \varepsilon) = \frac{\partial}{\partial x_i}\left[\left(\mu + \frac{\mu_t}{\sigma_s}\right)\frac{\partial s}{\partial x_i}\right] + \frac{s}{k}(c_{1s} G_k - c_{2s}\rho\varepsilon) \qquad \text{III.6}$$

$$G_k = \mu_t \frac{\partial u_i}{\partial x_i}\left(\frac{\partial u_i}{\partial x_j} + \frac{\partial u_j}{\partial x_i}\right) + \frac{2}{3}\rho k \delta_{ij}\frac{\partial u_i}{\partial x_j} \qquad \text{III.7}$$

In these equations, turbulent viscosity μ_t is defined as:

$$\mu_t = c_\mu \rho \frac{k^2}{s} \qquad \text{III.8}$$

The equations contain five adjustable constants C_μ, σ_k, σ_ε, $c_{1\varepsilon}$ and $c_{2\varepsilon}$. This model employs values for the constants that are arrived at by comprehensive data fitting for a wide range of turbulent flow [45]:

C_μ=0.09, σ_k=1.00 σ_ε=1.30 $c_{1\varepsilon}$=1.44 and $c_{2\varepsilon}$=1.92.

III.3.2. Boundary conditions

- Fluid inlet: $V_x = V_{in}$; $V_y = V_z = 0$; $T_f = T_{in}$
- Fluid outlet: Fully developed condition.
- Wall boundary condition:
- No-slip conditions exist at the inside surface of the absorber tube.
- The outer wall of the absorber tube is subjected to non-uniform heat flux (fig. 3) [40]:

$$Q = LCR * DNI \qquad \text{III.9}$$

Where the DNI is the Direct normal irradiance (DNI=1000 W/m^2)

- The outer wall of the glass cover in this receiver model has a mixed boundary condition to account for both radiation and convection heat transfer losses.

$$Q_{loss} = A_{co}\sigma\varepsilon(T_{gc}^4 - T_{sky}^4) + A_{co}h_v(T_{gc} - T_{amb}) \qquad \text{III.10}$$

The sky temperature is defined as [46]:

$$T_{sky} = 0.00552 \cdot T_{amb}^{1.5} \qquad \text{III.11}$$

Where T_{amb} is ambient temperature (T_{amb}=300 K)

And the convective heat transfer coefficient of the wind is given by [47]:

$$h_w = 4V_w^{0.58} \cdot d_{go}^{-0.48} \qquad \text{III.12}$$

Where V_w is the wind speed, (V_w=2.5 m/s) and d_{go} is the glass cover outer diameter.

The HTF used in this study is the Therminol®VP1. It is a eutectic mixture of 73.5% di-phenyl oxide and 26.5% di-phenyl and as such can be used in existing liquid or vapour systems [48].

All the equations are discretised by the finite volume method. All the equations are solved by the second order scheme, the coupling between the pressure and the velocity is based on the simple algorithm [45].

III.3.3. Monte Carlo Ray Tracing method

The simulation of the Local Concentration Ration (LCR) of the conventional PTC is adopted by SolTrace software developed at the National Renewable Energy Laboratory (NREL) to model concentrating solar power optical systems and analyse their performance and it is based on the Monte Carlo Ray Tracing method (MCRT) [49].

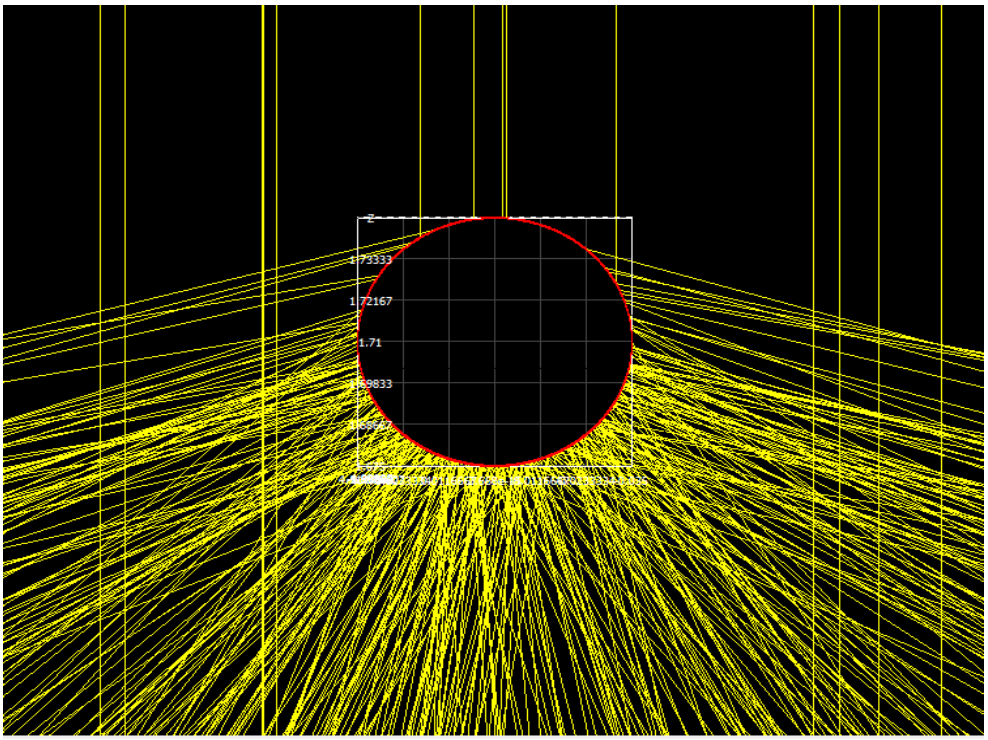

Figure III.3: *Sun's rays reflected by the concentrator on the absorber tube*

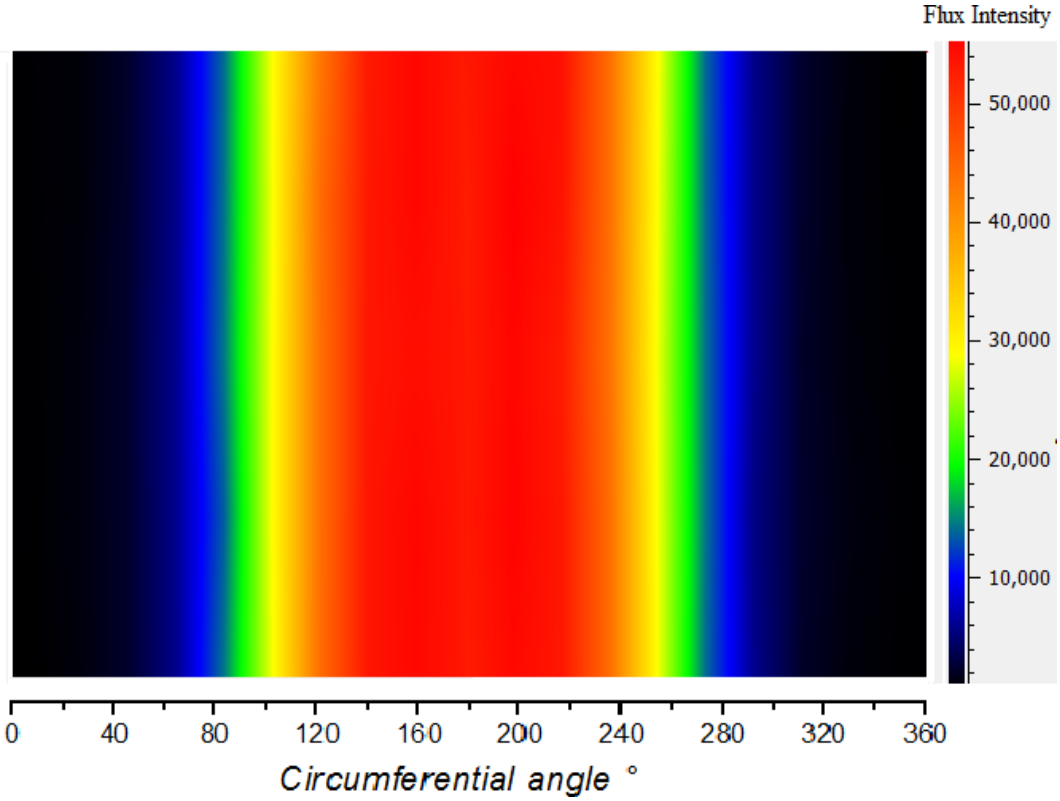

Figure III.4: *Flux density on the absorber tube*

Figure III.5 presents the local concentration ratio distribution over the outer surface of the absorber tube obtained from SolTrace and compared with the Local concentration ratio from ref. [40]. It can be seen that the heat flux distribution is non-uniform over the circumferential surface of the absorber tube.

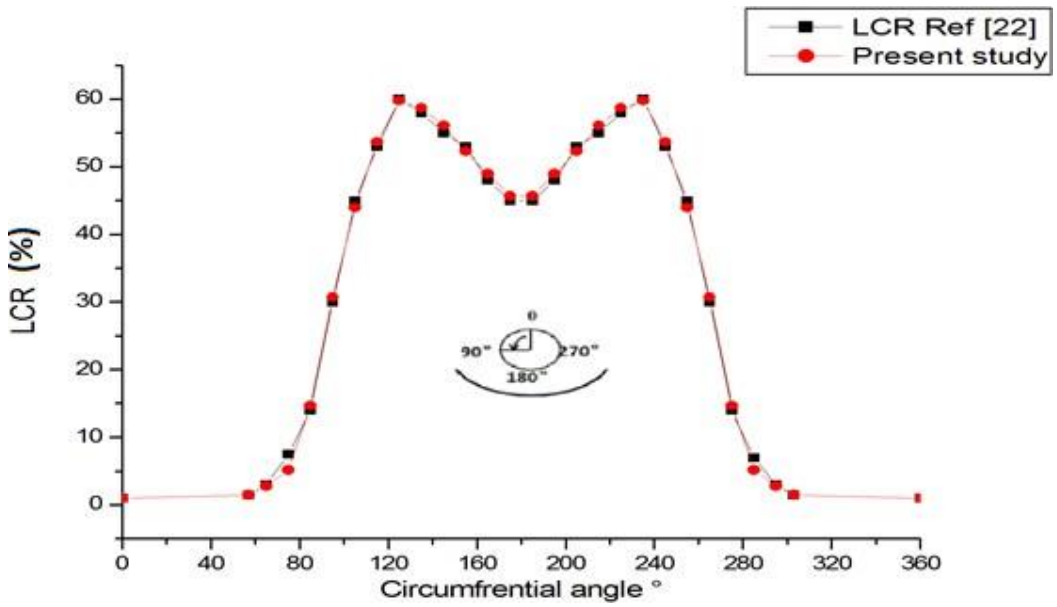

Figure III.5: *Heat transfer phenomena within the absorber tube*

III.4. Model Validation

For the purpose, the numerical results of Nusselt number and the Darcy friction factor in the case of smooth pipe are compared with correlations obtained from literature. The average Nusselt Number is given by:

$$\overline{Nu} = \frac{\bar{h}\, d_{ai}}{\lambda} \qquad \text{III.13}$$

And

$$\bar{h} = \frac{\bar{Q}}{T_{ai} - T_f} \qquad \text{III.14}$$

Where Q is the average heat flux on the absorber tube, T_{ai} is the average temperature of the inner wall of the absorber tube and T_f is the average temperature of the HTF.

The Darcy friction factor for turbulent flow is defined as:

$$f = \frac{2d_{ai}\Delta P}{L\rho u^2} \qquad \text{III.15}$$

Where d_{ai} and L are the inner diameter and the length of the absorber tube respectively.

The Nusselt number given by Gnielinski [50] is defined as:

$$Nu = \frac{\frac{(Re-1000)Pr}{8}}{1+12.7\left(\frac{}{8}\right)^{0.5}\left(Pr^{\frac{2}{3}}-1\right)} \qquad \text{III.16}$$

Where the friction factor f can be determined from an appropriate relation such as the first Petukhov's equation [50, 51] for turbulent flow in smooth tube:

$$f = (0.79\, lnRe - 1.64)^{-2} \qquad \text{III.17}$$

For $0.5 \leq \mathrm{Pr} \leq 2000$ and $3000 \leq \mathrm{Re} \leq 5\cdot10^6$

Another equation presented by Notter [51] to determine the average Nusselt number:

$$Nu = 5 + 0.015\, Re^{0.856}\, Pr^{0.347} \qquad \text{III.18}$$

Blasius [50] proposed a correlation to calculate the Darcy friction factor for fully developed flow inside circular smooth tubes:

$$f = 0.184\, Re^{-0.2} \qquad \text{III.19}$$

For: $\mathrm{Re} > 2\cdot10^4$

It is necessary to evaluate the thermo-hydraulic performance of the enhanced tube. The Performance Evaluation Criteria is a suitable tool to estimate the performance of the enhanced tube compared to the plain tube, and it is defined as [27, 53]:

$$PEC = \frac{(Nu/Nu_0)}{(f/f_0)} \qquad \text{III.20}$$

Another factor is presented to evaluate the improvement of the tube; the Nusselt number enhancement factor (δ_{Nu}) and it is expressed as [54]:

$$\delta_{Nu} = \frac{Nu_{Ins} - Nu_0}{Nu_0} \times 100 \qquad \text{III.21}$$

Chapter IV

IV.1. Introduction

It can be seen from the conventional parabolic trough collector that the bottom periphery of the absorber tube is subjected to concentrated solar radiation and the top one is subjected to non-concentrated solar radiation. In order to improve the heat transfer between the HTF and the absorber tube and minimize the circumferential temperature difference and the heat losses to the ambient different technics are investigated in this chapter using numerical simulation based on finite volume method.

IV2 Numerical simulation

IV.2.1. Model validation

As discussed in the previous chapter the numerical results in the case of smooth pipe are compared with the results obtained from the experimental correlations.

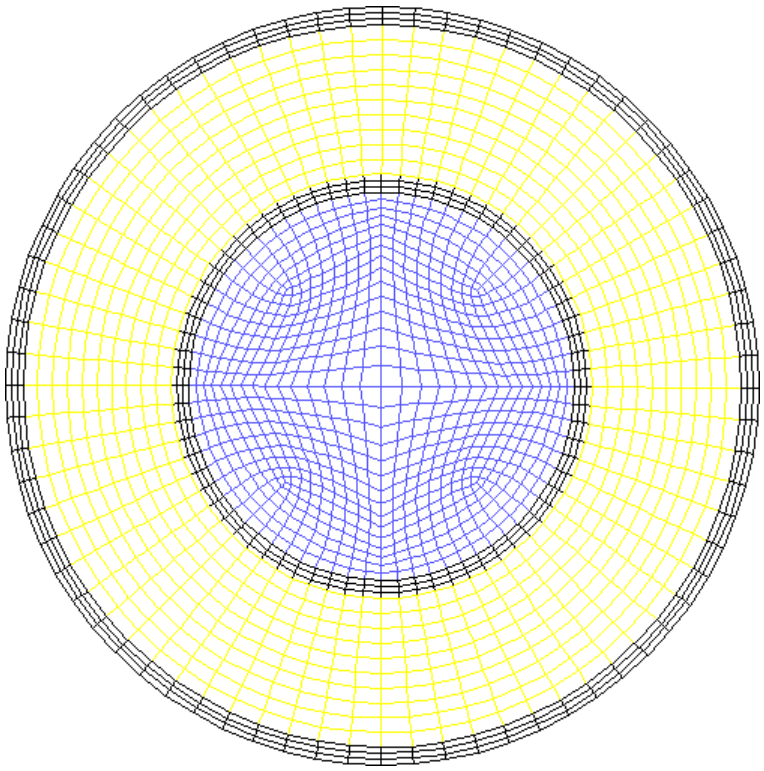

Figure IV.1: *The mesh used in the numerical model*

Figure VI.1 shows the mesh used in the numerical model for the smooth tube in order to validate the numerical results with those obtained from the literature.

Figure VI.2 and Figure VI.3 show the comparison between the numerical results and the results calculated by correlations obtained from literature of the Nusselt number *Nu* and the Darcy friction factor *f* respectively.

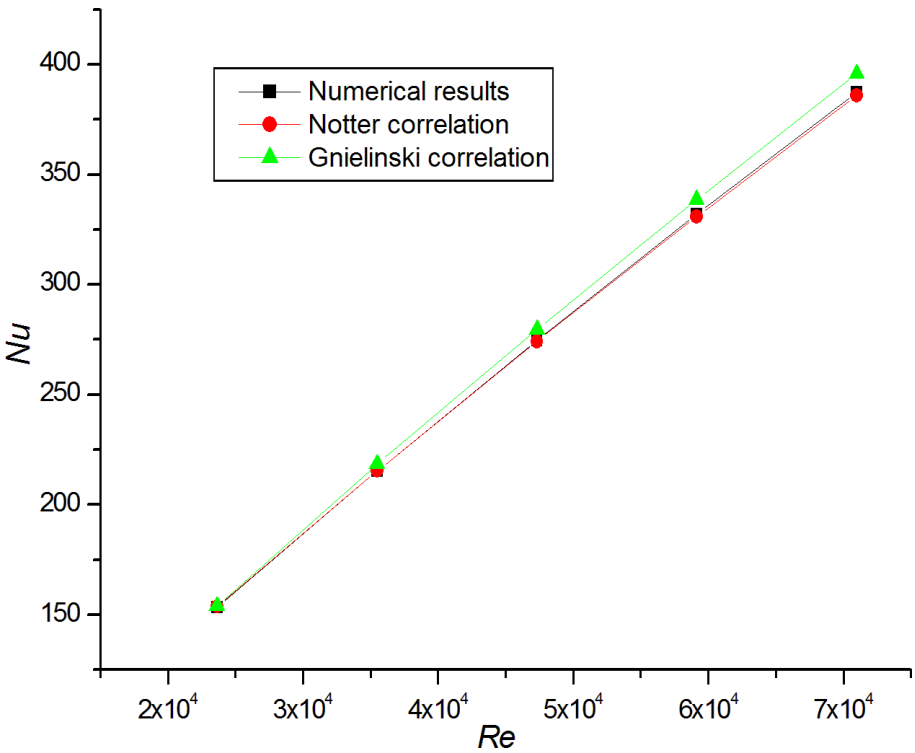

Figure IV.2: *Variation of Nu number with Re number for plain tube*

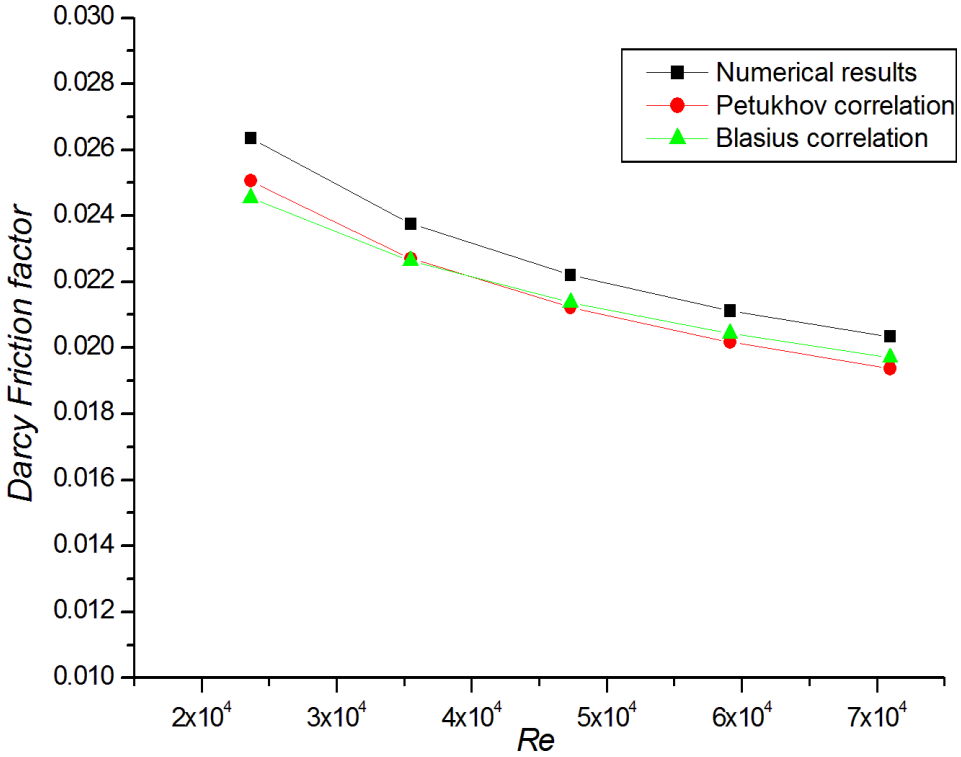

Figure IV.3: *Variation of f number with Re number for plain tube*

From these figures, it can be seen that the curves agree well with each other with a maximum deviation of 2.14% for *Nu* number. The maximum errors for the friction factor are 4.91% and 6.87% for correlations of Petukhov and Blasius respectively. As the error between the numerical model and the literature's correlations is minor, the numerical model can be considered for further investigation.

IV.3. Technics to enhance the Heat transfer

IV.3.1. Focal inserts

With the aim to enhance the heat transfer between the absorber tube and the heat transfer fluid and decrease the circumferential temperature gradient of the receiver, transversal inserts are planted on the bottom part of the absorber tube inner surface (Figure IV.4).

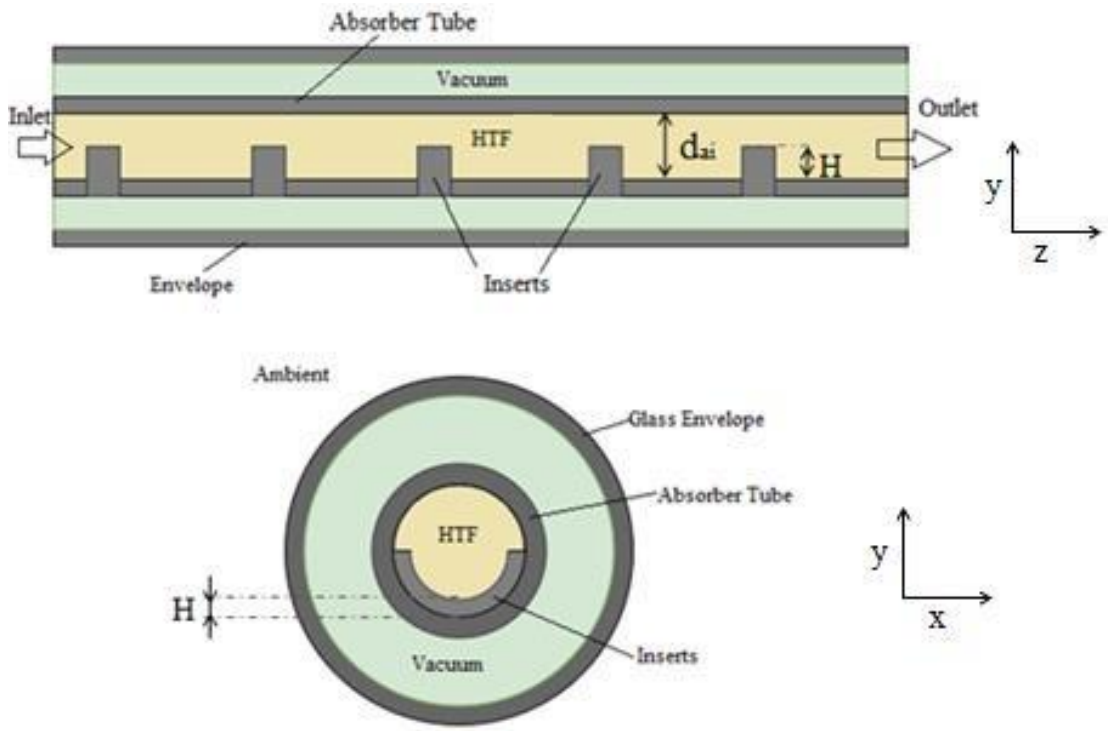

Figure IV.4: S*chematic diagram of the enhanced tube with transversal focal inserts*

The geometrical parameters as the height and the width of the inserts are investigated as shown in figure IV.4 and figure IV.5. For this purpose, we introduced four different heights of inserts H/d_{ai}=0.078, 0.109, 0.14 and 0.171.

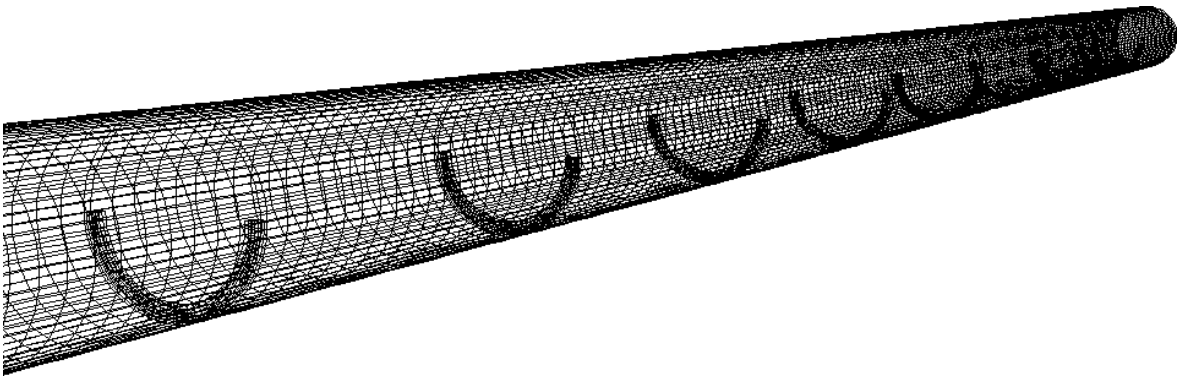

Figure IV.5: *The mesh used in the numerical model of focal inserts*

Figure IV.6 shows the effect of the inserts on the *Nu* number as a function of *Re* number. From this figure it can be seen that the *Nu* number increase with increase of the *Re* number for both smooth and enhanced tubes and for the same *Re* number, the *Nu* number increase with increase of height of the inserts and the *Nu* number is always higher than that of the Smooth tube.

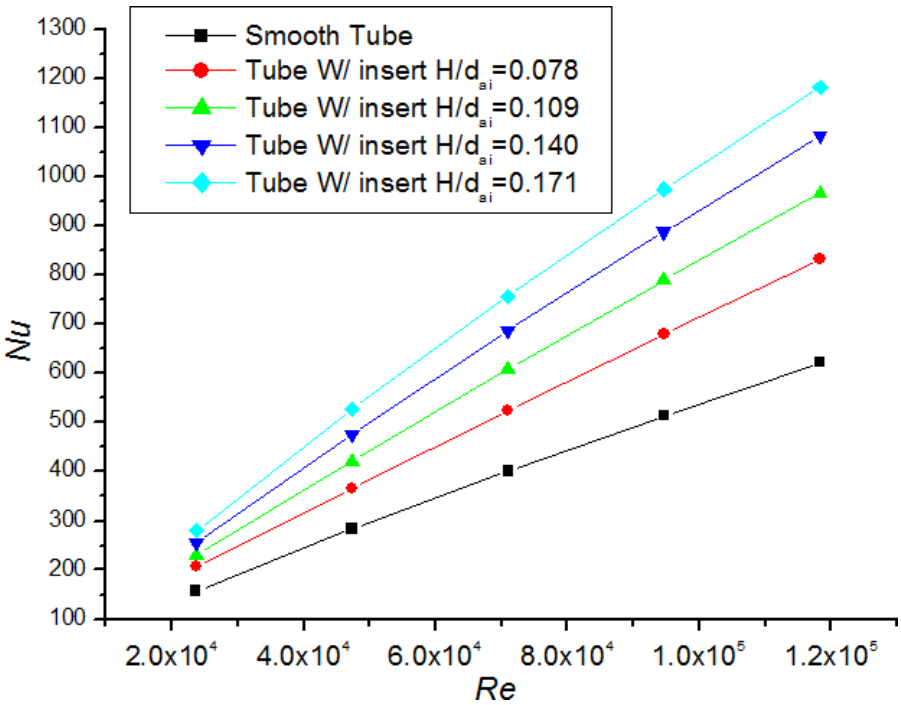

Figure IV.6: *Variation of Nu as a function of Re for different H/d_{ai} values*

Figure IV.7 shows the variation of the fiction factor coefficient as a function of Reynolds number for different height of inserts. It can be seen that the f decreases with the increase of Re number and it increase with the increase of the insert's height at the same *Re* number because of the increase of pressure drop due to turbulence energy dissipation and vortices.

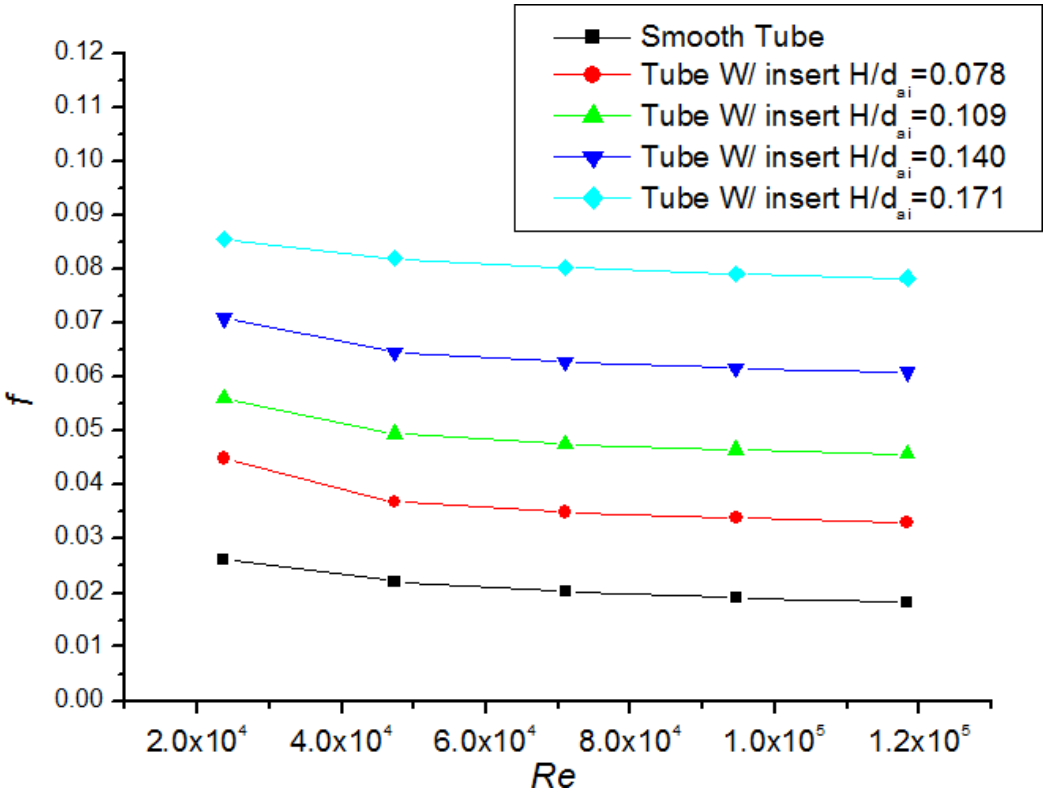

Figure IV.7: *Variation of f as a function of Re for different H/d$_{ai}$ values*

To evaluate the thermo-hydraulic performance of the enhanced tube comparing to the smooth tube we introduced the Performance Evaluation Criteria (PEC) as it is defined in the previous chapter. From Figure IV.8 it can be seen that the PEC of the enhanced tubes is always higher than 1 and the tube with higher inserts (H/d$_{ai}$=0.171) gives the best result for Re number less than $1.2 \cdot 10^5$.

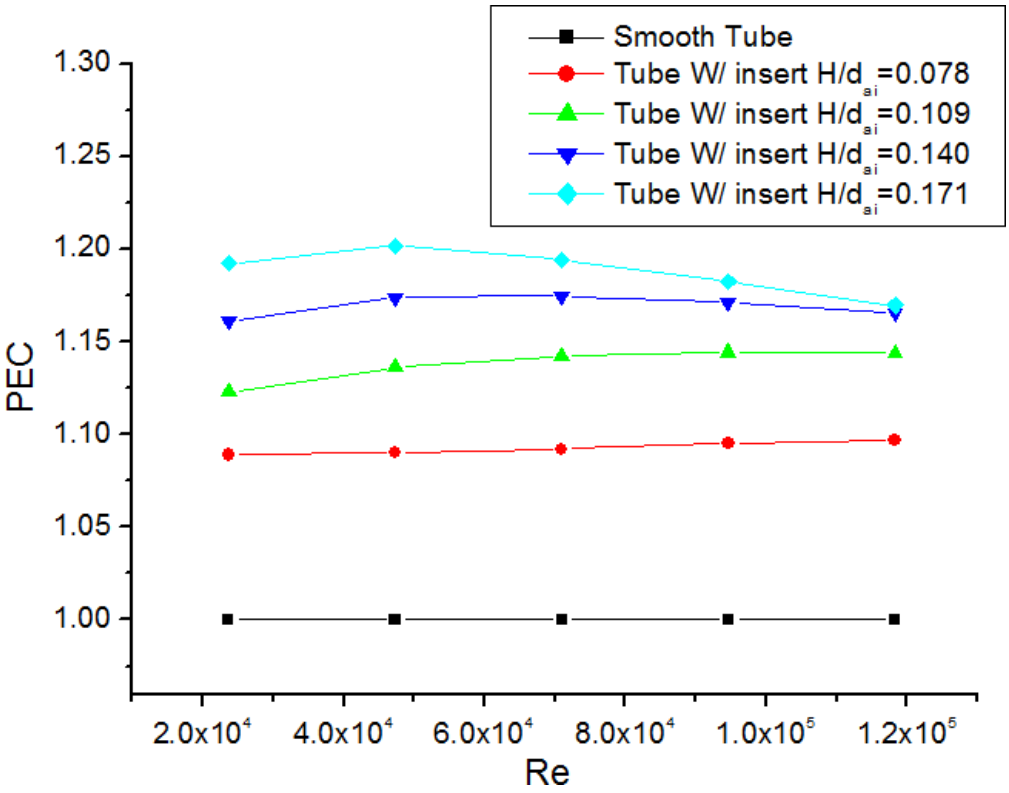

Figure IV.8 *Variation of PEC as a function of Re for different H/dai values*

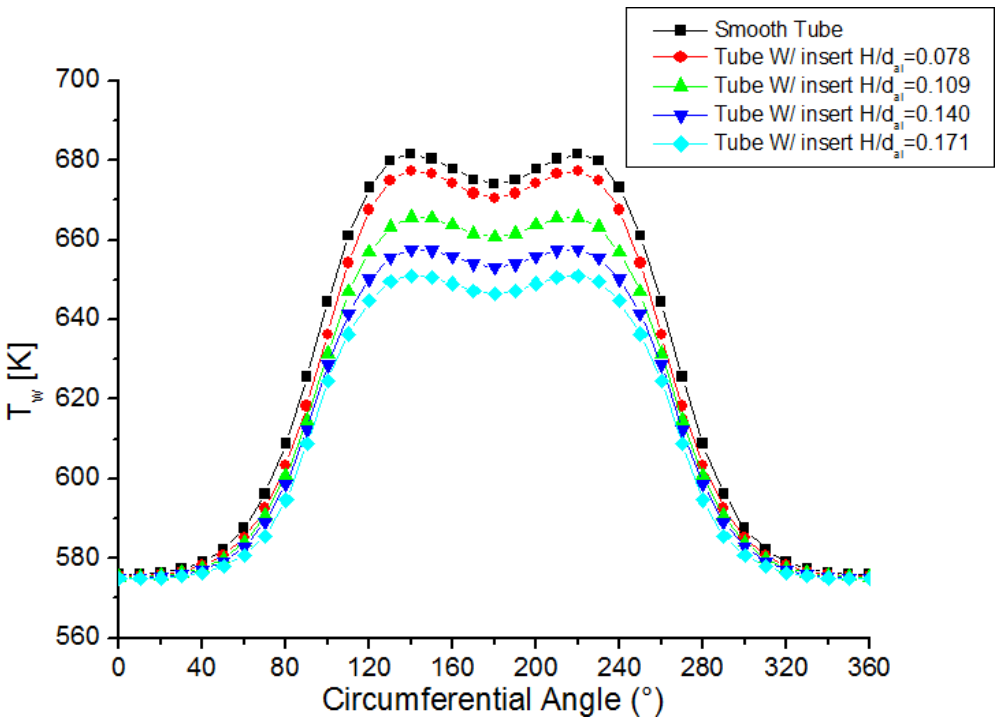

Figure IV.9 *Temperature distribution variation with the change of circumferential angle for different H/d$_{ai}$ value*

As seen in Figure IV.9 the circumferential temperature distribution on the wall of the absorber tube is non-uniform because of the non-uniformity of the heat flux. We can also observe that the maximum temperature is on the bottom periphery of the absorber tube. It can be seen that the temperature difference decreases with the increase of the H/d_{ai} value of the inserts. This will be helpful to diminish the heat losses and augment the lifetime of the absorber tube.

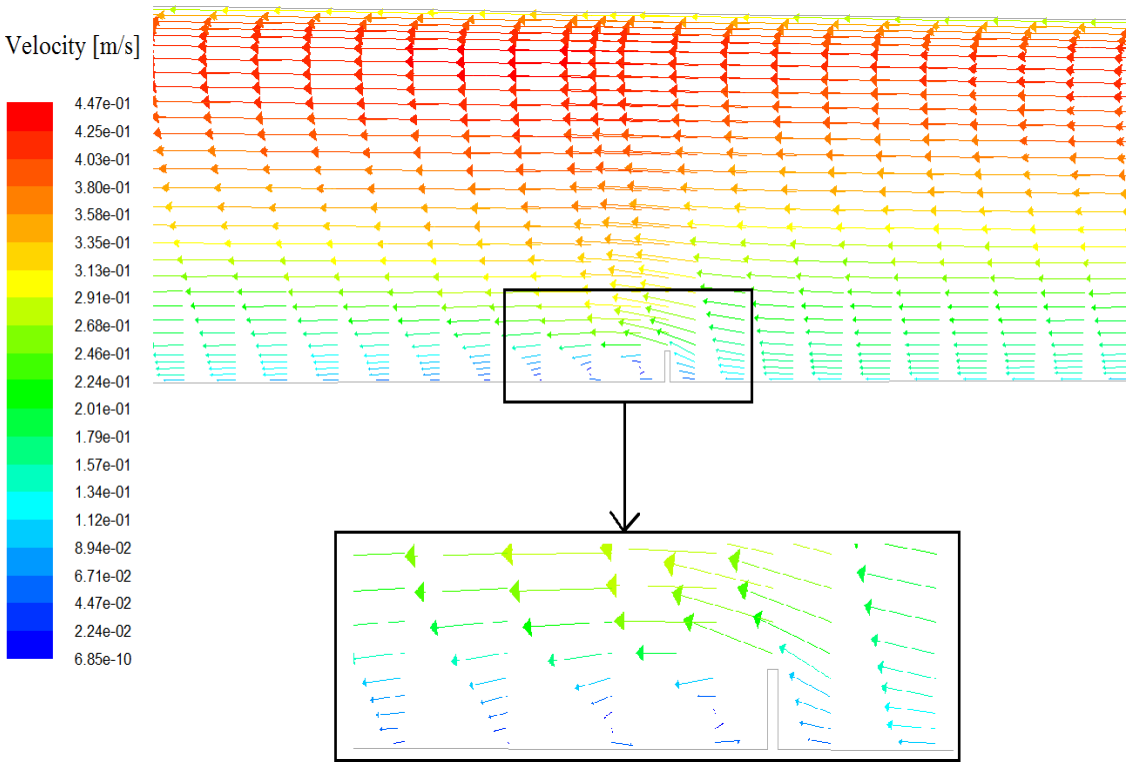

Figure IV.10: *Velocity vector distribution of an enhanced tube ($H/d_{ai}=0.171$ and $Re=71\cdot10^3$).*

Figure IV.10 shows the contours of velocity vector distribution for smooth tube and the enhanced tube with inserts ($H/d_{ai}=0.171$) for $Re=71\cdot10^3$. As seen in this figure the inserts increase the velocity field compared to smooth tube and generates vortexes on the bottom part of the absorber tube, and this augments the turbulence inside the tube and homogenize the temperature distribution of the HTF inside the tube.

Figure IV.11 illustrates the contours of the temperature distribution of the HTF at the outlet for both smooth tube (Fig 11.a) and enhanced tubes (Fig.11.b-e) with different height (H/d_{ai}) and Re=71·10^3. As seen from this figure the temperature of the HTF homogenized comparing to the smooth tube.

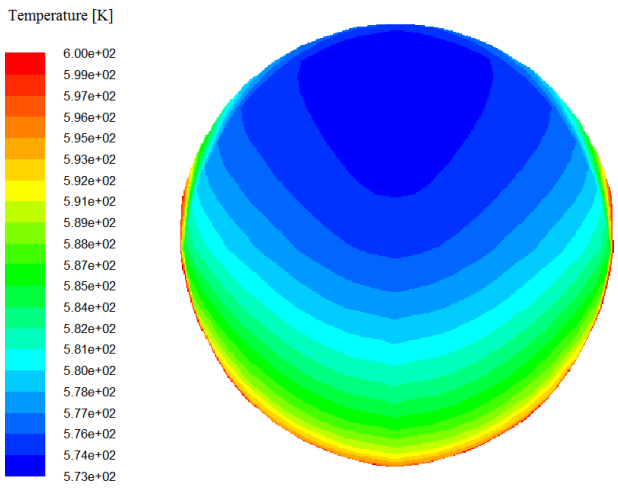

a) Smooth Tube

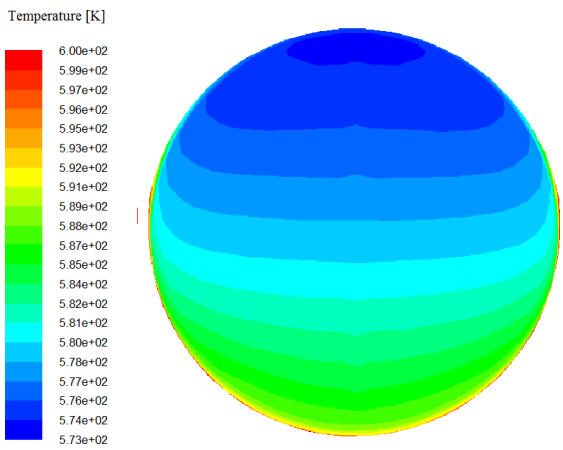

b) H/d_{ai}=0.078

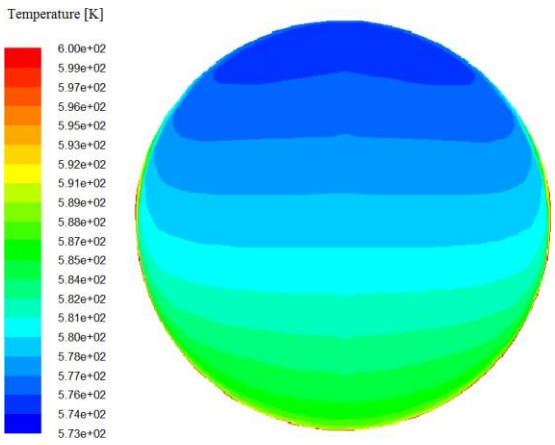

c) H/d_{ai} =0.109

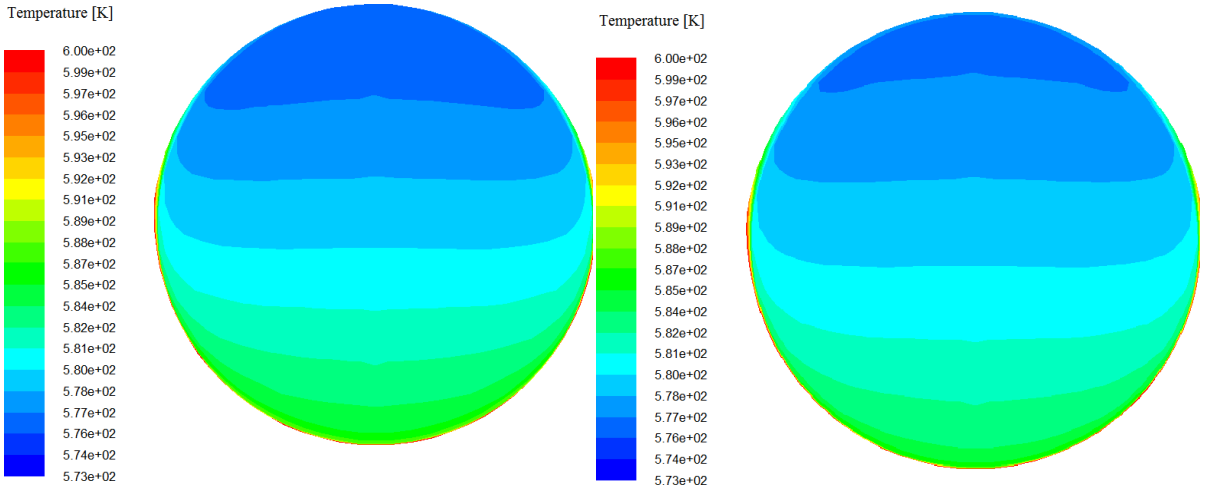

c) H/d_{ai} =0.140 d) H/d_{ai} =0.171

Figure IV.11: *Contours of the temperature distribution of the HTF at the outlet.*

IV. 3.2. Cylindrical inserts

A new type of cylindrical inserts was introduced into the absorber tube and investigated under non-uniform heat flux condition (Figure IV.12).

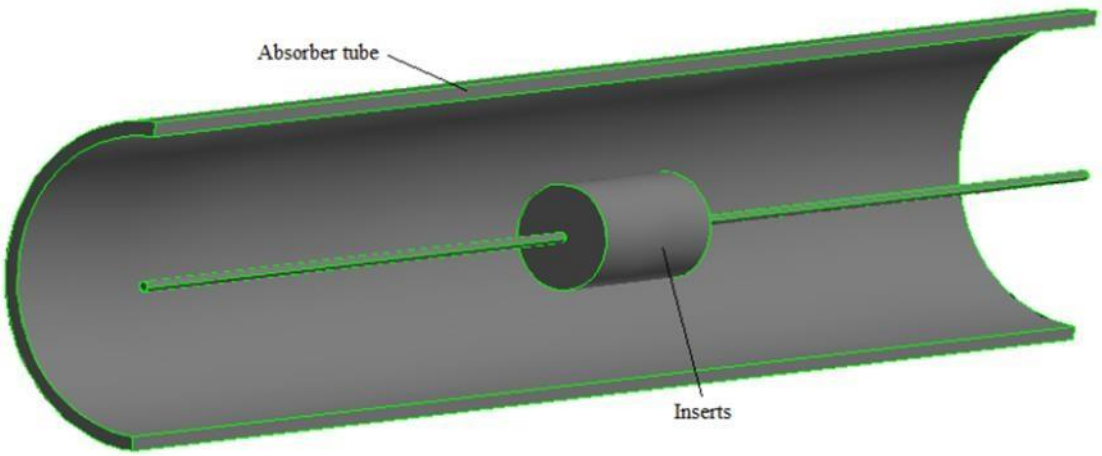

a) : Cylindrical inserts

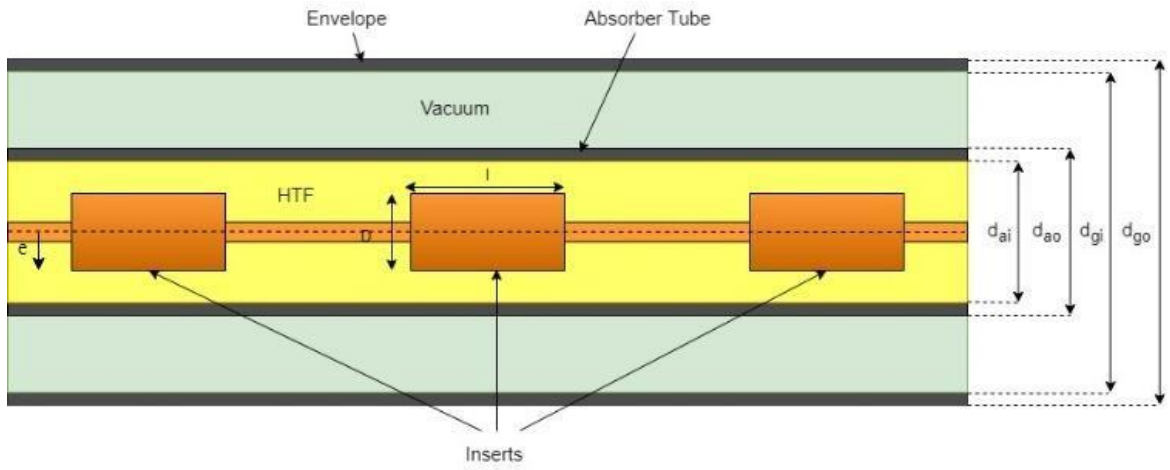

b) : Cylindrical inserts

Figure IV.12: *Schematic diagram of the enhanced tube cylindrical inserts*

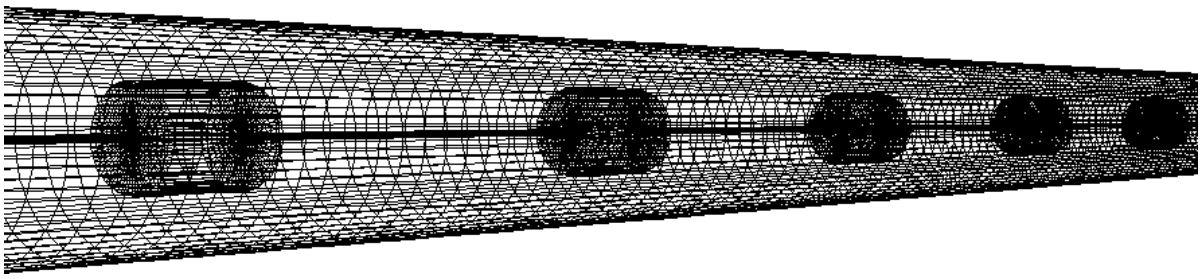

Figure IV.13: *The mesh used in the numerical model of the tube with cylindrical inserts*

The geometrical parameters of the cylindrical inserts like the diameter and the length of inserts and the position of the inserts are investigated for different *Re* number as follow.

IV. 3.2.1. Effect of (D/d_{ai}) on the heat transfer performance

In this section the effect of the dimensionless diameter (D/d_{ai}) is investigated.

Fig. IV.14 shows the *Nu* number as a function of *Re* number for different diameters ratio

(D/d_{ai}). It can be seen from this figure that the Nu number increases with the increase of Re number for both plain and tube formed by cylindrical inserts and increase also with the increase of *D*. It is noticed that the Nu of the enhanced tube is always higher than that of the plain tube. Each insert considered as a vortex generator to increase turbulence inside the tube.

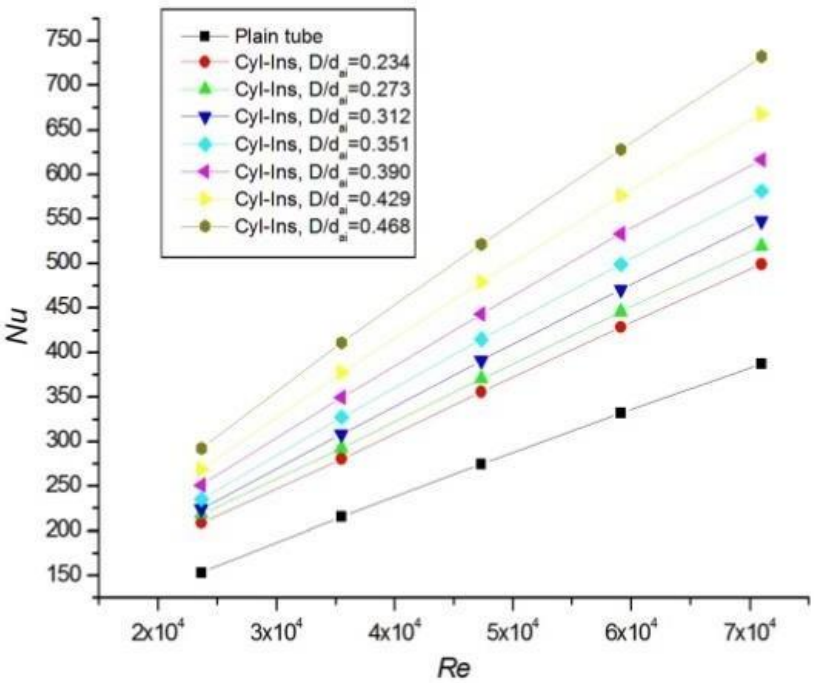

Figure IV.14: *Variation of Nu as a function of Re for different D/d_{ai} values*

The Nusselt number enhancement factor (δ_{Nu}) is expressed as [54]:

$$\delta_{Nu} = \frac{Nu_{Cyl-Ins} - Nu_0}{Nu_0} \times 100 \qquad \text{IV.1}$$

It can be seen from Figure IV.15 that this factor reaches a value of 91 % of improvement for the *D/dai*=0.468 and at lower *Re* number.

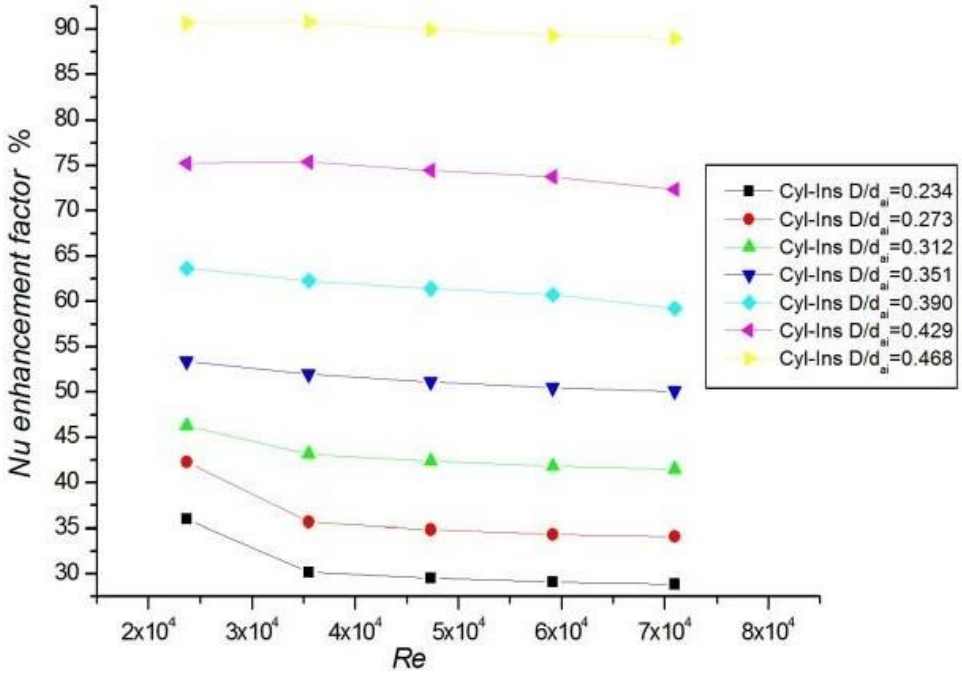

Figure IV.15: *Variation of Nu number enhancement factor as a function of Re*

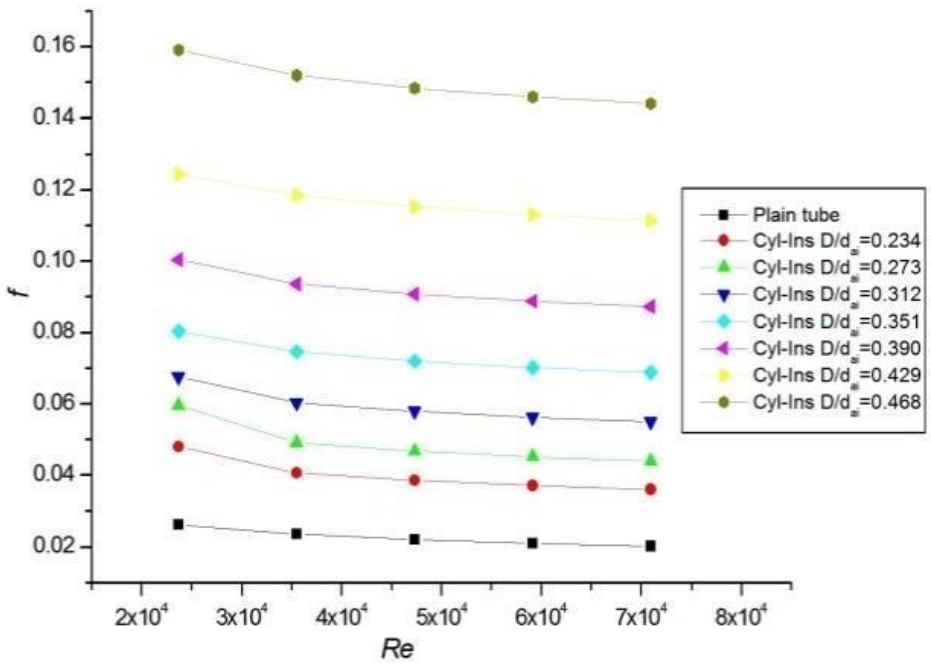

Figure IV.16: *Variation of f as a function of Re for different D/d_{ai} values*

Figure IV.16 presents the Darcy friction factor as a function of Re number for different diameters ratio (D/d_{ai}). The *f* decreases with the increase of *Re* number for all the tube and at the same re number, the *f* increases with the increase of *D*, this is due to the increase of pressure drop when inserts are introduced Figure IV.17.

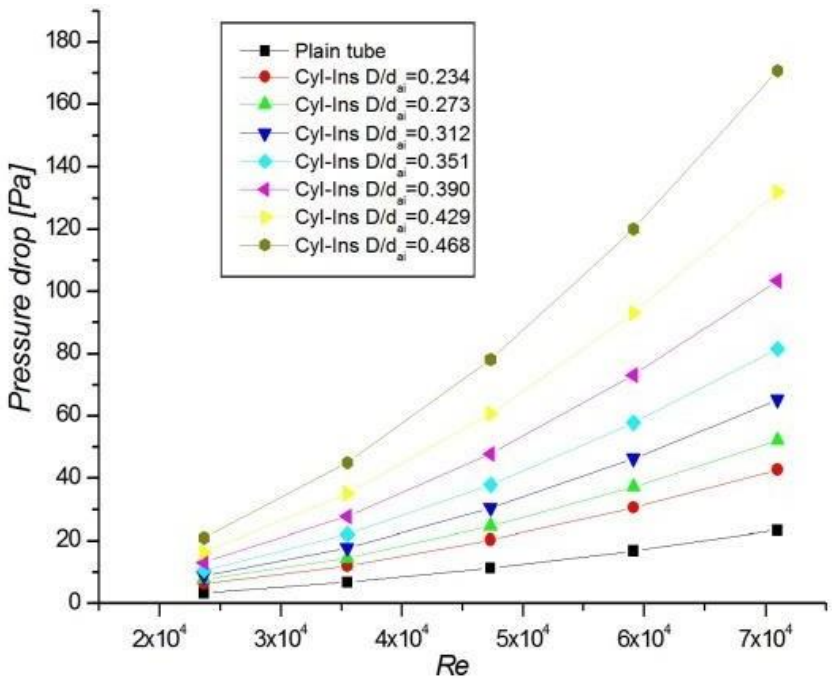

Figure IV.17: Variation of ΔP as a function of *Re* for different D/d_{ai} values

Based on the above analyses, it can be concluded that the introduction of the cylindrical inserts increases the heat transfer between the inner wall of the absorber tube and the HTF, while the pressure drop in the absorber tube of receiver also increases with the using of Inserts. It is necessary to evaluate the thermo-hydraulic performance of the enhanced tube.

Figure IV.18 presents the variation of the *PEC* as a function of *Re* number for different values of diameters (D/d_{ai}). It can be seen that the *PEC* decreases with the increase of *RE* number. It is noticed also that the *PEC* of the smaller inserts gives a better performance compared to the other configurations. It can be seen that the PEC of inserts D/d_{ai}=0.234, 0.273, 0.312 and

0.351 always higher than 1. The other configurations that D/d_{ai} is superior to 0.390 are slightly mingled and gives a *PEC* lower than 1 for the highest *Re* number because of the pressure drop as mentioned above, although they give a better *Nu* number.

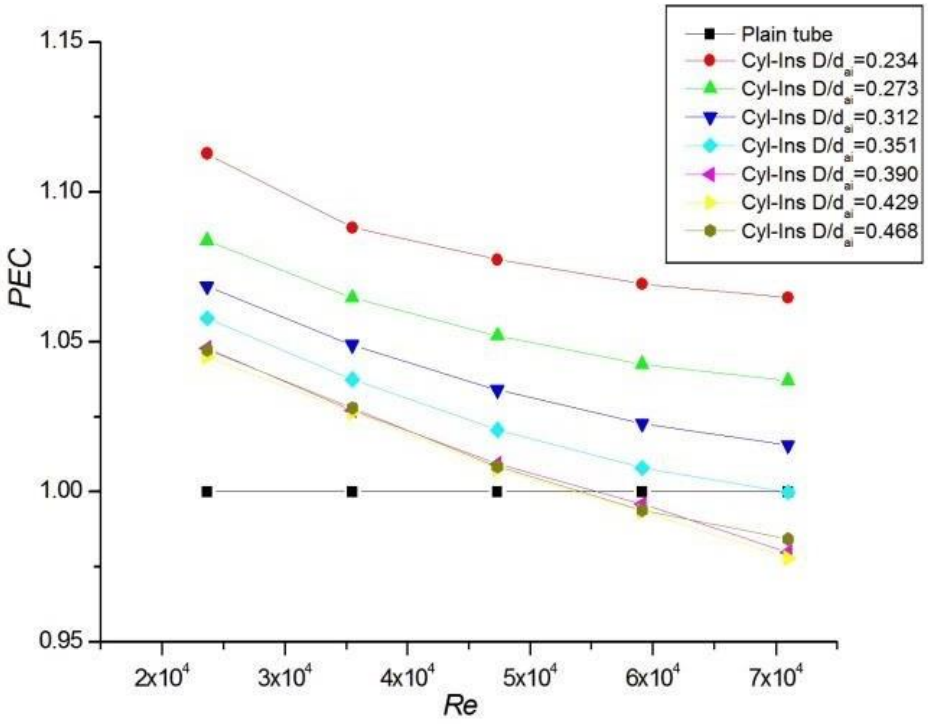

Figure IV.18: *Variation of PEC as a function of Re for different D/d_{ai} values*

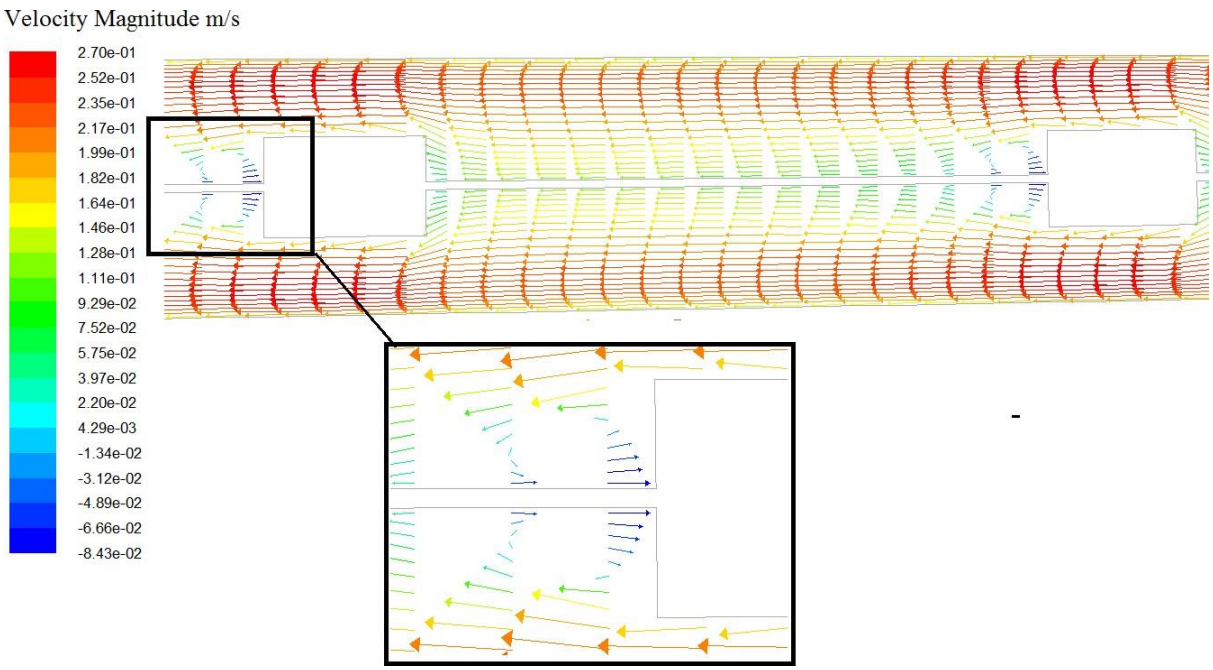

Figure IV.19: *Velocity vector distribution of an enhanced tube (H/d_{ai}=0.468 and $Re=4.73\cdot10^4$)*

The distribution of the velocity vectors inside the enhanced tube *D/dai*=0.468 and for *Re*=$4.73\cdot10^4$ is presented in Figure IV.19. It can be shown that the velocity increase at the narrowed space between the inserts and the inner wall of the tube. The increase of the velocity increases the heat transfer between the wall and the HTF, which leads to decreases the circumferential temperature of the wall. It can be seen also that the inserts generate vortices and homogenize the temperature of the HTF which gives a better heat transfer.

The circumferential temperature distribution of the absorber tube at the *Re* number of $4.73\cdot10^6$ is presented in Figure IV.20. It can be seen from the figure that the circumferential temperature is non-uniform over the absorber tube's cross section for both plain tube and enhanced tube. It can be seen also that the peak temperature decreases with the increase of the dimensionless diameter (*D/dai*). The peak temperature decreases from 722.72 K for the plain tube to 696.77 K for enhanced tube with inserts of *D/dai*=0.468, (53 K) while the difference

in the overall circumferential temperature for both the plain tube and the enhanced tube are 144.52 K and 94.17 K. A remarkable decreasing in the circumferential temperature is estimated approximately by 34.84%.

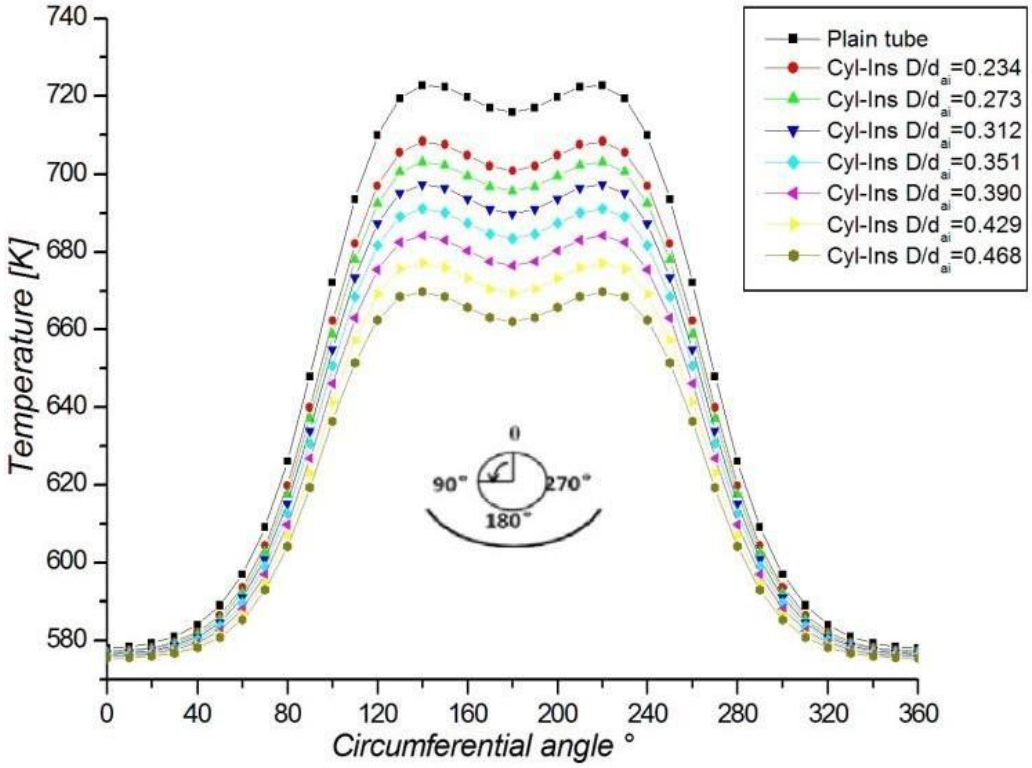

Figure IV.20: *Temperature distribution variation with the change of circumferential angle for different D/d_{ai} value*

Figure IV.21 illustrates the contour of temperature distribution on Kelvin at the outlet of the absorber tube for both plain tube Fig. 13.a and tubes formed by inserts for different diameters Figure IV.21 (b-h). It can be noticed that the average temperature of the fluid at the outlet increases and homogenizes with the increase of the dimensionless diameters (D/d_{ai}).

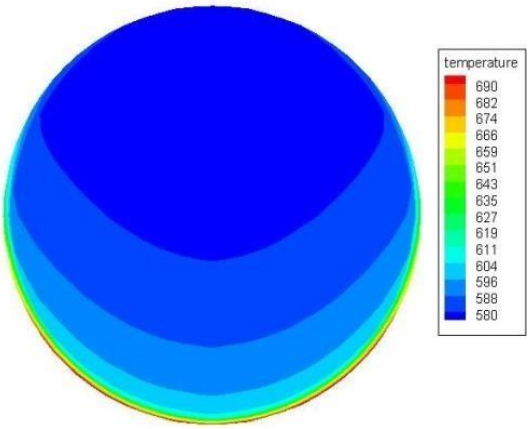

a) Plain tube

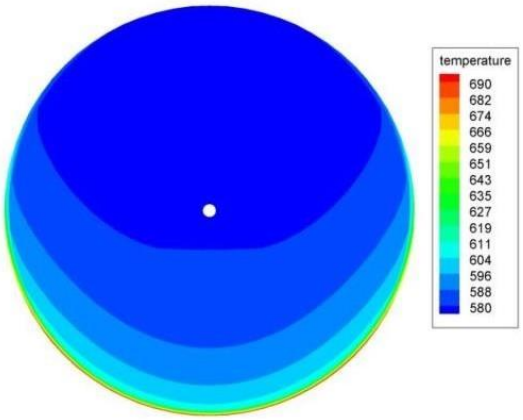

b) Cyl-Ins D/d_{ai}=0.234

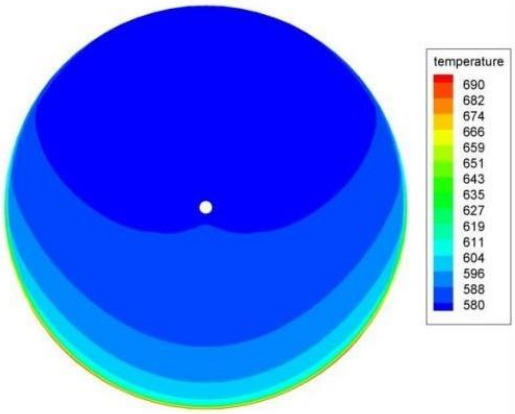

c) Cyl-Ins D/d_{ai}=0.273

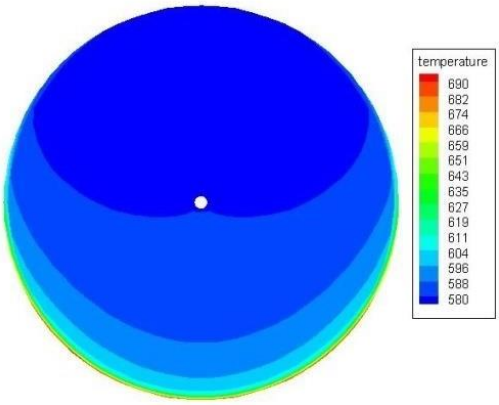

d) Cyl-Ins D/d_{ai}=0.312

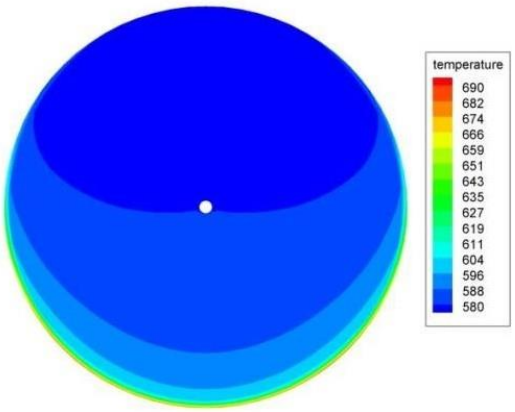

e) Cyl-Ins D/d_{ai}=0.351

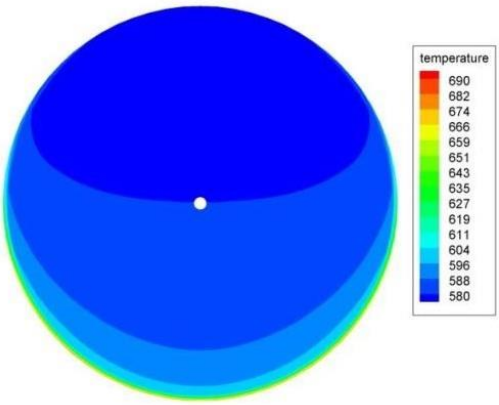

f) Cyl-Ins D/d_{ai}=0.390

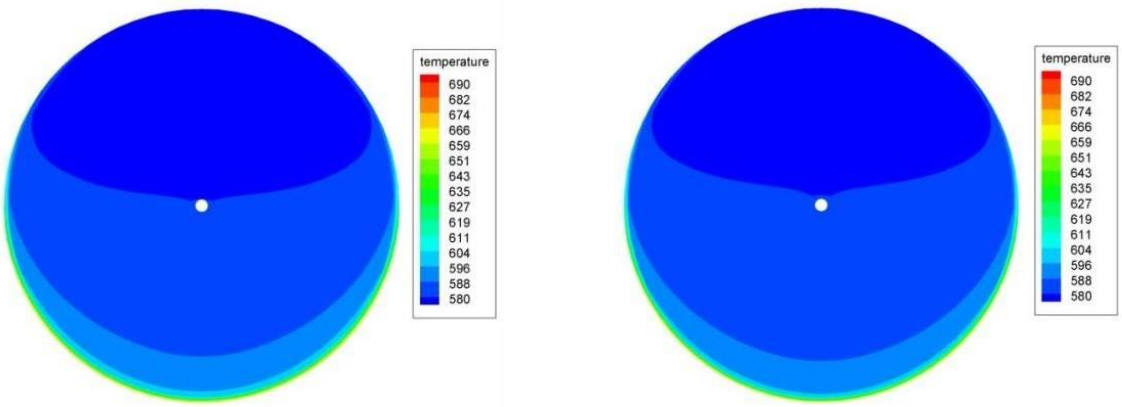

g) Cyl-Ins D/d_{ai}=0.429 h) Cyl-Ins D/d_{ai}=0.468

Figure IV.21: *temperature distribution of the HTF at the outlet*

IV. 3.2.2. Effect of (l/D) on the heat transfer performance

The effects of the length of inserts are investigated in this section.

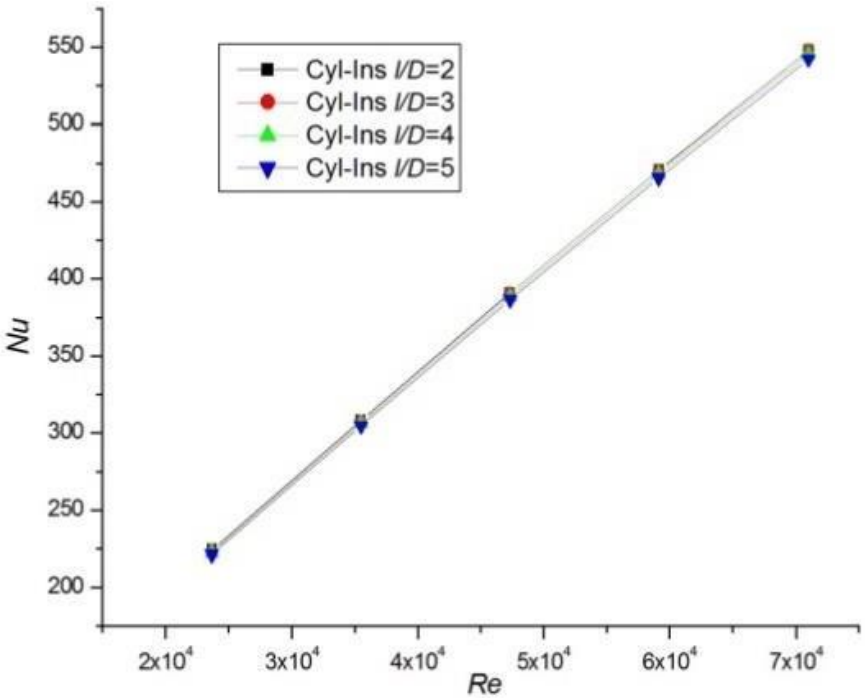

Figure IV.22: *Variation of Nu as a function of Re for different l/D values*

Figure IV.22 show the *Nu* number as a function of *Re* number for different *l/D* values. It can be seen that the Nu number increases with the increase of *Re* number and at the same *Re* number the Nu number are slightly mingled with each other.

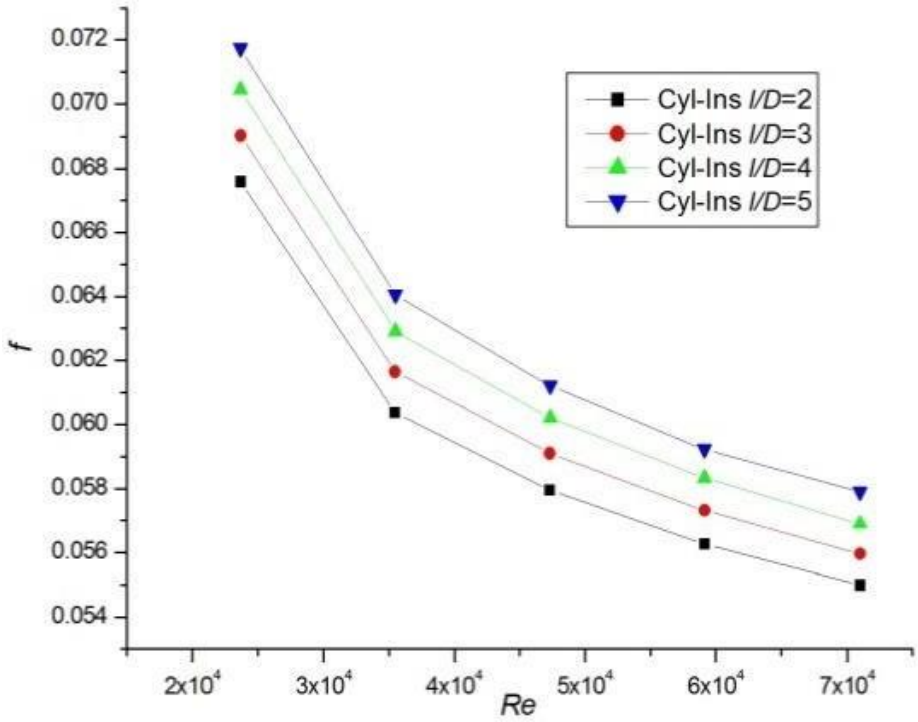

Figure IV.23: *Variation of f as a function of Re for different l/D values*

Figure IV.23 presents the Darcy friction factor as a function of *Re* number. It can be noticed that as the length of inserts increases the *f* increase, and this is due to the increase of the contact area between the HTF and the wall of the inserts.

Figure IV.24 shows the performance Evaluation Criteria for different *l/D* values as a function of *Re* number. It can be seen that the *PEC* decreases with the increase of *Re* number and it decreases also with the increase of the length of inserts. It can be seen that the *PEC* decreases under the value of 1 for the inserts with *l/D*=5 at $Re=5\cdot10^4$. It can be concluded that the smallest length gives the best results.

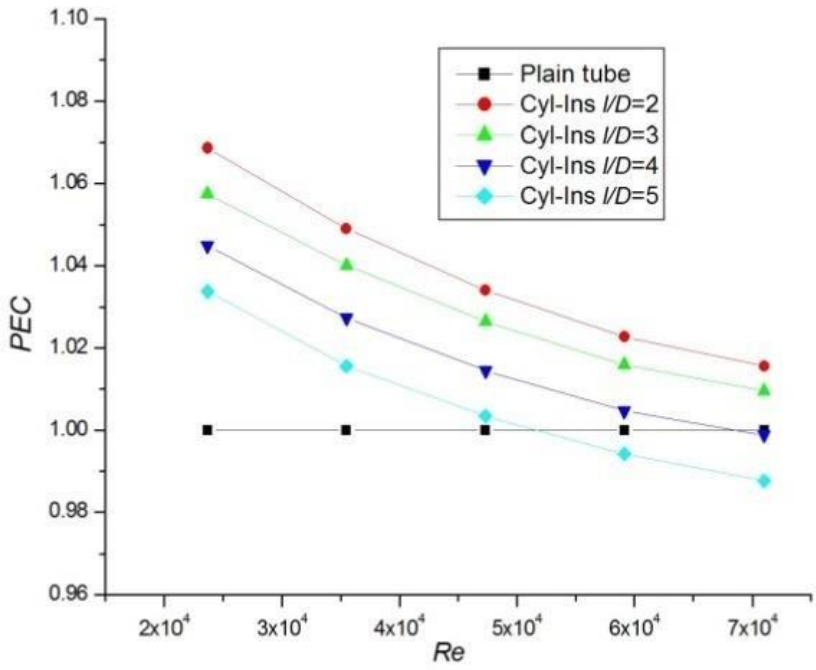

Figure IV.24: *Variation of PEC as a function of Re for different l/D values*

IV. 3.2.3. Effect of the eccentricity (e/D) of the cylindrical inserts on the heat transfer performance:

In this part we analysed the thermo hydraulic performance of the enhanced tube for different eccentricity (*e/D*) values with (D/d_{ai}=0.312 and *l/D*=2). For this purpose, the cylindrical inserts are introduced into the tube with a distance (*e/D*) far away from the centre of the absorber tube.

Figure IV.25 shows the *Nu* number as a function of the *Re* number for Different *e/D* values. It can be seen that the *Nu* number increases with the increase of *Re* number and it increases also with the increase of the distance *e/D* as illustrated in Figure IV.26. It can be noticed from this figure that the *Nu* number has a remarkable value for the inserts placed at the farther distance from the centre (close to the inner wall of the absorber tube) with an enhancement factor of

33.68% and 90.32% compared to the centred inserts tube and the smooth tube respectively.

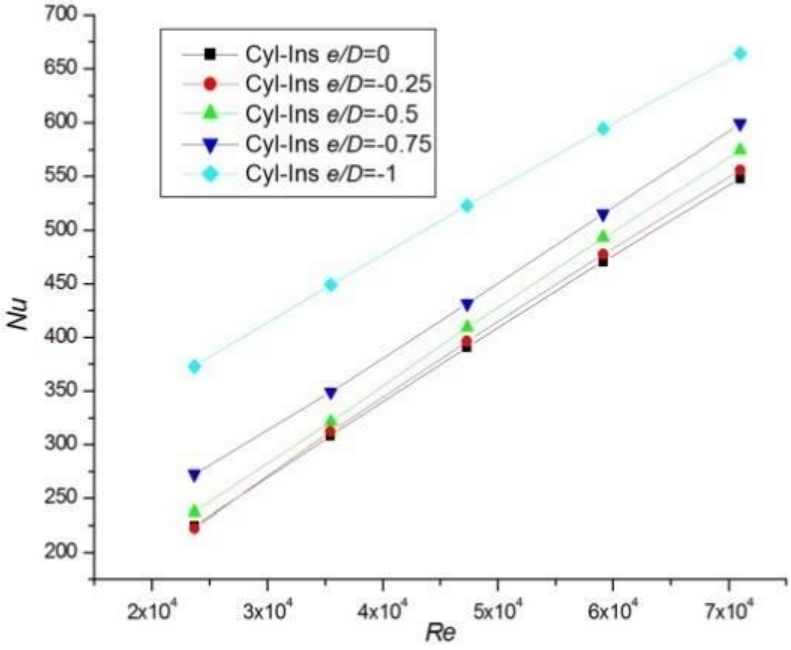

Figure IV.25: *Variation of Nu as a function of Re for different e/D values*

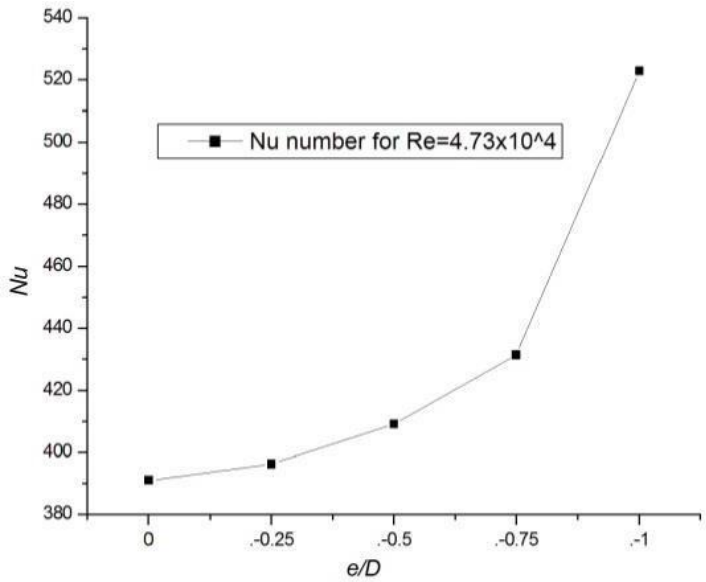

Figure IV.26: *Variation of Nu as a function of e/D for Re=4.73·10^4*

Figure IV.27 presents the Darcy friction factor as a function of the *Re* number for Different *e/D* values. It can be seen that the *f* decreases with the increase of *Re* number and as the *Re* number increases, the values of the *f* for different *e/D* are slightly mingled and this is due to the pressure drop as shown in Figure IV.28.

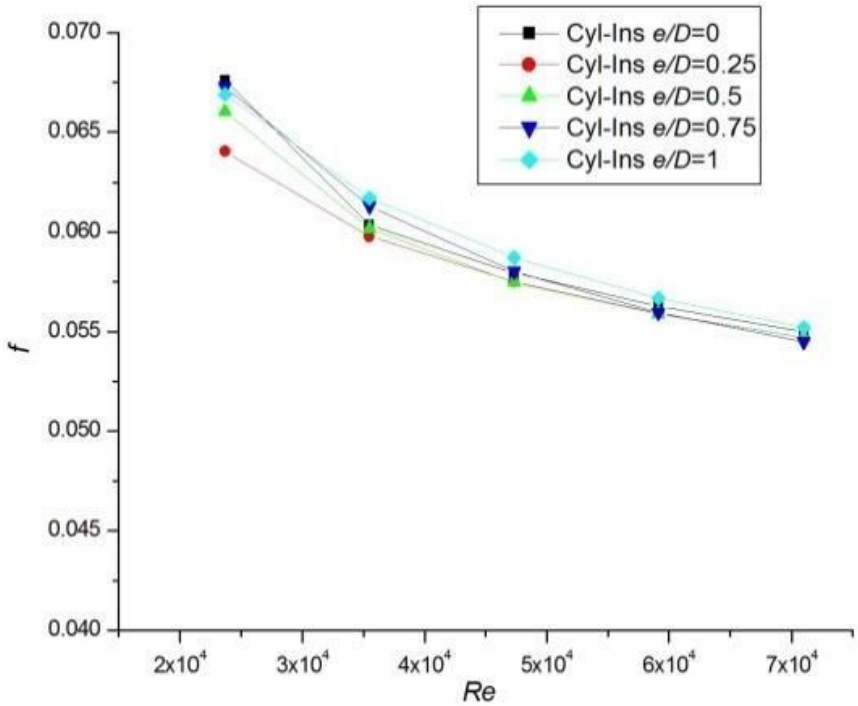

Figure IV.27: *Variation of f as a function of Re for different e/D values*

Figure IV.29 shows the *PEC* for different *e/D* values as a function of *Re* number. From this figure we can see that the *PEC* decreases with the increase of *Re* number and it is always higher than 1 for all *Re* number. It can also be noticed that for lower *Re* number the *PEC* increases considerably with the increase of the *e/D* and has a value of 1.782 for *e/D*=1 and *Re*= $2.36 \cdot 10^4$ and this is due to the remarkable augmentation of the *Nu* number.

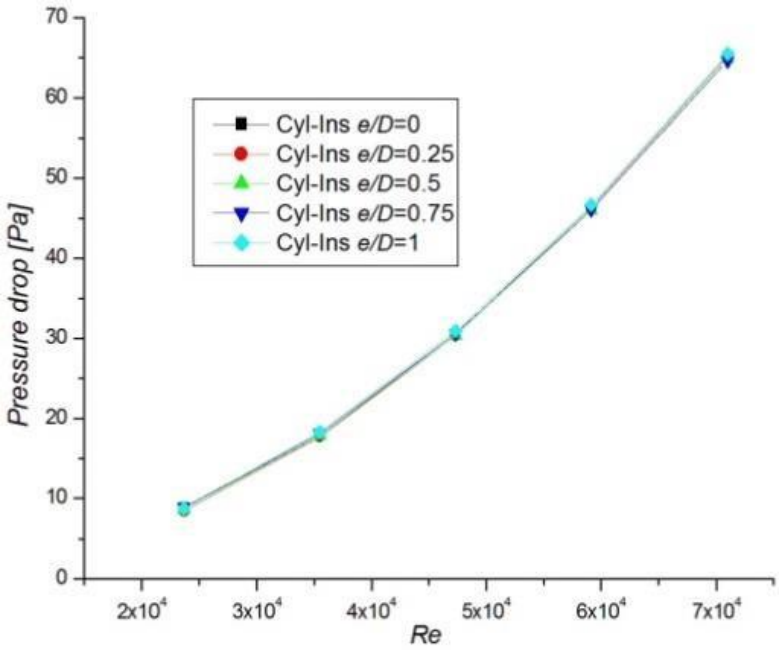

Figure IV.28: *Variation of pressure drop as a function of Re for different e/D values*

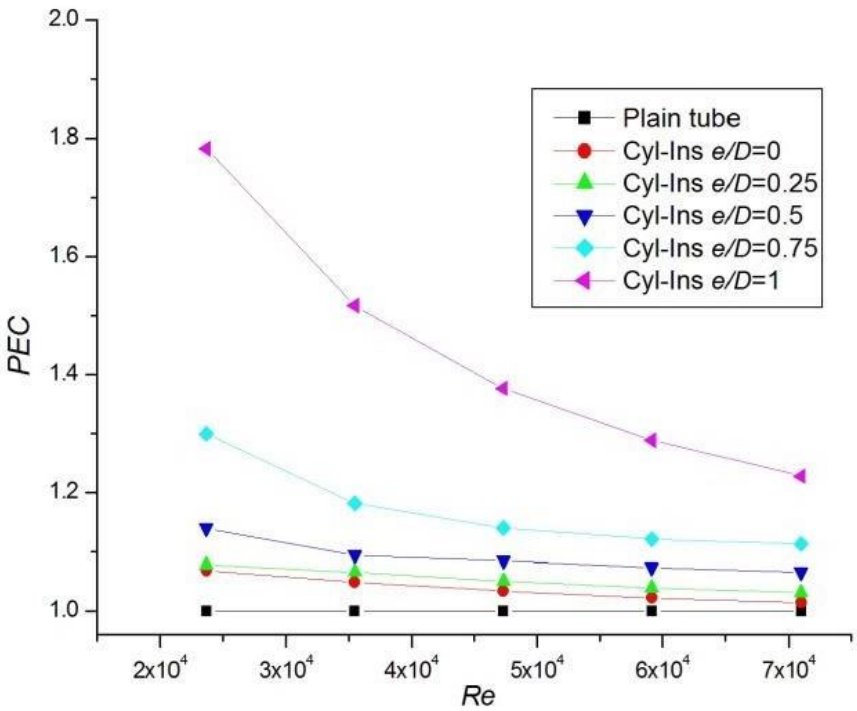

Figure IV.29: *Variation of PEC as a function of Re for different e/D values*

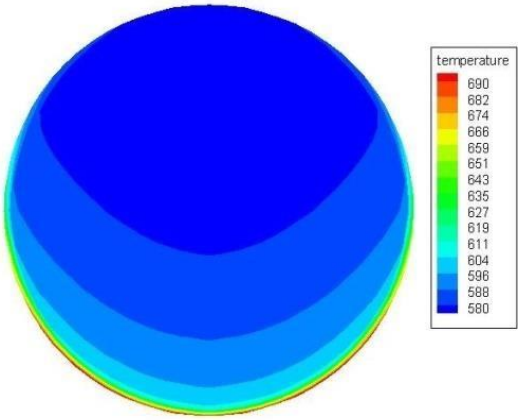

a) Plain tube

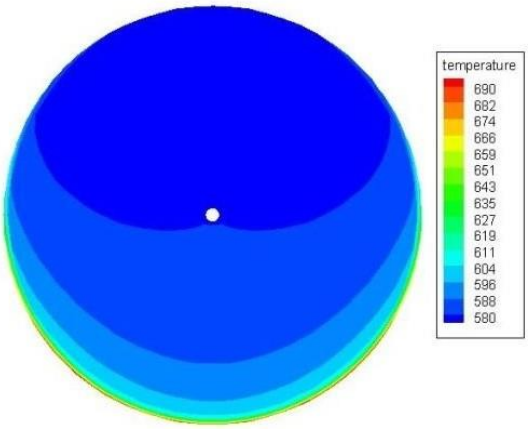

b) Cyl-Ins *e/D*=0

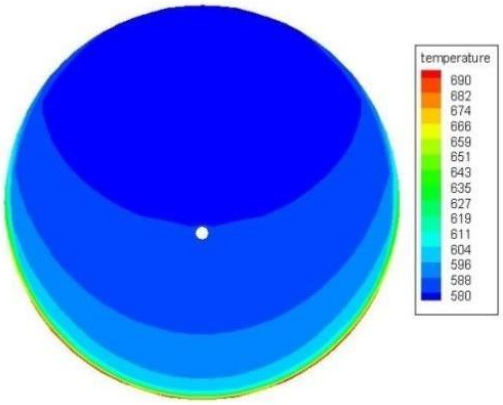

c) Cyl-Ins Cyl-Ins *e/D*=0.25

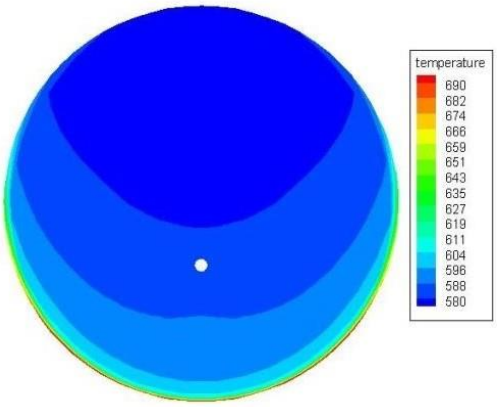

d) Cyl-Ins Cyl-Ins *e/D*=0.5

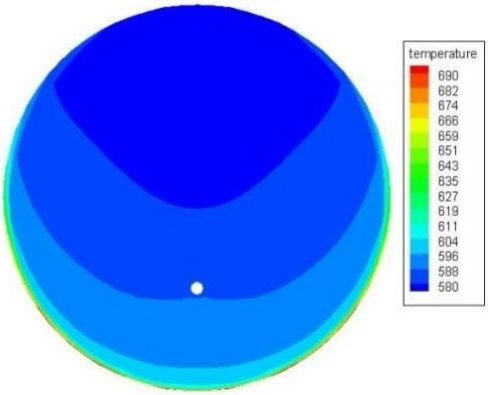

e) Cyl-Ins Cyl-Ins *e/D*=0.75

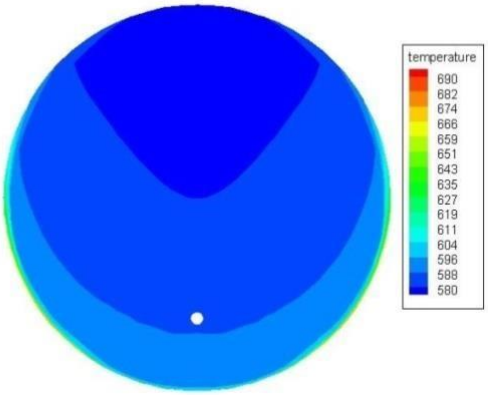

f) Cyl-Ins Cyl-Ins *e/D*=1

Figure IV.30: *Temperature distribution of the HTF at the outlet*

Figure IV.30 illustrates the contour of temperature distribution on Kelvin at the outlet of the absorber tube for both plain tube Fig. 22.a and tubes formed by inserts for different eccentricities Fig. 22 (b-f). It can be seen that the average temperature of the fluid at the outlet increases and homogenizes with the increase of the dimensionless eccentricity (*e/D*).

IV. 3.3. Parabolic Trough collector with secondary reflector (Annex I)

The biggest problem that can be encountered in the Parabolic Trough Collector is the tube wear, and this is due to the non-uniformity of the temperature distribution over the circumferential angle of the tube. In this part, the absorber tube is moved downward away the focal line of the parabola and a secondary reflector is added overhead the tube in order to reduce the heat flux gradient and homogenize it as shown in (Figure IV.31).

The simulation method of the ray's path is adopted by SolTrace software. The sun rays reflected by the primary concentrator hit the bottom part of the absorber tube and a portion of these rays are reflected again on the upper part of the absorber tube by the secondary reflector

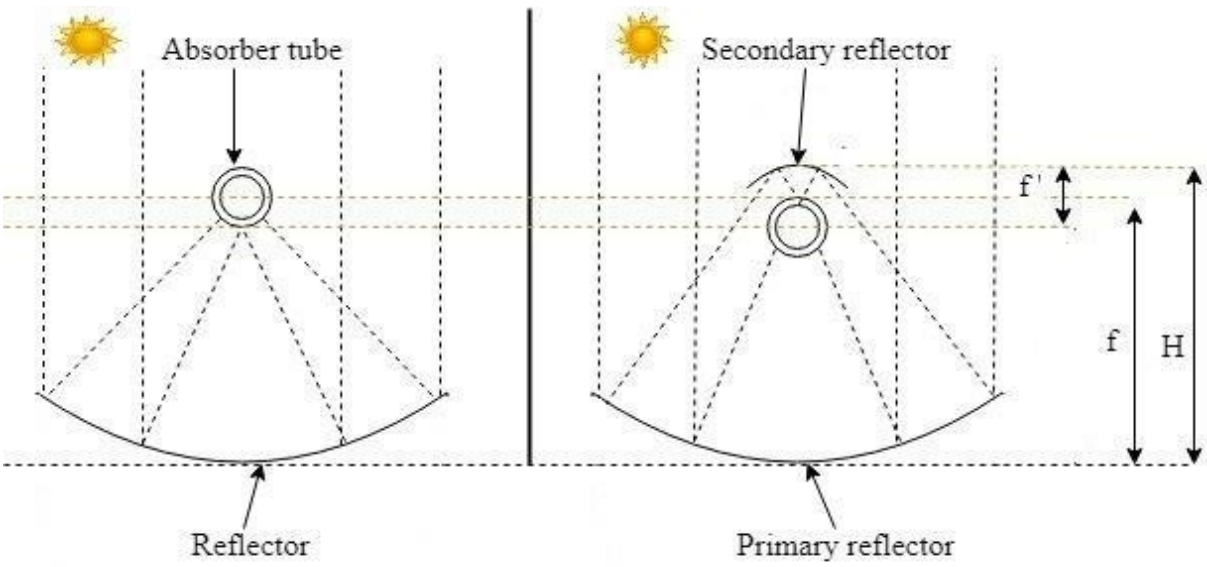

Figure IV.31: *Schematic diagram of the receiver with reflectors*

IV. 3.3.1. Ray tracing and heat flux analysis

In this part of this section, the LCR obtained from SolTrace software for both the conventional PTC and the PTC with secondary reflector are investigated.

Figure IV.32 shows the path of the rays reflected by the concentrator on the absorber tube. It can be seen from this figure that the absorber tube of the conventional PTC (Figure IV.32.a) is subjected to a concentrated solar flux on the bottom part while the upper one is subjected to a non-concentrated solar flux; and by moving the absorber tube downward and adding a second ary reflector; the solar rays can reach the upper part after reflected by the additional reflector as shown in Figure IV.32.b

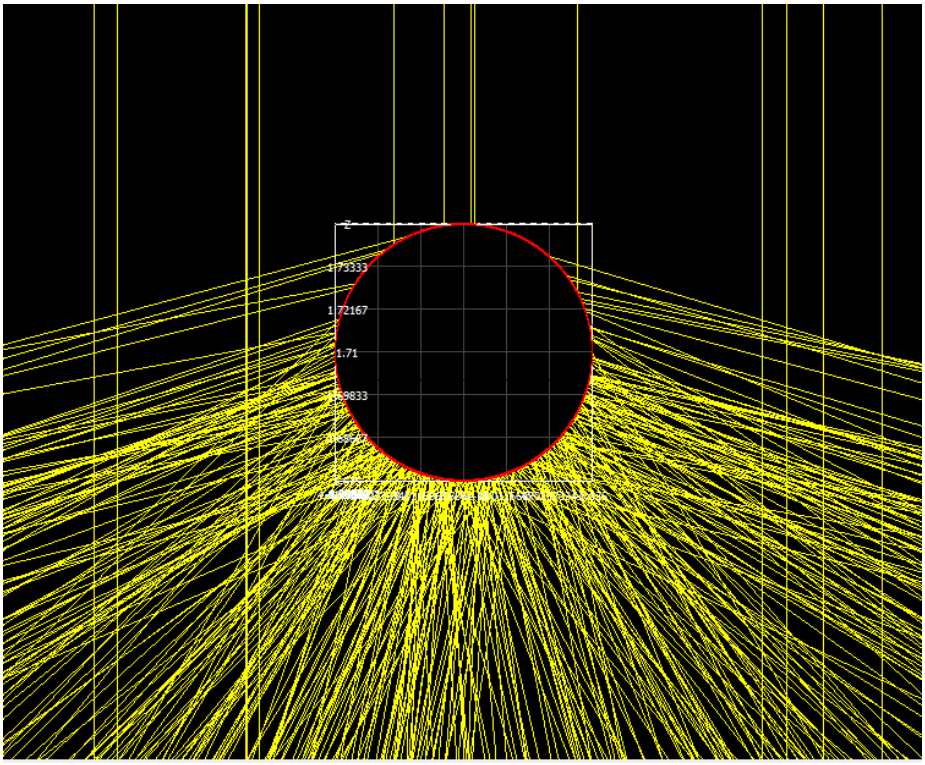

a) Conventional Parabolic Trough Collector

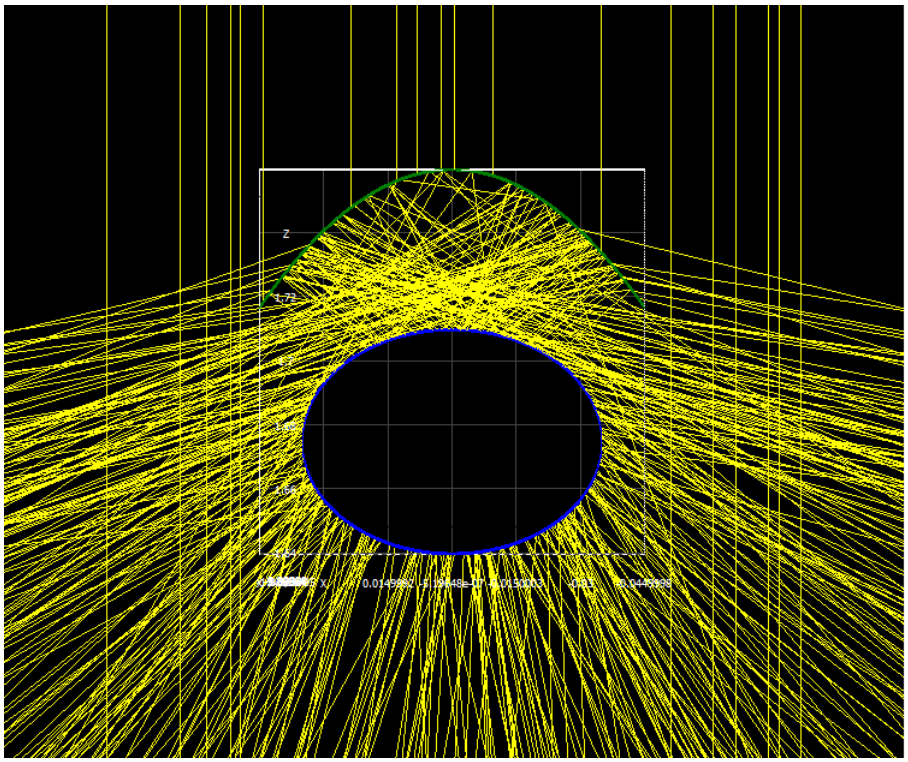

b) Parabolic Trough Collector with SR

Figure IV.32: *Ray's path reflected by the concentrator on the absorber tube*

Figure IV.33 shows the flux map of the conventional PTC and the enhanced PTC. From these figures it can be seen that the heat flux of the conventional PTC is non-uniform with a large gradient while by adding a secondary reflector the gradient of the flux decreases and becomes homogenous.

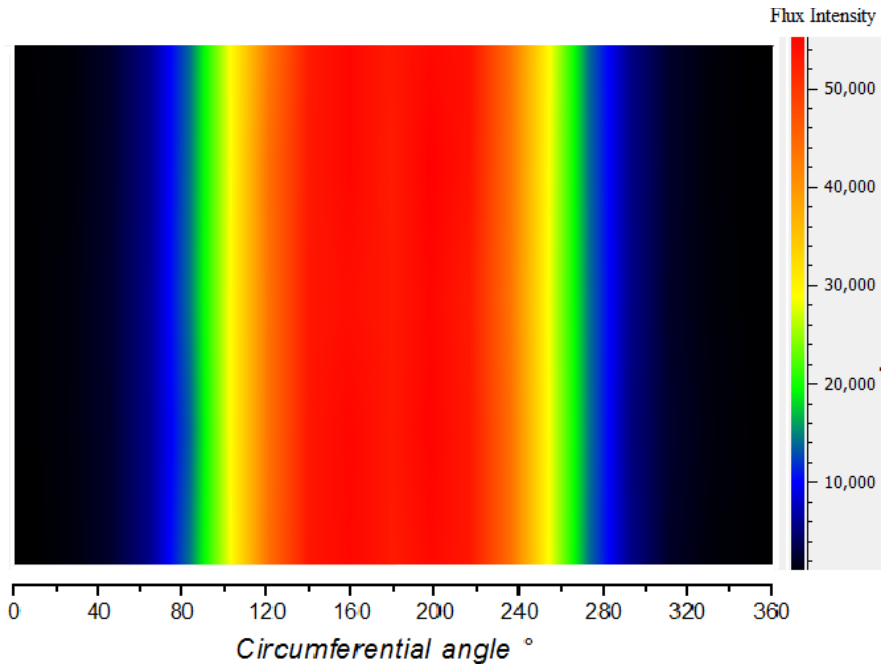

a) Conventional Parabolic Trough Collector

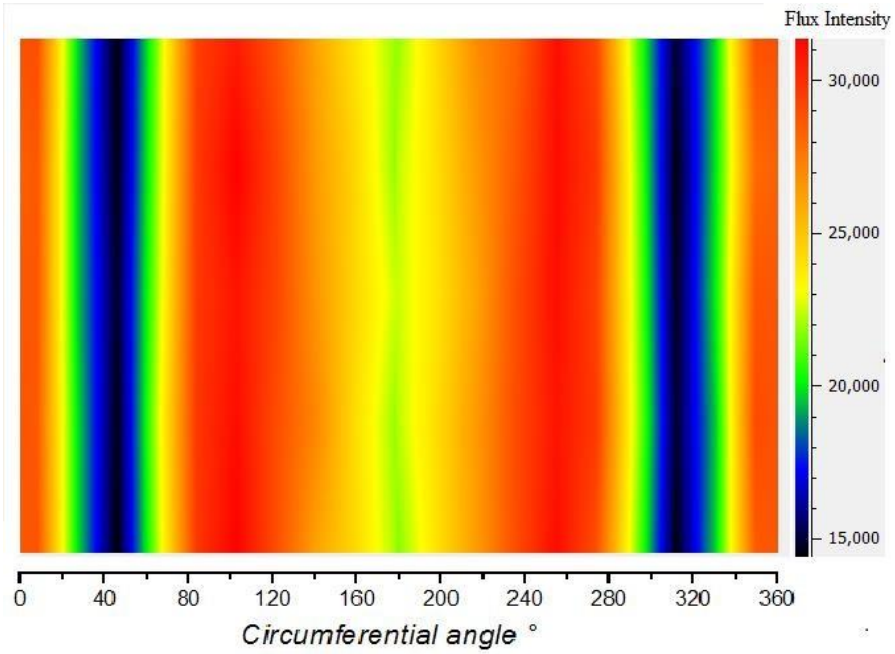

b) Parabolic Trough Collector with SR

Figure IV.33: *Flux map of the conventional PTC and the enhanced PTC*

The LCR for both conventional PTC and the PTC with secondary reflector are shown in Figure IV.34.It can be seen that the LCR decreases and becomes slightly uniform by adding the secondary reflector and the maximum value of the heat flux decreases to 31000 $W \cdot m^{-2}$ and the minimum value increases to 15000 $W \cdot m^{-2}$, while for the conventional PTC the peak value

is 55000 W·m^{-2} and the minimum value is 1000 W·m^{-2}. The gradient of the heat flux over the circumferential angle of the absorber tube is enhanced and reduced by 70.37 %.

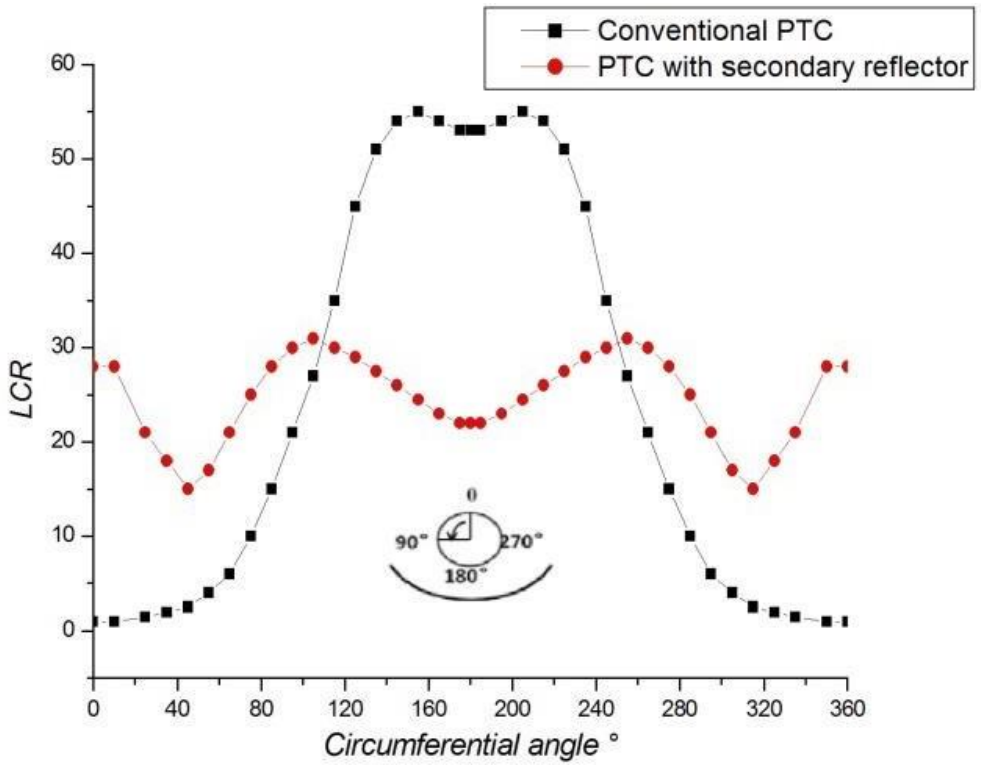

Figure IV.34: *The Local Concentration Ratio distribution on the outer surface of the absorber tube as a function of circumferential angle*

IV. 3.3.2. Temperature distribution analysis

In the second part of this section, the thermal performance and the efficiency of the conventional PTC and the PTC with the secondary reflector are investigated under the same conditions.

Figure IV.35 presents the temperature distribution over the circumferential angle of both the conventional PTC and the enhanced one at the middle-distance L=2m and for *Re*=47.31·10^4. It can be seen that the temperature gradient is reduced significantly and becomes

homogenous. It can be also noticed that by adding a secondary reflector the maximum temperature is decreased from 739.84 K to 663.98 K and the minimum temperature is increas ed from 580.44 K to 639.82 K, and the temperature gradient difference is reduced from 159.3 K to 24.16 K.

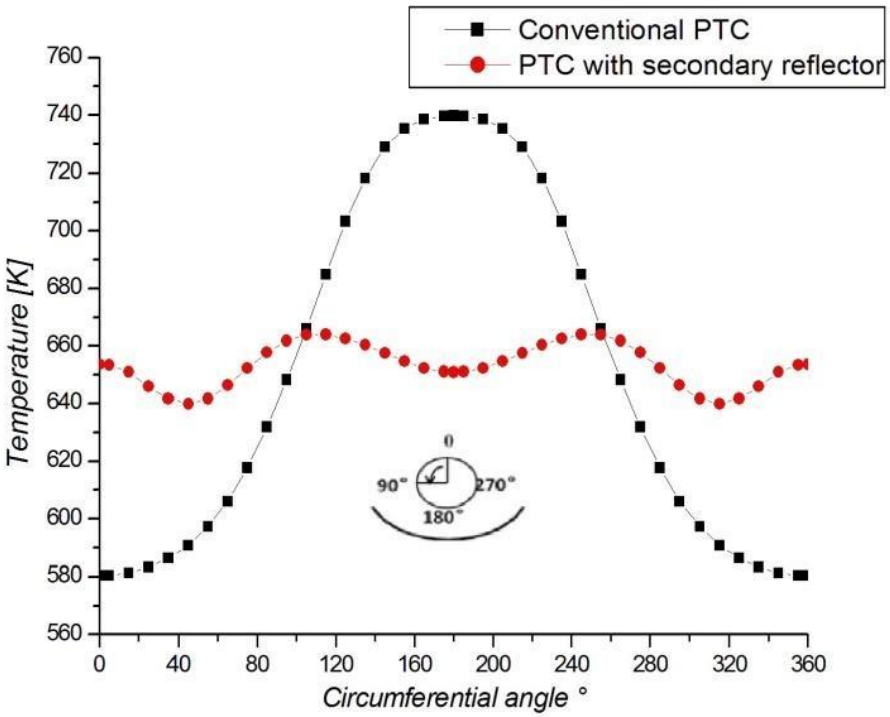

Figure IV.35: *Temperature distribution on the outer surface of the absorber tube as a function of circumferential angle*

The contour of temperature distribution over the wall of both conventional tube and tube with secondary reflector are shown in Figure IV.36 From this figure it can be seen that that the temperature distribution of the conventional PTC (Figure IV.30.a) is non-uniform and by adding another reflector the temperature distribution becomes more uniform (Figure IV.30.b)

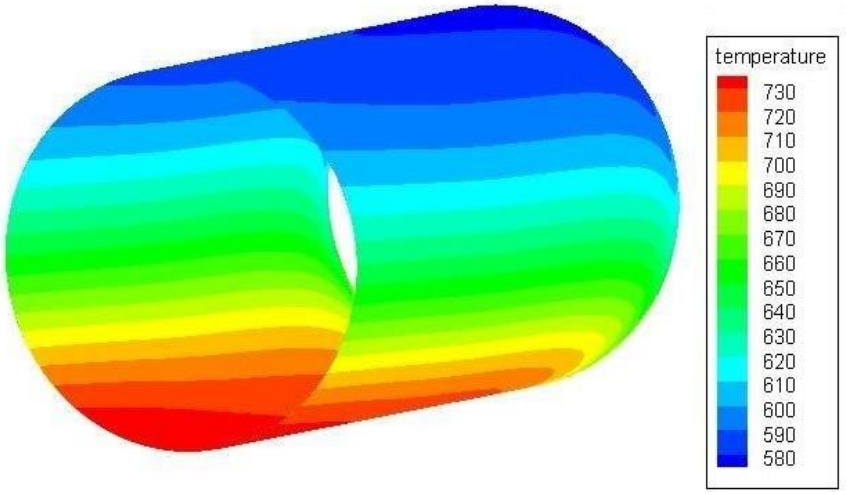

a) Conventional Parabolic Trough Collector

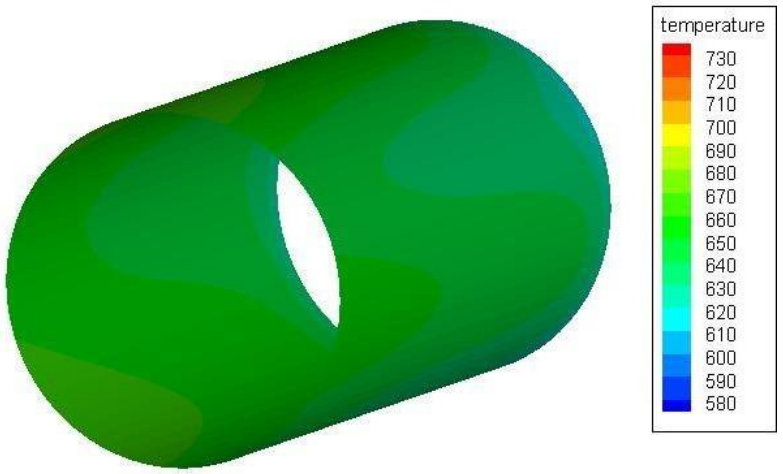

b) Parabolic Trough Collector with SR

Figure IV.36: *The contour of the temperature distribution of the absorber tube*

IV. 4. Conclusion

In this chapter the evaluation of the numerical study is carried out to evaluate the heat transfer enhancement of a receiver tube of parabolic trough collector by introducing different type of insert inside the tube and the introduction of the secondary reflector. The numerical results show that the tubes with inserts give better heat transfer compared to the smooth tube with a sacrifice of pressure drop. In the other hand the parabolic through collector with a homogenized reflector reduce the circumferential temperature gradient of the absorber tube.

Chapter V

V.1. Introduction

Algeria is the largest country in the entire African continent, with an area of 2.381.741 km². The country has a population of 42 million people, with a forecast of reaching 45 million by 2025. Algeria's economy is based on hydrocarbons and represent 98% of its exports, 40% of public revenues and around 35% of GDP. The forecast of the increase in electricity consumption from 75 TWh (terawatt-hours) to 150 for the year 2030 concludes in the investment in other energy sources, mainly in renewable energies, and the national energy potential based on renewables is clearly dominated by solar energy.

V.2. Geographical location:

The geographical location of Algeria is one of the most important solar potentials in the world. The duration of insolation over the national territory exceeds 2000 hours per year, reaching up to 3900 hours in the Sahara. The average energy received on a unit surface is of the order of 5 kWh, which represents about 1700 kWh/m^2 per year in the north of the country and 2650 kWh/m^2 per year in the south.

The northern coastal area receives an annual average daily irradiation of 5.5 kWh·m^{-2}, the central area receives 6 kWh·m^{-2} and the southern area 6.5 kWh·m^{-2} or more.

In the case of Tamanrasset, the annual average of daily irradiation reaches up to 7.5 kWh/m^2.

V.3. Algeria's weather

Algeria has various climates and regions; the three most important regions are as shown in the figure:

V.3.1. Mediterranean: In the coastal strip the sunshine is greater than 2500 hours per year.

V.3.2. Semi-arid / Steppe: In the High Plains and in the centre of the country the insolation is between 3000 and 3500 hours per year.

V.3.3. Desert: In the Sahara region the sunshine is greater than 3500 hours of per year.

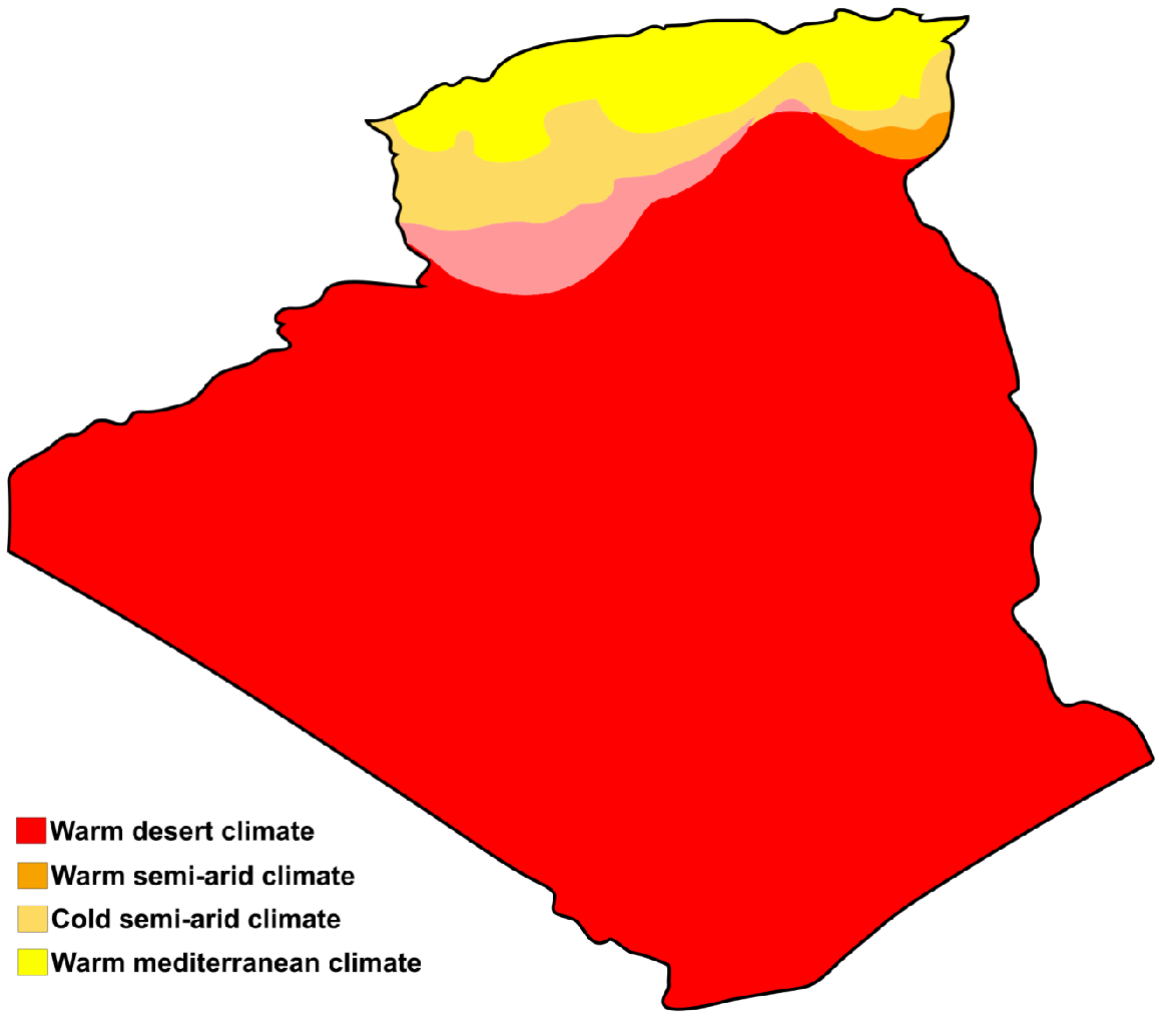

Figure V.1. *The Algerian map with different climates*

V.4. Solar irradiation Estimation

V.4.1. Hottel's model

Solar radiation of the clear sky irradiance modelling is necessary in many applications of solar energy. A number of models of varying complexity have been proposed in the literature, spanning from simple empirical formulae to highly sophisticated spectral codes. Solar irradiance is defined as the amount of electromagnetic energy incident on a surface per unit time and per unit area. The energy emitted by the Sun passes through space until it is

intercepted by planets. Solar irradiance includes extra-terrestrial irradiance and surface irradiance. Extra-terrestrial irradiance refers to the upper bound irradiance which is not affected by the aerosphere and weather conditions but depends on the Earth's rotation and revolution and it's related to the latitude, the Sun elevation angle, date and the time of the day. There are many models for solar irradiance which are used to calculate the value of radiation at different locations and these models are utilized for horizontal and inclined surface.

For clear sky, Hottel has given a simple model in order to evaluate the transmittance of sun's radiation. The elevation, day number, and the zenith angle of the location are the only required input [55].

It is known that the atmospheric transmittance is defined as

$$r = \frac{DNI}{G_s} \qquad \text{V.1}$$

As defined in the chapter 1

$$G_s = G_{sc}\ [1 + 0.034\ cos\ (\frac{360(N-3)}{365.25})] \qquad \text{V.2}$$

Where the G_{sc} is the solar constant

$$G_{sc} = 1367\ W \cdot m^{-2} \qquad \text{V.3}$$

Hottels [56] defined the solar transmittance as:

$$r = a_0 + a_1 e^{-kcos\theta_z} \qquad \text{V.4}$$

Where:

$$DNI = G_s * (a_0 + a_1 e^{-kcos\theta_z}) \qquad \text{V.5}$$

Where a_0, a_1 and k are constants

- For the altitude less than 2.5 km (Annex II):

$$a_0 = 0.4237 - 0.00821(6 - A)^2 \qquad \text{V.6}$$

$$a_1 = 0.5055 - 0.00595(6.5 - A)^2 \qquad \text{V.7}$$

$$k = 0.2711 - 0.01858(2.5 - A)^2 \qquad \text{V.8}$$

And for urban zones:

$$a_0 = 0.2538 - 0.0063(6 - A)^2 \quad \text{V.9}$$

$$a_1 = 0.7678 - 0.01858(6.5 - A)^2 \quad \text{V.10}$$

$$k = 0.249 - 0.081(2.5 - A)^2 \quad \text{V.11}$$

And θ_z is the zenith angle (See chapter 1).

V.4.2. Results

Using the Excel program for the direct normal irradiance calculations for the six Algerian towns chosen; Tamanrasset, Adrar, Ghardaia, Oran, Algies and annaba. (Annex II)

The figures V.2 to V.7 show the direct normal irradiance on a horizontal plane surface.

It can be seen that the DNI increase with the increase of the time until reach a maximum value and then decrease. The maximum value is reached when the elevation of the sun is in its highest value.

It can be noticed that for the six towns the DNI is always higher in 21st of June which is the summer solstice and it is due to the declination angle of the earth. In the other hand, it can be seen that the DNI is lower in 21st of December (Winter Solstice) it's totally the reverse of the summer solstice.

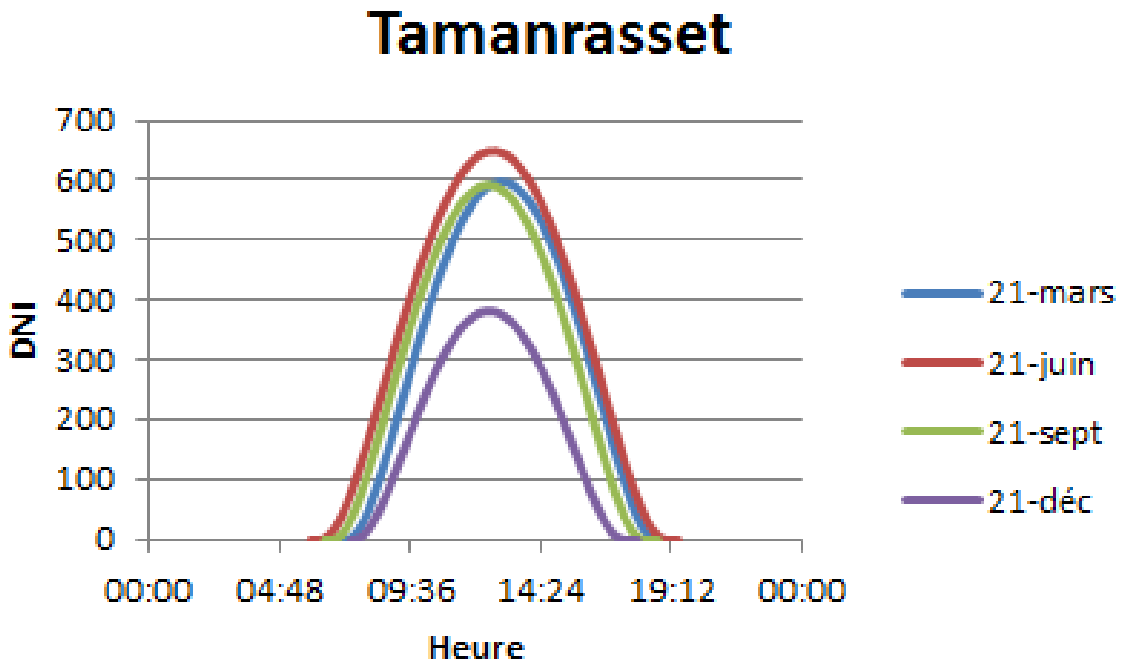

Figure V.2: *The DNI evolution during the day for the Tamanrasset region*

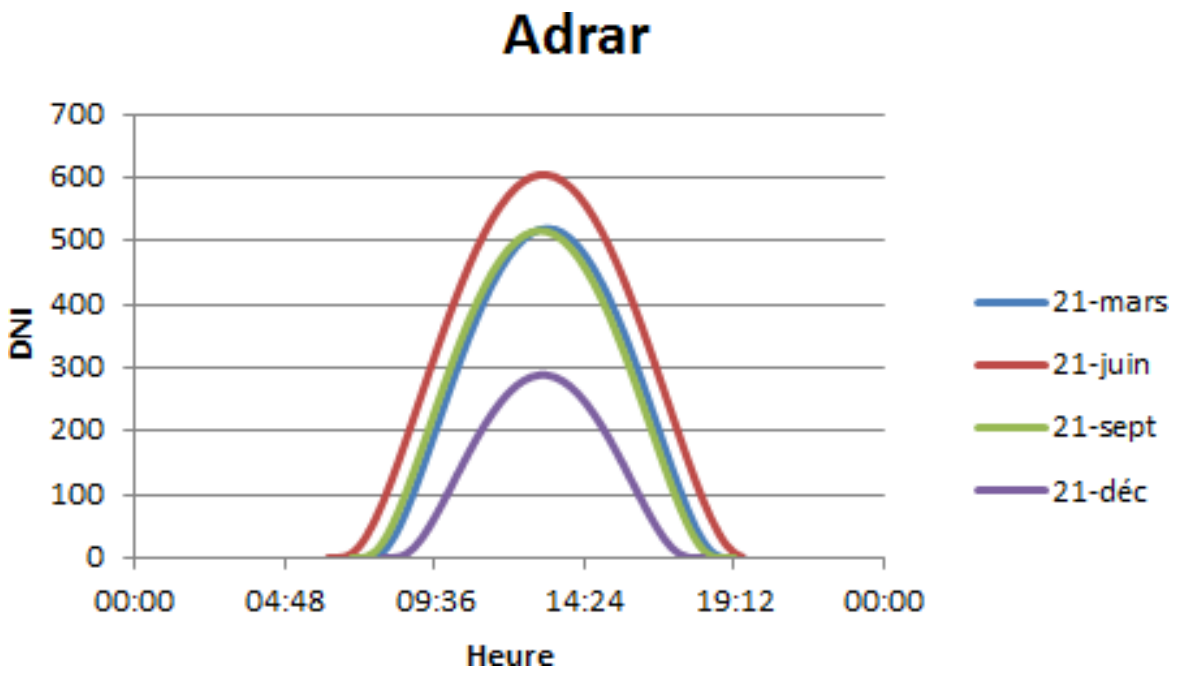

Figure V.3: *The DNI evolution during the day for the Adrar region*

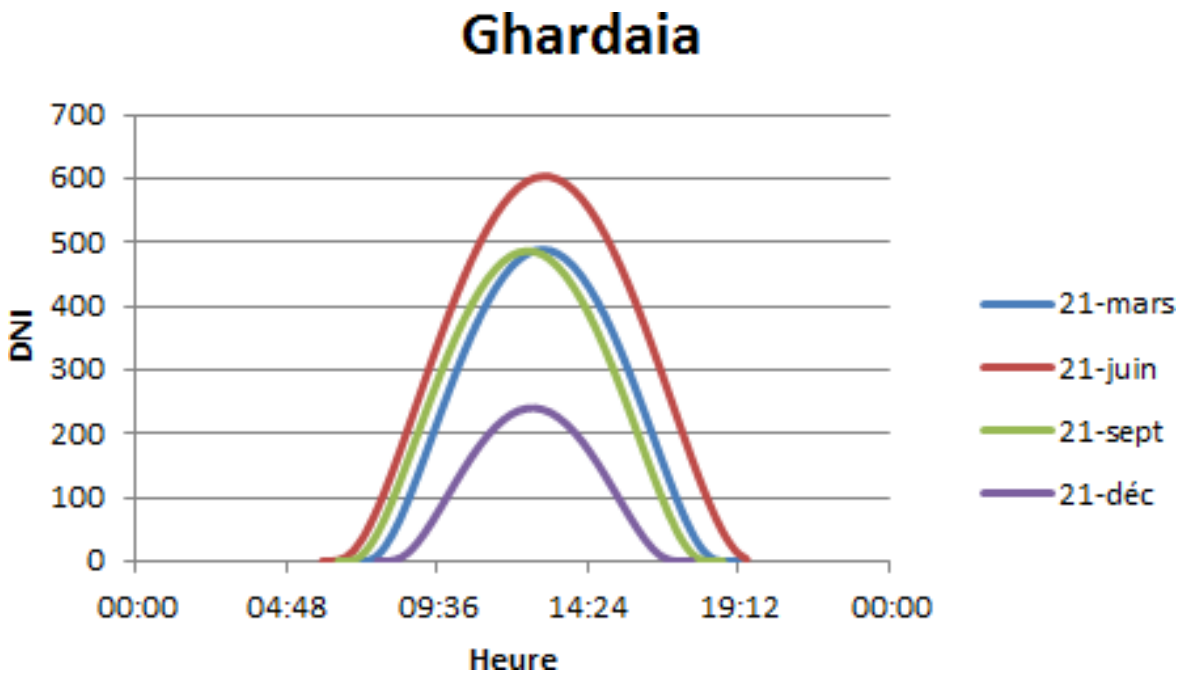

Figure V.4: *The DNI evolution during the day for the Ghardaia region*

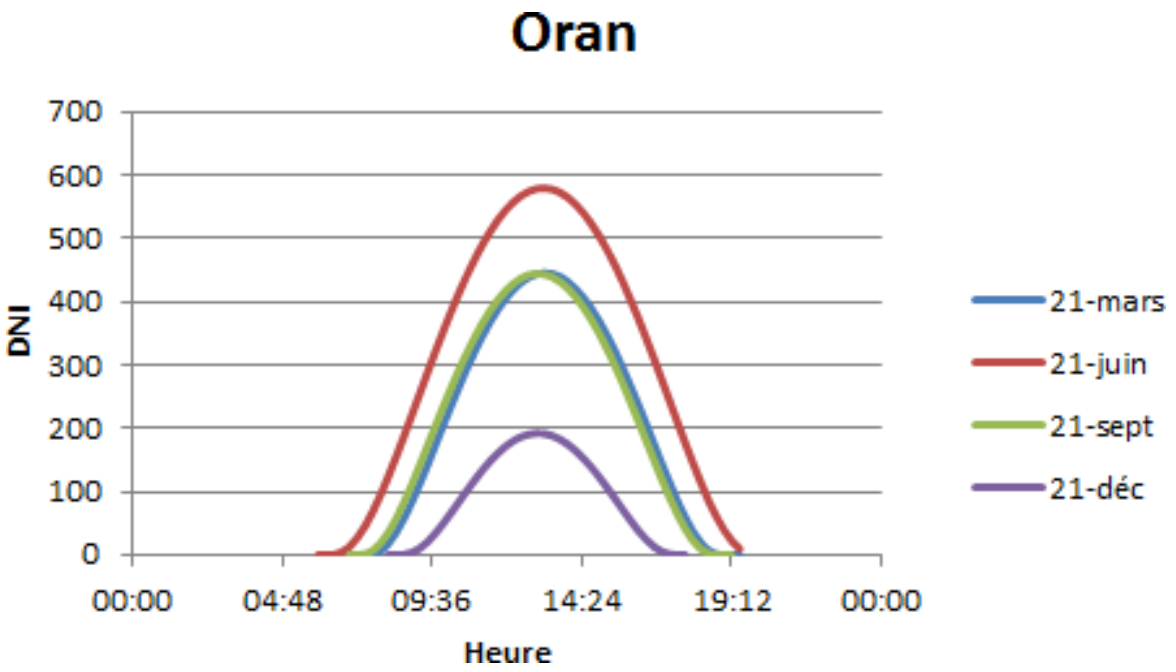

Figure V.5: *The DNI evolution during the day for the Oran region*

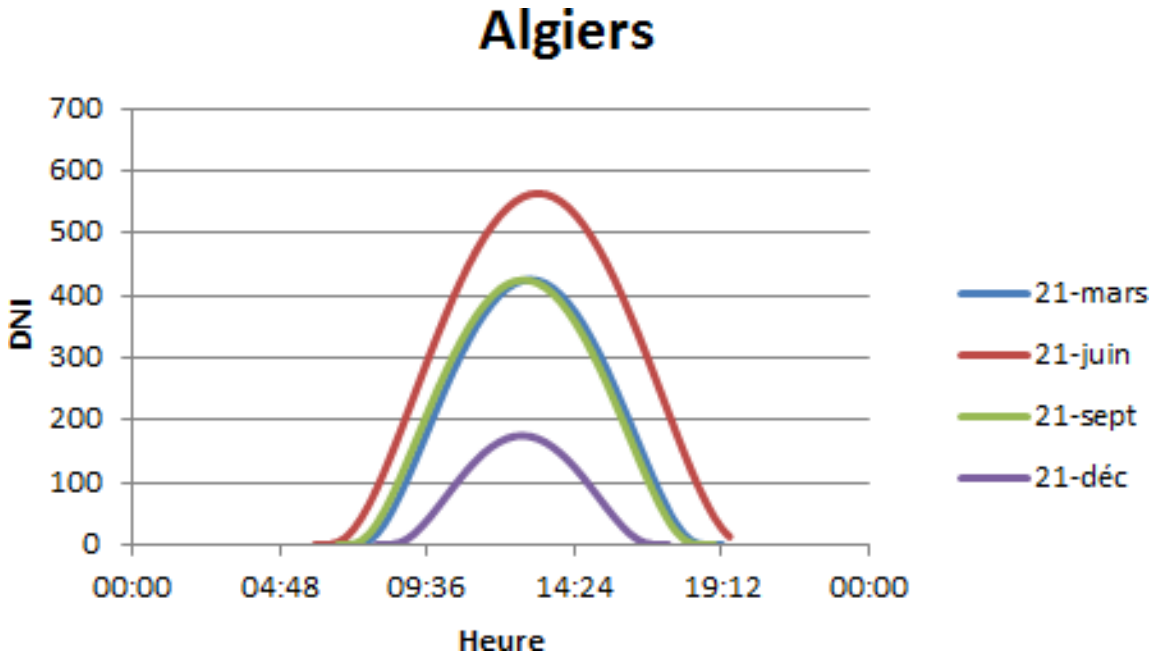

Figure V.6: *The DNI evolution during the day for the Algies region*

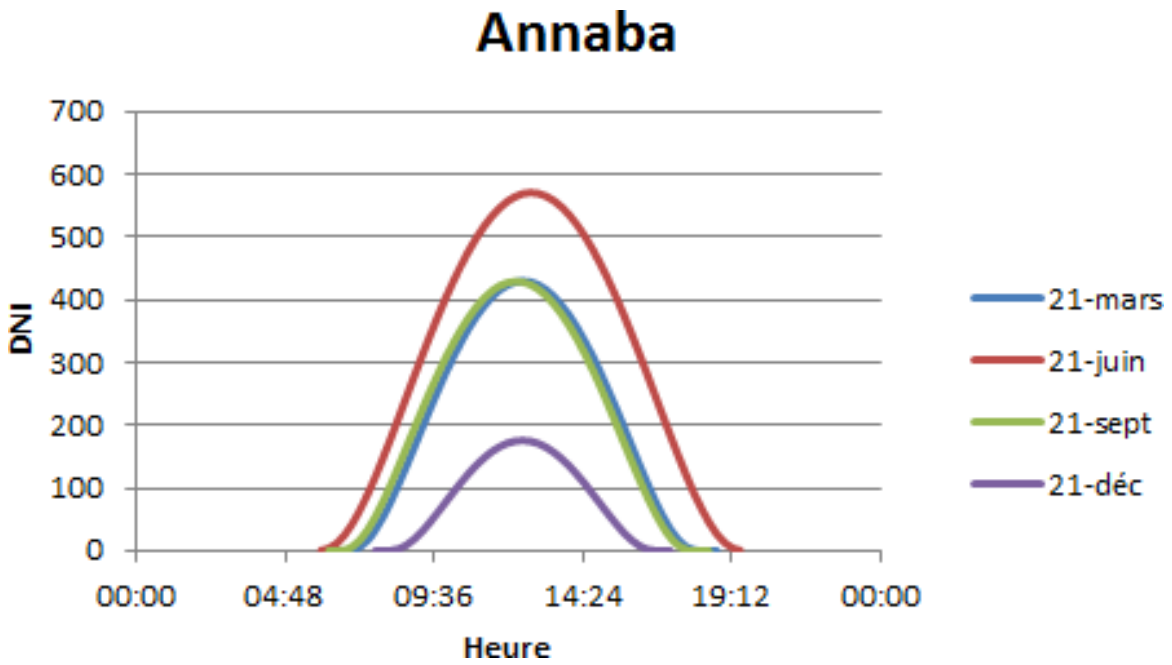

Figure V.7: *The DNI evolution during the day for the Annaba region*

The figures V.8 to V.11 show the DNI evolution of the sex regions in function of the time. It can be seen that the DNI increase with the increase of the tie and reach a maximum value then

decrease for all regions. It can be noticed also that the DNI for the Sahara regions are always higher than that of the north regions especially for the Tamanrasset region during the four period of the year.

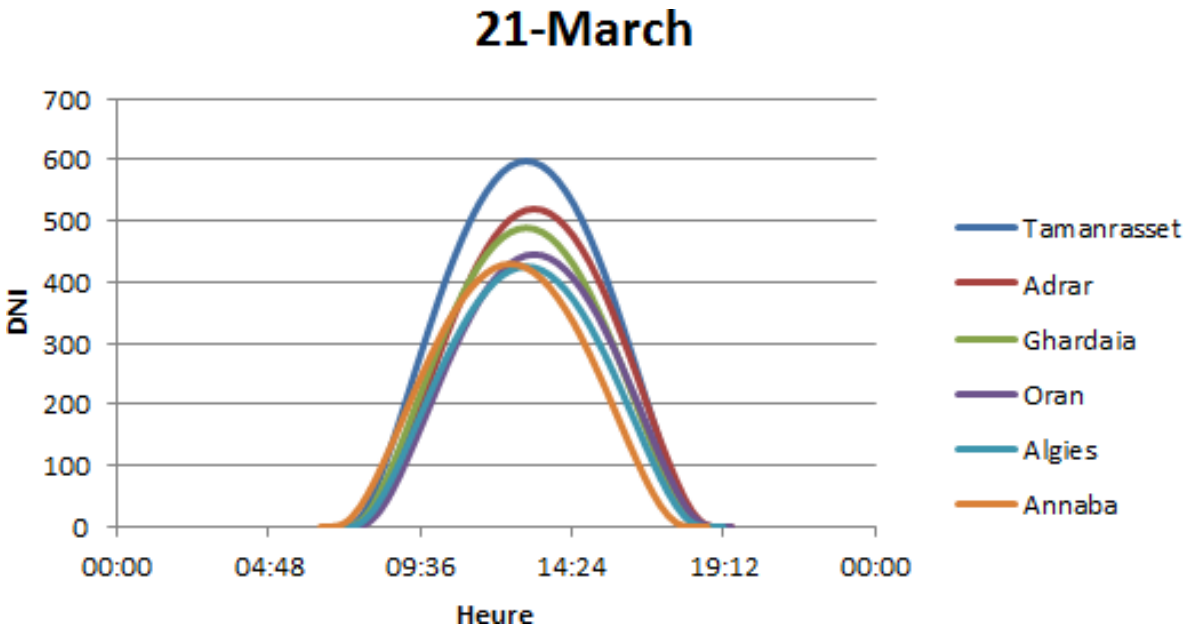

Figure V.8: *The DNI evolution during the day for the 21st March*

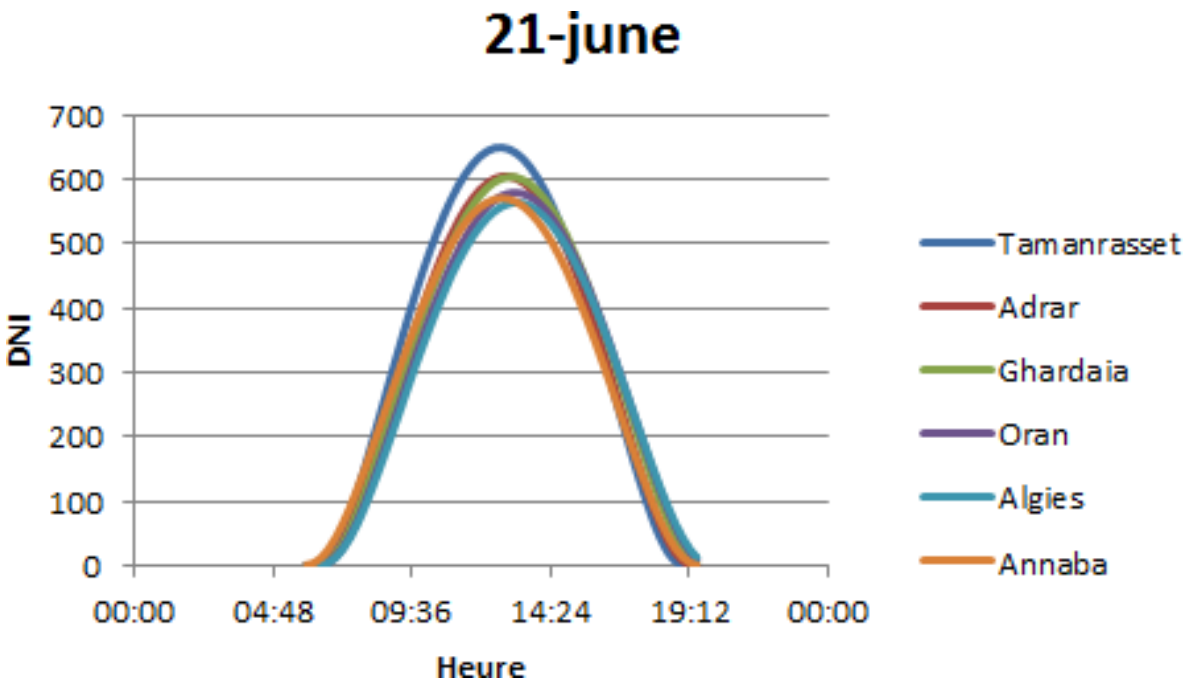

Figure V.9: *The DNI evolution during the day for the 21st June*

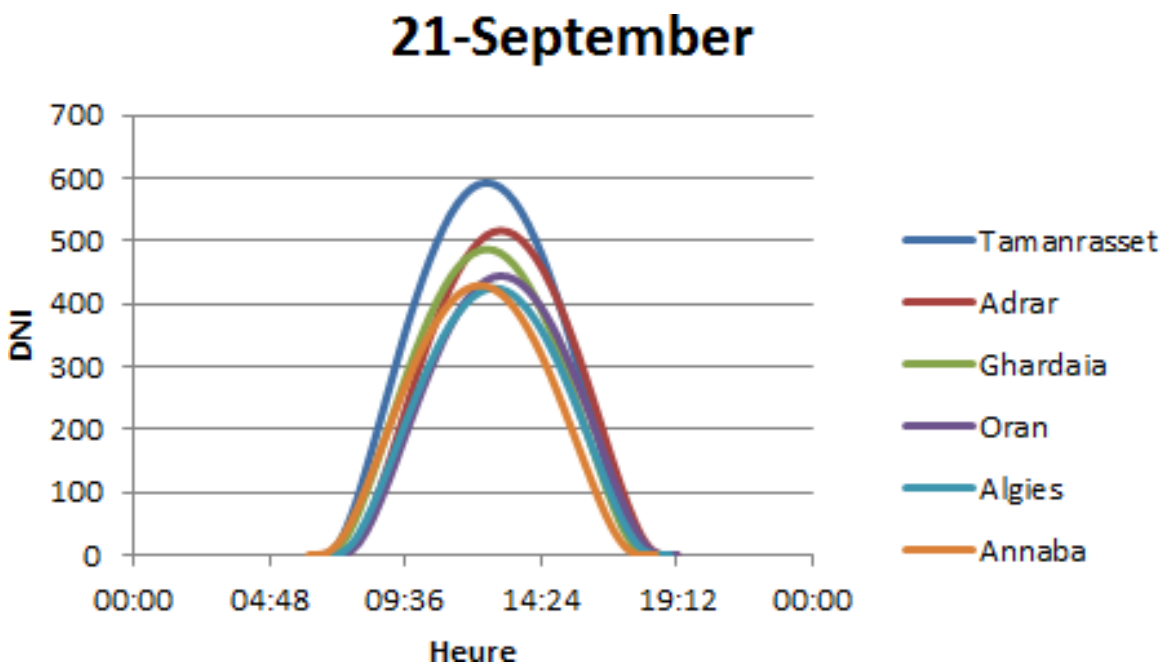

Figure V.10: *The DNI evolution during the day for the 21st September*

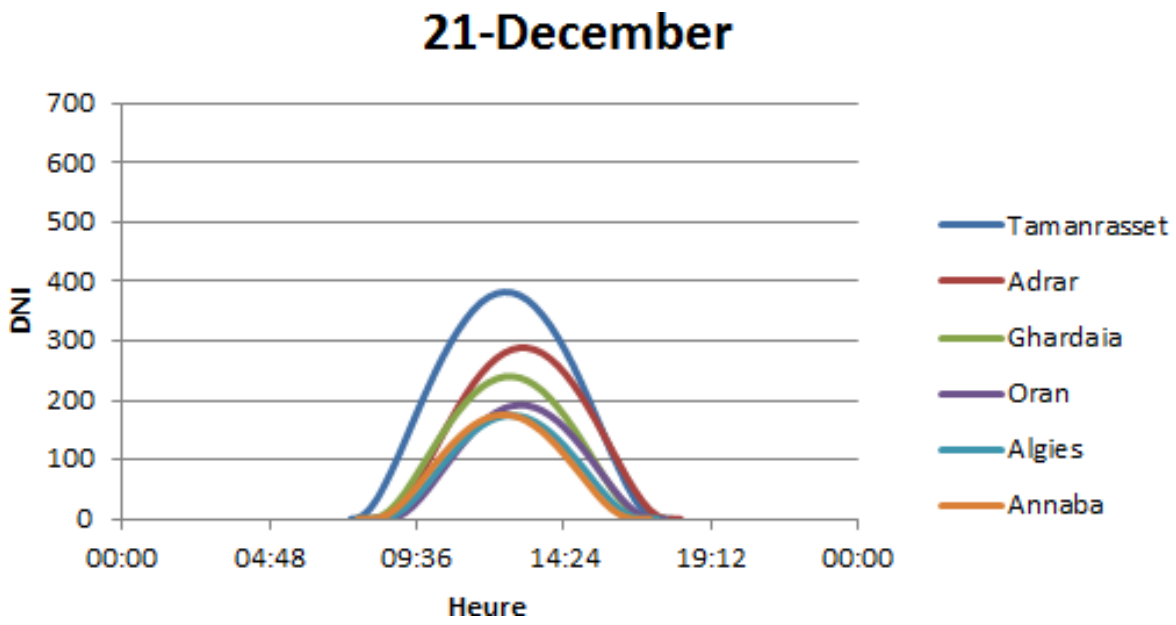

Figure V.11: *The DNI evolution during the day for the 21st December*

V.5. Conclusion

The Calculations of the DNI in different region of Algeria are presented in this chapter using the Hottel's model with the help with an Excel program is presented in this chapter. The results are presented in the form of graphs to show the evolution of the Direct Normal Irradiance during the day. It can be concluded that the Sahara's regions receive the great amount of energy compared with the north regions.

Conclusion

Different methods was presented by different researchers and engineers in the world in order to increase the life time of the parabolic trough absorber tube by active, passive or combined technics. In this thesis, a comprehensive and brief review of solar thermal collector especially the parabolic trough collector and various technic to enhance the heat transfer between the absorber tube and the heat transfer fluid was presented. Also, a new model of the parabolic trough technology is discussed. The parameters and climatic conditions of different sites in Algeria were analysed to determine the direct normal irradiance in every region.

The use of the inserts inside the receiver tube enhances the heat transfer and reduces the circumferential temperature which is the major cause of the absorber tube damage.

The cylindrical and the focal inserts increase the heat transfer between the absorber tube inner wall and the heat transfer fluid with a penalty of pressure drop because of the friction factor.

By adding the secondary reflector to the conventional parabolic trough collector, the circumferential temperature of the absorber tube was enhanced and homogenised which is a beneficial concept to increase the lifetime of the receiver tube.

The climatic analysis of the different regions of Algeria showed that the direct normal irradiance increases with the increase of the hours of the day and in the Saharan regions the DNI is always higher than that of the north ones and in Tamanrasset region that the highest value of the DNI.

IIETA International Information and Engineering Technology Association
Advancing the World of Information and Engineering

Instrumentation Mesure Métrologie
Vol. 18, No. 3, June, 2019, pp. 275-280
Journal homepage: http://iieta.org/journals/i2m

Numerical Investigation and Solar Flux Distribution Analysis of Parabolic Trough Solar Collector by Adding Secondary Reflector

Haddouche Mohammed Reda*, Benazza Abdelylah

Laboratory of Materials and Reactive Systems, Djillali Liabes University, Sidi Bel Abbes 22000, Algeria

Corresponding Author Email: haddouchereda@outlook.com

https://doi.org/10.18280/i2m.180307

Received: 10 March 2019
Accepted: 8 May 2019

Keywords:
heat transfer enhancement, parabolic trough collector, non-uniform heat flux, Nusselt number, secondary reflector, computational fluid dynamic

ABSTRACT

The biggest problem that can be encountered in the Parabolic Trough Collector is the tube wear, and this is due to the non-uniformity of the temperature distribution over the circumferential angle of the tube. In this paper the absorber tube is moved downward away the focal line of the parabola and a secondary reflector is added overhead the tube in order to reduce the heat flux gradient and homogenize it. The simulation method of the ray's path is adopted by Soltrace software. The numerical results of the enhanced Parabolic Trough Collector show that the heat flux gradient can be enhanced and reduced by 70.37 % and the temperature gradient can be reduced from 159.39 K to 24.16 K by adding the secondary reflector.

1. INTRODUCTION

The absorber tube is the major component and the key parameter of a parabolic trough solar collector. The non-uniformity of the solar flux distribution over the outer surface of the absorber tube leads to a large difference on the temperature distribution which can cause damages and failures. Nowadays the researchers and engineers in the field search to decrease the circumferential temperature gradient to avoid failures and increase the life time of the absorber tube.

Moreover, many researchers focus on the heat transfer enhancement between the absorber tube and the heat transfer fluid using different methods. Jie Deng et al. [1] investigated the heat transfer enhancement of a receiver tube by introducing concentric and eccentric rod inserts and using molten salt as HTF. Their results show that the usage of rod insert can enhance the heat transfer performance and reduces of the maximum tube wall temperature. Gong Xiangtao et al. [2] analysed the Heat transfer enhancement of a parabolic trough solar receiver with pin-fin arrays inserting. Their results show that the use of pin-fin arrays inserting increases the overall heat transfer performance and decreases the temperature gradient of the absorber tube. Xingwang Song et al. [3] carried out a numerical study of parabolic trough receiver with non-uniform heat flux and helical screw-tape inserts. They investigated the effect of solar incidence angle on heat flux distribution, the heat loss of a receiver, the maximum temperature on absorber tube outer surface and the maximum circumferential temperature difference. Some researchers tried to modify the shape and the geometry of the parabolic trough collector. Bin Zou et al. [4] presented a detailed study on the optical performance of parabolic trough solar collectors with Monte Carlo Ray Tracing method. Their results prove that the geometrical parameters, including aperture width, focal length and absorber diameter, have great effects on the optical performance of the PTC and the distribution of local concentration ratio around the absorber tube varies greatly with different geometrical configurations and for some special parameter conditions. Yassine Demagh et al. [5, 6] analysed the feasibility of an S-curved sinusoidal absorber of parabolic trough collector using Tonatiuh code to establish the heat flux density on the outer surface of the absorbers. Their results show that the highest values of the heat flux density decrease, what leads to reduce the temperature gradient; they concluded also that the S-curved absorber should be comparatively better than the conventional straight absorber tube. Tao Tao et al. [7] analysed a new trough solar concentrator. Their analysis shows that the trough width of the system is the important factor that determines the performance of the system. Fei Cao et al. [8, 9] analysed the thermal performance and stress of the elliptical cavity receiver tube in the parabolic trough solar collector. Panna Lal Singh et al. [10] studied experimentally the heat loss of trapezoidal cavity absorbers for linear solar concentrating collector. Their results show that the values of the heat loss coefficient for the trapezoidal cavity absorber were lower as compared to the concentric glass covered absorber. X. Xiao et al. [11] analysed experimentally and numerically the heat transfer of a V-cavity absorber for linear parabolic trough solar collector. They found that the V-cavity absorber with the rectangular fins has a better heat transfer performance. And the average outlet temperature of the heat transfer fluid increases and the temperature of the heating surface decreases adding rectangular fins, which confirms that the rectangular fins in the absorber can enhance the heat transfer and decrease the heat loss. A. Kajavali et al. [12] investigated the heat transfer enhancement in a parabolic trough collector with a modified absorber. Their numerical analysis conducted that the single tube absorber showed a lower solar energy recovery than the modified absorber. Wang Kun et al. [13] presented a numerical study for a new type parabolic trough solar collector with uniform solar flux distribution. Their analysis show that the solar flux distribution can be homogenized by adding a secondary

reflector which leads to reduce significantly the maximum temperature and the circumferential temperature difference of the absorber tube wall.

In this paper the absorber tube is moved downward away the focal line and a secondary parabola is added to reduce the heat flux gradient over the circumferential angle of the absorber tube and increase the reliability of the absorber tube .

2. PHYSICAL MODEL

The conventional parabolic trough collector is designed to capture the direct solar irradiance over a large parabolic shaped surface and concentrate it onto its focal line. The concentrator is a sheet metal bended to a parabolic shape and painted with reflective surface to reflect solar irradiation on its focal line. The absorber tube is the major component of PTC, in which solar radiation is focused and converted to thermal energy by an intermediate of a heat transfer fluid (HTF). From (Figure 1a) it can be seen that the absorber tube is subjected to a non-uniform heat flux while the bottom periphery of is subjected to concentrated solar radiation and the top one is subjected to non-concentrated solar radiation. The non-uniformity of the solar flux distribution over the outer surface of the absorber tube leads to a large difference on the temperature distribution which can cause damages.

In order to homogenize the heat flux and reduce the circumferential temperature gradient; the absorber tube is moved away from the focal line of the parabolic trough concentrator toward the concentrator and a secondary reflector is added overhead the tube. The two parabolas are arranged in an opposite manner. The sun rays reflected by the primary concentrator hit the bottom part of the absorber tube and a portion of these rays are reflected again on the upper part of the absorber tube by the secondary reflector as shown in (Figure 1b). Table 1 shows the geometrical parameters of the Parabolic Trough Collector.

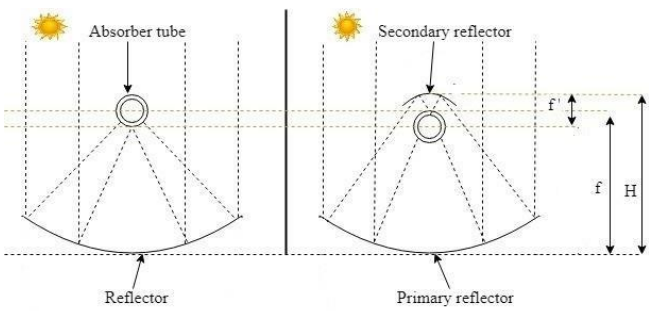

Figure 1. The schematic diagram of the parabolic trough collector

Table 1. The geometrical parameters of the parabolic trough collector

Focal length of the primary concentrator (f)	1.71 m
Focal length of the secondary reflector (f')	0.011m
Distance of the secondary reflector (H)	1.76 m
Aperture width of the primary concentrator	5.77 m
Aperture width of the secondary concentrator	0.09 m
Absorber tube inner radius	3.2 cm
Absorber tube outer radius	3.5 cm
Transmittance of the glass pipe	96 %
Cover inner radius	5.95 cm
Cover outer radius	6.25 cm

3. MATERIALS AND METHODS

3.1 The MCRT simulation

The simulation of the Local Concentration Ration (LCR) of the conventional PTC and PTC with secondary reflector is adopted by SolTrace software developed at the National Renewable Energy Laboratory (NREL) to model concentrating solar power optical systems and analyse their performance and it is based on the Monte Carlo Ray Tracing method (MCRT).

Figure 2 shows the path of the rays reflected by the concentrator on the absorber tube. It can be seen from this figure that the absorber tube of the conventional PTC (Figure 2a) is subjected to a concentrated solar flux on the bottom part while the upper one is subjected to a non-concentrated solar flux; and by moving the absorber tube downward and adding a secondary reflector; the solar rays can reach the upper part after reflected by the additional reflector as shown in Figure 2b.

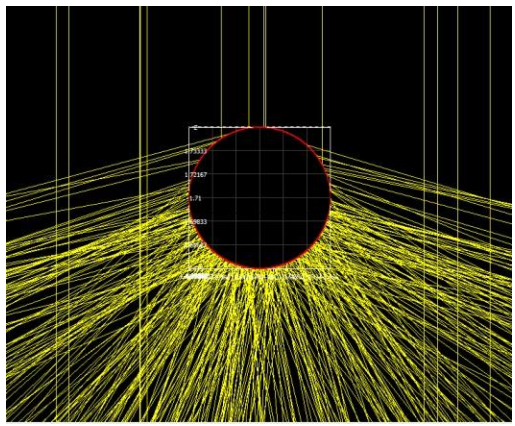

a) Conventional parabolic trough collector

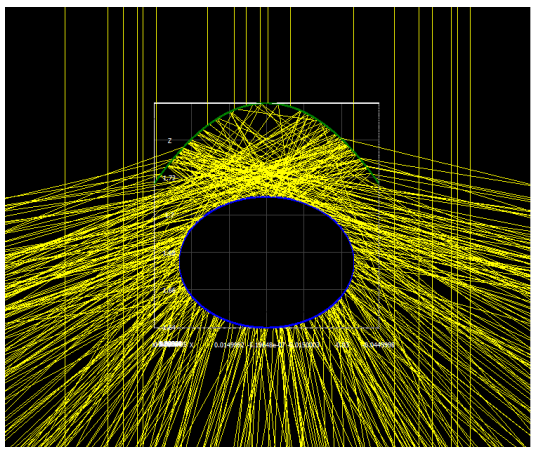

b) The schematic diagram of the parabolic trough

Figure 2. Ray's path reflected by the concentrator on the absorber tube

3.2 The CFD simulation

3.2.1 Governing equations

The equations which govern the computational fluid dynamics are continuity, momentum, energy and the standard k-ε equations [1]:

Continuity equation

$$\frac{\partial}{\partial x_j}(\rho u_i) = 0 \tag{1}$$

Momentum equation

$$\frac{\partial}{\partial x_i}(\rho u_i u_j) = -\frac{\partial P}{\partial x_i} + \frac{\partial}{\partial x_j}\left[(\mu+\mu_t)\left(\frac{\partial u_i}{\partial x_j}+\frac{\partial u_j}{\partial x_i}\right) - \frac{2}{3}(\mu+\mu_t)\frac{\partial u_i}{\partial x_i}\delta_{ij}\right] + \rho g_i \tag{2}$$

Energy equation

$$\frac{\partial}{\partial x_i}(\rho u_i T) = \frac{\partial}{\partial x_i}\left[\left(\frac{\mu}{\Pr}+\frac{\mu_t}{\sigma_t}\right)\frac{\partial T}{\partial x_i}\right] \tag{3}$$

The standard k-ε model has two model equations, one for k and one for ε [14]:

k-equation

$$\frac{\partial}{\partial x_i}(\rho u_i k) = \frac{\partial}{\partial x_i}\left[\left(\mu+\frac{\mu_t}{\sigma_k}\right)\frac{\partial k}{\partial x_i}\right] + G_k - \rho\varepsilon \tag{4}$$

ε- equation

$$\frac{\partial}{\partial x_i}(\rho u_i \varepsilon) = \frac{\partial}{\partial x_i}\left[\left(\mu+\frac{\mu_t}{\sigma_\varepsilon}\right)\frac{\partial \varepsilon}{\partial x_i}\right] + \frac{\varepsilon}{k}\left(c_{1\varepsilon}G_k - c_{2\varepsilon}\rho\varepsilon\right) \tag{5}$$

where, G_k represent the generation of turbulent kinetic energy

$$G_k = \mu_t \frac{\partial u_i}{\partial x_i}\left(\frac{\partial u_i}{\partial x_j}+\frac{\partial u_j}{\partial x_i}\right) + \frac{2}{3}\rho k \delta_{ij}\frac{\partial u_i}{\partial x_j} \tag{6}$$

In these equations, turbulent viscosity μ_t is defined as:

$$\mu_t = c_\mu \rho \frac{k^2}{\varepsilon} \tag{7}$$

The equations contain five adjustable constants $C\mu$, σk, $\sigma \varepsilon$, $c1\varepsilon$ and $c2\varepsilon$. This model employs values for the constants that are arrived at by comprehensive data fitting for a wide range of turbulent flow [15]:

$C\mu$=0.09, σk=1.00 $\sigma \varepsilon$=1.30 $c1\varepsilon$=1.44 and $c2\varepsilon$=1.92.

3.2.2 Boundary conditions

- Fluid inlet: $V_x = V_{in}$; $V_y = V_z = 0$; $T_f = T_{in}$
- Fluid outlet: Fully developed condition.
- Wall boundary condition:
- No-slip conditions exist at the inside surface of the absorber tube.
- The outer wall of the absorber tube is subjected to non-uniform heat flux (Figure 6):

$$Q = LCR \cdot DNI \tag{8}$$

where, the DNI is the Direct normal irradiance (DNI=1000 W/m^2).

- The outer wall of the glass cover in this receiver model has a mixed boundary condition to account for both radiation and convection heat transfer.
- The sky temperature is defined as [16]:

$$T_{sky} = 0.00552 \cdot T_{amb}^{1.5} \tag{9}$$

where, T_{amb} is ambient temperature (T_{amb}=300 K)

And the convective heat transfer coefficient of the wind is given by [18]:

$$hw = 4V_w^{0.58} \cdot d_{go}^{-0.48} \tag{10}$$

where, V_w is the wind speed, (V_w=2.5 m/s) and d_{go} is the glass cover outer diameter.

The HTF used in this study is the Therminol®VP1. It is a eutectic mixture of 73.5 % diphenyl oxide and 26.5 % diphenyl and as such can be used in existing liquid or vapor systems.

All the equations are discretised by the finite volume method. All the equations are solved by the first order scheme, the coupling between the pressure and the velocity is based on the simple algorithm [15]. The thermo-physical properties of the fluid are taken constant.

4. MORE MODEL VALIDATION

For this purpose the numerical results are compared with correlations obtained from literature. The average Nusselt Number is given by:

$$Nu = \frac{h d_{ai}}{\lambda} \tag{11}$$

And

$$h = \frac{Q}{T_{ai} - T_f} \tag{12}$$

where, Q is the average heat flux on the absorber tube, T_{ai} is the average temperature of the inner wall of the absorber tube and T_f is the average temperature of the HTF.

The Darcy friction factor for turbulent flow is defined as:

$$f = \frac{2 d_{ai} \Delta P}{L \rho u^2} \tag{13}$$

where, d_{ai} and L are the inner diameter and the length of the absorber tube respectively.

The Nusselt number given by Gnielinski [18] is defined as:

$$Nu = \frac{\frac{f}{8}(\mathrm{Re}-1000)\Pr}{1+12.7\left(\frac{f}{8}\right)^{0.5}\left(\Pr^{\frac{2}{3}}-1\right)} \tag{14}$$

where, the friction factor f can be determined from an appropriate relation such as the first Petukhov's equation [18, 19] for turbulent flow in smooth tube:

$$f = (0.79 \ln \mathrm{Re} - 1.64)^{-2} \quad (15)$$

For 0.5 ≤Pr≤2000 and 3000≤Re≤5x10^6

Another equation presented by Notter [18] to determine the average Nusselt number:

$$Nu = 5 + 0.015\,\mathrm{Re}^{0.856}\,\mathrm{Pr}^{0.347} \quad (16)$$

Blasius [17] proposed a correlation to calculate the Darcy friction factor for fully developed flow inside circular smooth tubes:

$$f = 0.184\,\mathrm{Re}^{-0.2} \quad (17)$$

For Re > 2x10^4

Figure 3 and Figure 4 show the comparison between the numerical results and the results calculated by correlations obtained from literature of the Nusselt number *Nu* and the Darcy friction factor *f* respectively. From these figures, it can be seen that the curves agree well with each other with a maximum deviation of 2.14 % for *Nu* number and the maximum error for the friction factor is 2.78 %.

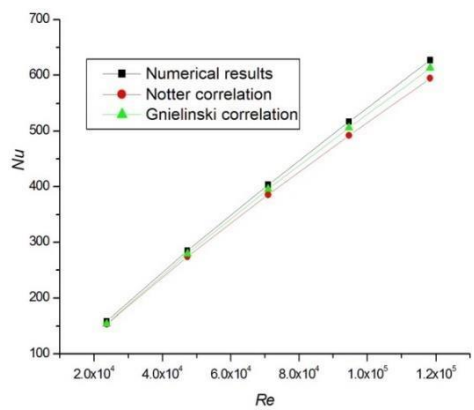

Figure 3. Variation of Nu number as a function of Re number

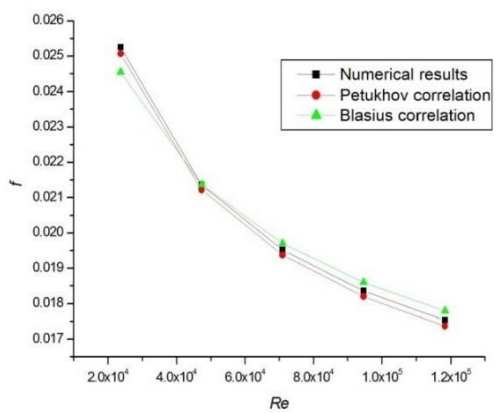

Figure 4. Variation of f number as a function of Re number

5. RESULTS AND DISCUSSION

5.1 Ray tracing and heat flux analysis

In the first part of this this paper; the LCR obtained from Soltrace software for both the conventional PTC and the PTC with secondary reflector are investigated.

Figure 5 shows the flux map of the conventional PTC and the enhanced PTC. From these figures it can be seen that the heat flux of the conventional PTC is non-uniform with a large gradient while by adding a secondary reflector the gradient of the flux decreases and becomes homogenous.

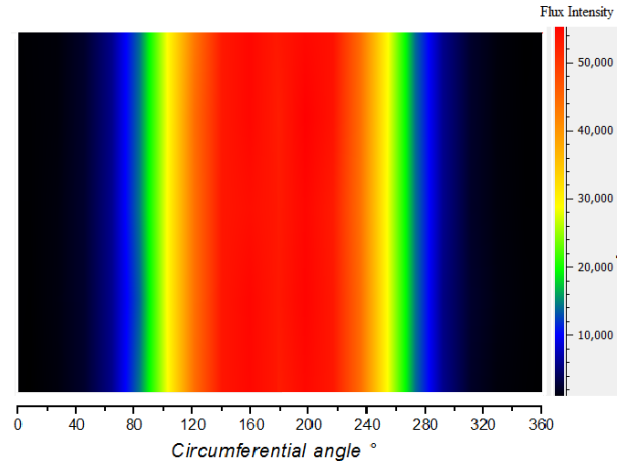

a) Conventional parabolic trough collector

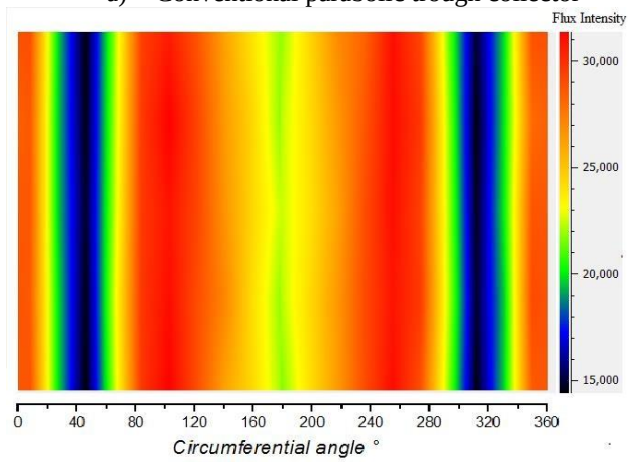

b) Parabolic trough collector with SR

Figure 5. Flux map of the conventional PTC and the enhanced PTC

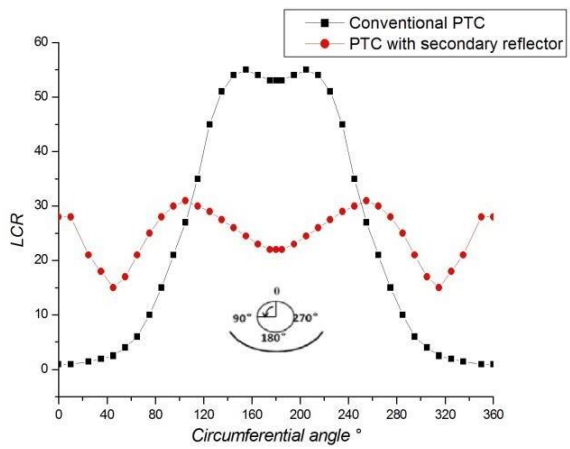

Figure 6. Variation of f number as a function of Re number

The LCR for both conventional PTC and the PTC with secondary reflector are shown in (Figure 6) .It can be seen

that the LCR decreases and becomes slightly uniform by adding the secondary reflector and the maximum value of the heat flux decreases to 31000 W/m² and the minimum value increases to 15000 W/m², while for the conventional PTC the peak value is 55000 W/m² and the minimum value is 1000 W/m². The gradient of the heat flux over the circumferential angle of the absorber tube is enhanced and reduced by 70.37 %.

5.2 Temperature distribution analysis

In the second part of this study; the thermal performance and the efficiency of the conventional PTC and the PTC with the secondary reflector are investigated under the same conditions.

Figure 7 presents the temperature distribution over the circumferential angle of both the conventional PTC and the enhanced one at the middle distance L=2m and for Re=47.31x10^4. It can be seen that the temperature gradient is reduced significantly and becomes homogenous. It can be also noticed that by adding a secondary reflector the maximum temperature is decreased from 739.84 K to 663.98 K and the minimum temperature is increased from 580.44 K to 639.82 K, and the temperature gradient difference is reduced from 159.39 K to 24.16 K.

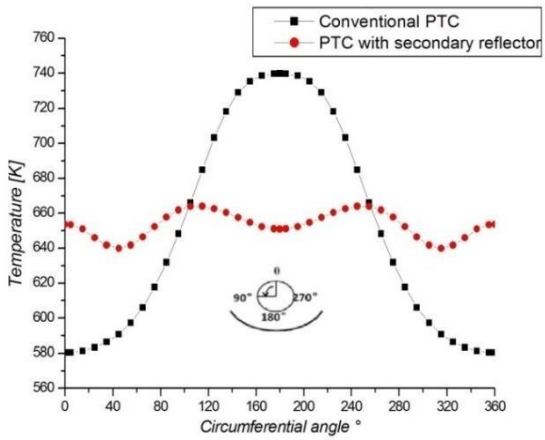

Figure 7. The temperature distribution on the outer surface of the absorber tube as a function of circumferential angle

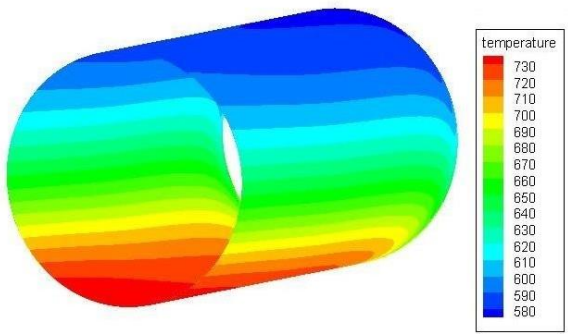

a) Conventional parabolic trough collector

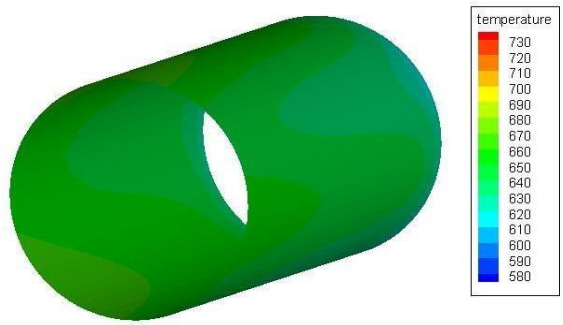

b) Parabolic Trough Collector with SR

Figure 8. The contour of the temperature distribution of the absorber tube

The contour of temperature distribution over the wall of both conventional tube and tube with secondary reflector are shown in Figure 6. From this figure it can be seen that that the temperature distribution of the conventional PTC (Figure 8a) is non-uniform and by adding another reflector the temperature distribution becomes more uniform (Figure 8b)

6. CONCLUSIONS

In this paper the heat flux distribution on the outer surface of the absorber tube of Parabolic Trough Collector is investigated and enhanced in order to reduce the temperature gradient of the tube by moving the absorber tube away from the focal line toward the parabola and adding a secondary reflector. The numerical results of the soltrace software indicate that the heat flux distribution is enhanced and the heat flux gradient can be reduced by adding another reflector overhead the absorber tube by 70.37 %, also the numerical results of the computational Fluid Dynamics show that the maximum temperature is decreased from 739.84 K to 663.98 K and the minimum temperature is increased from 580.44 K to 639.82 K, and the temperature gradient difference is reduced from 159.39 K to 24.16 K.

REFERENCES

[1] Chang, C, Sciacovelli, A., Wu, Z.Y., Li, X., Li, Y.L., Zhao, M.Z., Deng, J., Wang, Z.F., Ding, Y.L. (2018). Enhanced heat transfer in a parabolic trough solar receiver by inserting rods and using molten salt as heat transfer fluid. Applied Energy, 220: 337-350. https://doi.org/10.1016/j.apenergy.2018.03.091

[2] Bejan, A. (2015). Constructal thermodynamics. International Journal of Heat and Technology, 34(Special Issue 1): S1-S8. https://doi.org/10.18280/ijht.34S101

[3] Gong, X.T., Wang, F.Q., Wang, H.Y., Tan, J.Y., Lai Q.Z., Han, H.Z. (2017). Heat transfer enhancement analysis of tube receiver for parabolic trough solar collector with pin fin arrays inserting. Solar Energy, 144:

185-202. https://doi.org/10.1016/j.solener.2017.01.020
[4] Song, X.W., Dong, G.B., Gao, F.Y., Diao, X.G., Zheng, L.Q., Zhou, F.Y. (2014). A numerical study of parabolic trough receiver with nonuniform heat flux and helical screw-tape inserts. Energy, 77: 771-782. https://doi.org/10.1016/j.energy.2014.09.049
[5] Zou, B., Dong, J.K., Yao, Y., Jiang, Y.Q. (2017). A detailed study on the optical performance of parabolic trough solar collectors with Monte Carlo Ray Tracing method based on theoretical analysis. Solar Energy, 147: 189-201. https://doi.org/10.1016/j.solener.2017.01.055
[6] Demagh, Y., Bordja, I., Kabar, Y., Benmoussa, H. (2015). A design method of an S-curved parabolic trough collector absorber with a three-dimensional heat flux density distribution. Solar Energy, 122: 873-884. https://doi.org/10.1016/j.solener.2015.10.002
[7] Demagh, Y. (2018). Numerical investigation of a novel sinusoidal tube receiver for parabolic trough technology. Applied Energy, 218: 494-510. https://doi.org/10.1016/j.apenergy.2018.02.177
[8] Tao, T., Zheng, H.F., He, K.Y., Abdulkarim, M. (2011). A new trough solar concentrator and its performance analysis. Solar Energy, 85: 198-207. https://doi.org/10.1016/j.solener.2010.08.017
[9] Cao, F., Wang, L., Zhu, T.Y. (2017). Design and optimization of elliptical cavity tube receivers in the parabolic trough solar collector. International Journal of Photoenergy, 2017: 7 pages. https://doi.org/10.1155/2017/1471594
[10] Singh, P.L., Sarviya, R.M., Bhagoria, J.L. (2010). Heat loss study of trapezoidal cavity absorbers for linear solar concentrating collector. Energy Conversion and Management, 51(2): 329-337. https://doi.org/10.1016/j.enconman.2009.09.029
[11] Xiao, X., Zhang, P., Shao, D.D., Li, M. (2014). Experimental and numerical heat transfer analysis of a V-cavity absorber for linear parabolic trough solar collector. Energy Conversion and Management, 86: 49-59. https://doi.org/10.1016/j.enconman.2014.05.001
[12] Kajavali, A., Sivaraman, B., Kulasekharan, N. (2014). Investigation of heat transfer enhancement in a parabolic trough collector with a modified absorber. International Energy Journal, 14(4): 177-188.
[13] Wang, K., He, Y.L., Cheng, Z.D. (2014). A design method and numerical study for a new type parabolic trough solar collector with uniform solar flux distribution. Science China Technological Sciences, 57(3): 531-540. https://doi.org/10.1007/s11431-013-5452-6
[14] Launder, B.E., Splanding, D.B. (1974). The numerical computation of turbulent flows. Computer Methods in Applied Mechanics ANR Engineering, 3(2): 269-289. https://doi.org/10.1016/0045-7825(74)90029-2
[15] Versteeg, H.K., Malalasekera, W. (1995). An introduction to computational fluid dynamics. The Finite Volume Method. John Wiley and Sons Ink, New York.
[16] Swinbank, W.C. (1963). Long-wave radiation from clear skies. Quarterly Journal of the Royal Meteotological Society, 89(31): 339-348. https://doi.org/10.1002/qj.49708938105
[17] Mullick, S.C., Nanda, S.K. (1989). An improved technique for computing the heat loss factor of a tubular absorber. Solar Energy, 42(1): 1-7. https://doi.org/10.1016/0038-092X(89)90124-2
[18] Yunus, A.C. (2007). Heat and Mass Transfer: A Practical Approach. (Third eds), MC Graw Hill.
[19] Petukhov, B.S. (1970). Heat transfer and friction in turbulent pipe flow with variable physical properties. Advances in Heat Transfer, 6: 504-561. https://doi.org/10.1016/S0065-2717(08)70153-9
[20] Notter, R.H., Sleicher, C.A. (1972). A solution to the turbulent Graetz problem-III Fully developed and entry region heat transfer rates. Chemical Engineering Science, 27: 2073-2093.

NOMENCLATURE

CP	specific heat, J. kg^{-1}. K^{-1}
f	Friction factor
L	Receiver length,
Nu	Nusselt number
P	Pressure, Pa
Pr	Prandtl number
Q	Heat flux, $W.m^{-2}.K^{-1}$
Re	Reynolds number
T	Temperature, K
V	Velocity, $m.s^{-1}$

Greek symbols

ε	emissivity
λ	Thermal conductivity, $W.m^{-2}$. K^{-1}
ρ	solid volume fraction
μ	dynamic viscosity, kg. $m^{-1}.s^{-1}$

Subscripts

a	Absorber
e	Envelope
i	Inner
o	Outer
f	fluid
sky	Sky
w	Wall
a	Ambience

Annex II : Coordonnées géographiques des wilayas d'Algérie

Wilayas	Latitude	Longitude	Altitude
01 Adrar	27° 53′ 59N	0° 16′ 59W	275
02 Chlef	36° 09′ 53N	1° 20′ 06E	133
03 Laghouat	33° 47′ 59N	2° 52′ 59E	750
04 Oum Bouaghi	35° 52′ 39N	7° 06′ 49E	902
05 Batna	35° 33′ 19N	6° 10′ 43E	1048
06 Bejaia	36° 45′ 00N	5° 04′ 59E	0
07 Biskra	34° 51′ 00N	5° 43′ 59E	213
08 Bechar	31° 37′ 00N	2° 13′ 00W	747
09 Blida	36° 28′ 00N	2° 49′ 59E	274
10 Bouira	36° 22′ 48N	3° 54′ 05E	557
11 Tamanrasset	22° 46′ 59N	5° 31′ 00E	1319
12 Tebessa	35° 24′ 15N	8° 07′ 27E	851
13 Tlemcen	34° 52′ 42N	1° 18′ 54W	1032
14 Tiaret	35° 22′ 33N	1° 18′ 47E	994
15 Tizi Ouzou	36° 43′ 01N	4° 02′ 59E	182
16 Alger	36° 45′ 47N	3° 03′ 02E	0
17 Djelfa	34° 40′ 00N	3° 15′ 00E	1126
18 Jijel	36° 47′ 59N	5° 46′ 00E	47
19 Setif	36° 11′ 29N	5° 24′ 34E	1080
20 Saida	34° 49′ 59N	0° 09′ 00E	868
21 Skikda	36° 51′ 44N	6° 56′ 50E	25
22 Sidi Belabbes	35° 11′ 38N	0° 38′ 29W	483
23 Annaba	36° 53′ 59N	7° 46′ 00E	0
24 Guelma	36° 27′ 58N	7° 26′ 02E	256
25 Constantine	36° 21′ 54N	6° 36′ 53E	626
26 Medea	36° 16′ 00N	2° 45′ 00E	880
27 Mostaganem	35° 55′ 59N	0° 05′ 25E	97
28 M'sila	35° 43′ 32N	4° 31′ 40E	475
29 Mascara	35° 23′ 40N	0° 08′ 23E	492
30 Ouargla	31° 56′ 59N	5° 19′ 59E	150
31 Oran	35° 41′ 28N	0° 38′ 30W	110
32 El Bayadh	33° 41′ 10N	1° 00′ 50E	1304
33 Illizi	26° 28′ 59N	8° 28′ 00E	597
34 Bordj B. Arreridj	36° 04′ 00N	4° 46′ 00E	900
35 Boumerdes	36° 46′ 00N	3° 28′ 38E	41
36 Taref	36° 46′ 07N	8° 19′ 00E	14
37 Tindouf	27° 40′ 27N	8° 08′ 52W	386
38 Tissemsilt	35° 36′ 28N	1° 48′ 40E	849
39 El Oued	33° 19′ 59N	6° 52′ 59E	67
40 Khenchela	35° 26′ 09N	7° 08′ 36E	1152
41 Souk Ahras	36° 16′ 07N	7° 56′ 08E	686
42 Tipaza	36° 34′ 59N	2° 27′ 00E	69
43 Mila	36° 27′ 04N	6° 15′ 55E	486
44 Ain Defla	36° 04′ 00N	4° 32′ 59E	1164
45 Naama	33° 16′ 00N	0° 19′ 00W	1176
46 Ain emouchent	35° 18′ 45N	1° 08′ 43W	248
47 Ghardaia	32° 28′ 59N	3° 40′ 00E	572
48 Relizane	35° 44′ 33N	0° 33′ 33E	98

References

[1] Paul Breeze et al, Renewable Energy Focus Handbook, First edition, 2009, Elsevier, http://www.elsevierdirect.com/9780123747051

[2] John A. Duffie and William A. Beckman, Solar Engineering of Thermal Processes, fourth Edition, 2013, John Wiley & Sons.

[3] robert Foster, Majid Ghassemi, Alma Cota, SOLAR ENERGY, Renewable Energy and the Environment, 2010, Taylor and Francis Group.

[4] Peter Heller, The Performance of Concentrated Solar Power (CSP) Systems, Analysis, Measurement and Assessment, 2017 Elsevier.

[5] valeriano Ruiz Hernandez, Fondamentos de energia solar para ACS y climatizacion, buenas practicas, 2015, ATECYR.

[6] Volker Quaschning, Understanding Renewable Energy Systems, 2005, Carl Hanser Verlag GmbH and Co KG.

[7] A. Fernandez-Garcia, E. Zarza, L. Valenzuela and M. Perez, Parabolic-trough solar collectors and their applications, Renewable and Sustainable Energy Reviews, 14, (2010), 1695–1721.

[8] Y. Tian, C.Y. Zhao, A review of solar collectors and thermal energy storage in solar thermal applications, Applied Energy, 104, (2013), 538–553.

[9] V.K Jebasingh, G.M.Joselin Herbert, A review of solar parabolic trough collector, Renewable and Sustainable Energy Reviews, 54, (2016), 1085–1091.

[10] J.L. Navarro-Hermoso, G. Espinosa-Rueda, C. Heras, I. Salinas, N. Martinez, M. Gallas, Parabolic trough solar receivers characterization using specific test bench for transmittance, absorptance and heat loss simultaneous measurement, Solar Energy, 136, (2016), 268–277.

[11] Manuel J. Blanco Lourdes Ramirez Santigosa, Advances in Concentrating Solar Thermal Research and Technology, First edition, 2017, Elsevier.

[12] J. Sun, R. Wang, H. Hong, Q. Liu, An optimized tracking strategy for small-scale double axis parabolic trough collector, Applied Thermal Engineering (2016), doi: http://dx.doi.org/10.1016/j.applthermaleng.2016.10.187

[13] Ze-Dong Cheng, Ya-Ling He, Yu Qiu, A detailed nonuniform thermal model of a parabolic trough solar receiver with two halves and two inactive ends, Renewable Energy, 74, (2015), 139-147.

[14] S. Liu, M.Sakr, A comprehensive review on passive heat transfer enhancements in pipe exchangers, Renewable and Sustainable Energy Reviews, 19, (2013), 64–81.

[15] G. Kumaresan, P. Sudhakar, R. Santosh and R. Velraj, Experimental and numerical studies of thermal performance enhancement in the receiver part of solar parabolic trough collectors, Renewable and Sustainable Energy Reviews, (2017), http://dx.doi.org/10.1016/j.rser.2017.01.171.

[16] Chun Chang, Adriano Sciacovelli, Zhiyong Wu, Xin Li, Yongliang Li, Mingzhi Zhao, Jie Deng, Zhifeng Wang and Yulong Ding, enhanced heat transfer in a parabolic trough solar receiver by inserting rods and using molten salt as heat transfer fluid, Applied Energy, 220, (2018), 337–350.

[17] Evangelos Bellos and Christos Tzivanidis, Investigation of a star flow insert in a parabolic trough solar collector, Applied Energy, 224, (2018), 86–102.

[18] Evangelos Bellos, Christos Tzivanidis, Ilias Daniil and Kimon A. Antonopoulos, The impact of internal longitudinal fins in parabolic trough collectors operating with gases, Energy Conversion and Management, 135, (2017), 35–54.

[19] Gong Xiangtao, Wang Fuqiang, Wang Haiyan, Tan Jianyu, Lai Qingzhi and Han Huaizh, Heat transfer enhancement analysis of tube receiver for parabolic trough solar collector with pin fin arrays inserting, Solar Energy, 144, (2017), 185–202.

[20] Wei Wang, Yaning Zhang, Yongji Li, Huaizhi Han and Bingxi Li, Numerical study on fully-developed turbulent flow and heat transfer in inward corrugated tubes with double-objective optimization, International Journal of Heat and Mass Transfer, 120, (2018), 782–792.

[21] Aggrey Mwesigye, Tunde Bello-Ochende, Josua P. Meyer, Heat transfer and thermodynamic performance of a parabolic trough receiver with centrally placed perforated plate inserts. Appl Energy, (2014), http://dx.doi.org/10.1016/j.apenergy.2014.03.037

[22] Zhen Huang, Zeng-Yao Li, Guang-Lei Yu, Wen-Quan Tao, Numerical investigations on fully-developed mixed turbulent convection in dimpled parabolic trough receiver tubes, Appl. Therm. Eng. (2016), http://dx.doi.org/10.1016/j.applthermaleng.2016.10.012

[23] E. Bellos, C. Tzivanidis, K.A. Antonopoulos and G. Gkinis, Thermal enhancement of solar parabolic trough collectors by using nanofluids and converging-diverging absorber tube, Renewable Energy, 94, (2016), 213-222.

[24] Zaid S.Kareem, ShahrirAbdullah, TholudinM.Lazim, M.N.MohdJaafar and Ammar F.AbdulWahid, Heat transfer enhancement in three-start spirally corrugated tube: Experimental and numerical study, Chemical Engineering Science,134, (2015), 746–757.

[25] P. Wang, D.Y. Liu and C. Xu, Numerical study of heat transfer enhancement in the receiver tube of direct steam generation with parabolic trough by inserting metal foams, Applied Energy, 102, (2013), 449–460.

[26] Aggrey Mwesigye, Tunde Bello-Ochende, Josua P. Meye, Heat transfer and thermodynamic performance of a parabolic trough receiver with centrally placed perforated plate inserts. Appl. Energy (2014), http://dx.doi.org/10.1016/j.apenergy.2014.03.037

[27] Aggrey Mwesigye, Tunde Bello-Ochende and Josua P. Meyer, Heat transfer and entropy generation in a parabolic trough receiver with wall-detached twisted tape inserts, International Journal of Thermal Sciences, 99, (2016), 238-257.

[28] Xingwang Song, Guobo Dong, Fangyuan Gao, Xungang Diao, Liqing Zheng and Fuyun Zhou, A numerical study of parabolic trough receiver with nonuniform heat flux and helical screw-tape inserts, Energy, (2014), 1-12.

[29] Z. Huang, G.L. Yu, Z.Y. Li, W.Q. Tao, Numerical study on heat transfer enhancement in a receiver tube of parabolic trough solar collector with dimples, protrusions and helical fins, Energy Procedia, 69, (2015), 1306 – 1316.

[30] Z.D. Cheng, Y.L. He, F.Q. Cui, Numerical study of heat transfer enhancement by unilateral longitudinal vortex generators inside parabolic trough solar receivers, International Journal of Heat and Mass Transfer, 55, (2012), 5631–5641.

[31] Yogender Pal Chandra, Arashdeep Singh, Saroj Kumar Mohapatra, J.P. Kesari, Lokesh Rana, Numerical optimization and convective thermal loss analysis of improved solar parabolic trough collector receiver system with one sided thermal insulation, Solar Energy, 148, (2017), 36–48.

[32] Wang Fuqiang, Tan Jianyu, Ma Lanxin, Wang Chengchao, Effects of glass cover on heat flux distribution for tube receiver with parabolic trough collector system, Energy Conversion and Management, 90, (2015), 47–52.

[33] Fei Cao, Lei Wang, and Tianyu Zhu, Design and Optimization of Elliptical Cavity Tube Receivers in the Parabolic Trough Solar Collector, International Journal of Photoenergy, (2017), https://doi.org/10.1155/2017/1471594

[34] Wang K, He Y L, Cheng Z D. A design method and numerical study for a new type parabolic trough solar collector with uniform solar flux distribution. Sci China Tech Sci, (2014), 57, 531-540, http://dx.doi: 10.1007/s11431-013-5452-6

[35] Yassine Demagh, Ilyes Bordja, Yassine Kabar, Hocine Benmoussa, A design method of an S-curved parabolic trough collector absorber with a three-dimensional heat flux density distribution, Solar Energy, 122, (2015), 873–884.

[36] Hongbo Liang, Man Fan, Shijun You, Wandong Zheng, Huan Zhang, Tianzhen Ye, Xuejing Zheng, A Monte Carlo method and finite volume method coupled optical simulation method for parabolic trough solar collectors, Applied Energy, 201, (2017), 60–68.

[37] Roman Bader, Maurizio Barbato, Andrea Pedretti and Aldo Steinfeld, An air-based cavity-receiver for solar trough concentrators, proceedings of ASME 2010 4th International conference on Energy Sustainability.

[38] X. Xiao, P. Zhang, D.D. Shao, M. Li, Experimental and numerical heat transfer analysis of a V-cavity absorber for linear parabolic trough solar collector, Energy Conversion and Management, 86, (2014), 49–59.

[39] Vernon E. Dudley et al, Test results, SEGS LS2 Solar Collector, National technical information service, (1994).

[40] Yanjuan W., Qibin L., Jing L. and Hongguang J., A three-dimensional simulation of a parabolic trough solar collector system using molten salt as heat transfer fluid, Applied Thermal Engineering, 70, (2014), 462-476.

[41] Ze-Dong Cheng, Ya-Ling He, Yu Qiu, A detailed non-uniform thermal model of a parabolic trough solar receiver with two halves and two inactive ends, Renewable Energy, 74, (2015), 139-147.

[42] Ratzel A. C, Hickox C. E. and Gartling D. K, Techniques for reducing thermal conduction and natural convection heat losses in annular receiver geometries, Journal of Heat Transfer, 101, (1979), 108-113.

[43] Chun Changa, Adriano Sciacovelli, Zhiyong Wu, Xin Li, Yongliang Li, Mingzhi Zhao, Jie Deng, Zhifeng Wang, Yulong Ding, Enhanced heat transfer in a parabolic trough solar receiver by inserting rods and using molten salt as heat transfer fluid, Applied Energy, 220, (2018), 337–350.

[44] Launder B.E. and SplandingG D.B, The numerical computation of turbulent flows, computer methods in applied mechanics anr engineering, 3, (1974), 269-289.

[45] Versteeg H.K. and Malalasekera W., An introduction to computational fluid dynamics, the finite volume method, John Wiley and Sons Ink, New York, 1995.

[46] Swinbank W. C., Long-wave radiation from clear skies, Division of Meteorological Physics, Aspendale, Australia, (1963), 339-348.

[47] Mullick S. C. and Nanda S. K.: An improved technique for computing the heat loss factor of a tubular absorber, Solar Energy. 42, (1989), 1-7.

[48] Heat transfer fluids by SOLUTIA, Applied chemistry, creative solutions.

[49] NREL. SolTrace, optical modeling software.

[50] Yunus A. C.: Heat and mass transfer A PRACTICAL APPROACH, MC Graw Hill, Third ed, 2007.

[51] Petukhov .B. S., Heat transfer and friction in turbulent pipe flow with variable physical properties, High Temperature Institute, Academy of Science of the USSR. Moscow, (1970), 504-561.

[52] Notter R. H. and Sleicher C. A., A solution to the turbulent Graetz problem-III Fully developed and entry region heat transfer rates, Chemical Engineering Science, 27, (1972), 2073-2093.

[53] Khwanchit W. and Smith E., Enhancement of heat transfer using CuO/water nanofluid and twisted tape with alternate axis, International Communications in Heat and Mass Transfer, 38, (2011), 742–748.

[54] Gong Xiangtao, Wang Fuqiang, Wang Haiyan, Tan Jianyu, Lai Qingzhi, Han Huaizhi, Heat transfer enhancement analysis of tube receiver for parabolic trough solar collector with pin fin arrays inserting, Solar Energy, 144, (2017), 185–202.

[55] Ahmad Islahi, Saani Shakil, Mostafa Hamed, Hottel's Clear Day Model for a typical arid city – Jeddah, International Journal of Engineering Science Invention, 4, (2015), 32-37.

[56] Richard E. Bird and Roland L. Hulstrom, A simplified clear sky model for direct diffuse insolation on horizontal surfaces, Solar energy research institute, USA, (1981).